NAVAL POSTGRADUATE SCHOOL
Monterey, California

THESIS

FILMWISE CONDENSATION ON LOW INTEGRAL-FIN TUBES OF DIFFERENT DIAMETER

by

Thomas Louis Van Petten

December 1988

Thesis Co-Advisors: P. J. Marto
A. S. Wanniarachchi

Approved for public release; distribution is unlimited.

Unclassified

Security Classification of this page

REPORT DOCUMENTATION PAGE

1a Report Security Classification: Unclassified	1b Restrictive Markings
2a Security Classification Authority	3 Distribution Availability of Report: Approved for public release; distribution is unlimited.
2b Declassification/Downgrading Schedule	
4 Performing Organization Report Number(s)	5 Monitoring Organization Report Number(s)
6a Name of Performing Organization: Naval Postgraduate School; 6b Office Symbol (*If Applicable*): 69	7a Name of Monitoring Organization: Naval Postgraduate School
6c Address (*city, state, and ZIP code*): Monterey, CA 93943-5000	7b Address (*city, state, and ZIP code*): Monterey, CA 93943-5000
8a Name of Funding/Sponsoring Organization: National Science Foundation; 8b Office Symbol (*If Applicable*): CBT-8603-582	9 Procurement Instrument Identification Number
8c Address (*city, state, and ZIP code*): Washington, D.C. 20550	10 Source of Funding Numbers: Program Element Number / Project No / Task No / Work Unit Accession No

11 Title (*Include Security Classification*) Filmwise Condensation on Low Integral-Fin Tubes of Different Diameter

12 Personal Author(s) Thomas Louis Van Petten

13a Type of Report	13b Time Covered	14 Date of Report (*year, month,day*)	15 Page Count
Master's Thesis	From To	December 1988	168

16 Supplementary Notation The views expressed in this thesis are those of the author and do not reflect the official policy or position of the Department of Defense or the U.S. Government.

17 Cosati Codes			18 Subject Terms (*continue on reverse if necessary and identify by block number*)
Field	Group	Subgroup	Filmwise Condensation, Low Integral-Fin Tubes, Modified Wilson Plot Technique, Outside Heat-Transfer Coefficient

19 Abstract (*continue on reverse if necessary and identify by block number*)

Heat transfer measurements were made for filmwise condensation of R-113, steam and ethylene glycol on three sets of finned tubes which differed only in root diameter. The fin root diameters were 12.7 mm, 19.05 mm and 25.0 mm. A comparison of the enhancement ratios (based on constant vapor-side temperature drop) revealed that, within the range of diameter tested, the effect of root diameter was small. Results indicated that two or more trends may exist while increasing root diameter.

With the exception of the small-diameter tubes with steam, a change in root diameter did not effect the optimum fin spacing for each fluid tested. The optimum fin spacing for the small-diameter tubes with steam was approximately 2.0 mm, while the medium- and large-diameter tubes had an optimum fin spacing of 1.5 mm. The optimum fin spacing for R-113 and ethylene glycol was found to be 0.5 mm and 1.0 mm, respectively.

A comparison between the outside heat-transfer coefficients of the medium-diameter tubes for R-113 and steam with past NPS investigation showed an agreement within ±3 percent and ±10 percent, respectively.

20 Distribution/Availability of Abstract	21 Abstract Security Classification
[X] unclassified/unlimited [ ] same as report [ ] DTIC users	Unclassified
22a Name of Responsible Individual: Professor P. J. Marto	22b Telephone (*Include Area code*): (408) 646-2989 / 22c Office Symbol: 69Mx

DD FORM 1473, 84 MAR 83 APR edition may be used until exhausted security classification of this page

All other editions are obsolete Unclassified

Approved for public release; distribution is unlimited.

Filmwise Condensation on Low Integral-Fin Tubes of Different Diameter

by

Thomas Louis Van Petten
Lieutenant, United States Navy
B.S., U.S. Naval Academy, 1982

Submitted in partial fulfillment of the
requirements for the degree of

MASTER OF SCIENCE IN MECHANICAL ENGINEERING

from the

NAVAL POSTGRADUATE SCHOOL
December 1988

ABSTRACT

Heat transfer measurements were made for filmwise condensation of R-113, steam and ethylene glycol on three sets of finned tubes which differed only in root diameter. The fin root diameters were 12.7 mm, 19.05 mm and 25.0 mm. A comparison of the enhancement ratios (based on constant vapor-side temperature drop) revealed that, within the range of diameter tested, the effect of root diameter was small. Results indicated that two or more trends may exist while increasing root diameter.

With the exception of the small-diameter tubes with steam, a change in root diameter did not effect the optimum fin spacing for each fluid tested. The optimum fin spacing for the small-diameter tubes with steam was approximately 2.0 mm, while the medium- and large-diameter tubes had an optimum fin spacing of 1.5 mm. The optimum fin spacing for R-113 and ethylene glycol was found to be 0.5 mm and 1.0 mm, respectively.

A comparison between the outside heat-transfer coefficients of the medium-diameter tubes for R-113 and steam with past NPS investigation showed an agreement within ±3 percent and ±10 percent, respectively.

TABLE OF CONTENTS

LIST OF TABLES

LIST OF FIGURES

TABLE OF SYMBOLS

A	surface area for heat transfer consistent with U (m^2)
A_c	cross-sectional area of test tube (m^2)
A_{df}	$\pi D_f L$ (m^2)
A_f	surface area of fin (m^2)
A_i	effective inside area (m^2)
A_o	total external surface area, $A_r+\eta_f A_f$ (m^2)
A_p	profile area of fin (m^2)
A_r	surface area of smooth tube (m^2)
C_i	Sieder-Tate-type coefficient
c_p	specific heat at constant pressure ($J/kg \cdot K$)
D_f	fin diameter (m)
D_r	root diameter (m)
e	fin height (m)
g	gravitational constant (9.806 m/s^2)
h	condensing coefficient based on A_{df} ($W/m^2 \cdot K$)
h_b	condensing coefficient for flooded portion ($W/m^2 \cdot K$)
h_{BK}	Beatty-Katz outside heat-transfer coefficient($W/m^2 \cdot K$)
h^*_{BK}	modified Beatty-Katz condensing coefficient ($W/m^2 \cdot K$)
h_f	condensing coefficient of the fin ($W/m^2 \cdot K$)
h_{fg}	specific enthalpy of vaporization (J/kg)
h_h	condensing coefficient for smooth horizontal tube ($W/m^2 \cdot K$)
h_i	inside heat-transfer coefficient ($W/m^2 \cdot K$)

h_o	outside heat-transfer coefficient ($W/m^2 \cdot K$)
k_c	thermal conductivity of cooling water ($W/m \cdot K$)
k_l	condensate thermal conductivity ($W/m \cdot K$)
k_m	thermal conductivity of copper ($W/m \cdot K$)
L	length of exposed tube (133 mm)
LMTD	log-mean-temperature difference (K)
L_1	length of inlet portion of tube in nylon bushing (m)
L_2	length of outlet portion of tube in nylon bushing (m)
$\dot{m}$	mass flow rate (kg/s)
Nu_d	average Nusselt number for finned tube
Nu_{du}	average Nusselt number for unflooded portion
Nu_{df}	average Nusselt number for flooded portion
p	fin pitch (m)
Pr	Prandtl number
P_w	wetted perimeter (m)
Q	heat-transfer rate (W)
q	heat flux (W/m^2)
Re	Reynolds number
R_i	inside resistance ($m^2 \cdot K/W$)
R_v	vapor-side resistance ($m^2 \cdot K/W$)
R_w	wall resistance ($m^2 \cdot K/W$)
s	interfin spacing for rectangular fin(m)
s_b	interfin spacing at base (m)
t	fin thickness for rectangular fin (m)
t_b	fin thickness at base (m)

T_c	average coolant temperature (K)
T_{sat}	vapor saturation temperature (K)
t_t	fin thickness at tip (m)
$\tilde{T}_{wd}$	dimensionless average wall temperature for flooded portion
$\tilde{T}_{wu}$	dimensionless average wall temperature for unflooded portion
T_1	cooling water inlet temperature (K)
T_2	cooling water outlet temperature (K)
U	overall heat-transfer coefficient ($m^2 \cdot K/W$)
v	test tube average cooling water velocity (m/s)
α	dimensionless coefficient
β	fin-tip half angle (degrees)
$\epsilon_{\Delta T}$	enhancement ratio based on constant ΔT
ϵ_q	enhancement ratio based on constant q
Ψ	condensate retention angle (degrees)
μ_c	dynamic viscosity of cooling water at bulk temperature ($N \cdot s/m^2$)
μ_l	condensate dynamic viscosity ($kg/m \cdot s$)
μ_w	dynamic viscosity cooling water at inner wall temperature ($N \cdot s/m^2$)
ρ_c	test tube bulk cooling water density (kg/m^3)
ρ_l	condensate density (kg/m^3)
η	surface efficiency $(1 - (1 - \eta_f) A_r/(A_r + A_f))$
η_f	fin efficiency
η_1	fin efficiency for inlet portion of tube,
η_2	fin efficiency for outlet portion of tube

σ	surface tension (N/m)
ΔT_{vs}	temperature drop across the condensate film (K)
ΔT	cooling water temperature rise (K)
ΔT_f	average temperature difference across condensate film (K)

ACKNOWLEDGMENTS

The author would like to take this opportunity to thank Professor P. J. Marto for his advice and guidance in completing this thesis effort. Special appreciation is extended to Dr. A. S. Wanniarachchi for his support, patience, and expertise throughout this research project. Additionally, a special note of thanks is due to Mr. T. McCord and the machine shop personnel for their invaluable assistance.

The author also wishes to acknowledge Alice Case and LT Robert Vince for their efforts in helping to complete this paper.

Lastly, the author expresses his sincere gratitude to his best friend, his wife Jennifer, who without her support and sacrifice this investigation would never have been completed.

I. INTRODUCTION

A. BACKGROUND

Heat exchangers play an intricate role in the design, building and mission capabilities of today's naval vessels. Main engine and auxiliary condensers ensure the safe operation of the main engines and auxiliary equipment as well as the generation of electrical power. Air-conditioning condensers help to provide the climate control for ship's company and sensitive equipment. The development of high-powered shipboard sensors, computers, and weaponry has stretched present shipboard air-conditioning units to capacity. As a result, the modernization of naval vessels has required several tons of additional cooling capacity. Of course, this addition means that more space and weight must be allocated to this equipment. The Naval Postgraduate School (NPS), in association with David Taylor Research Center and with support from the National Science Foundation, is presently involved in research aimed at reducing the size and weight of condensers. These efforts can reduce ship's tonnage, save fuel, and provide space for other uses.

B. CONDENSATION

There are two modes of condensation: dropwise and filmwise. The random formation and departure of discrete droplets on the condensing surface is known as dropwise condensation. This mode is very efficient because the hot vapor is able to come in closer contact with

the cooler condenser surface because of the presence of very small droplets. Unfortunately, sustained dropwise condensation has not been practical despite decades of research. Filmwise condensation is a process in which the entire surface is covered with a thin, continuous film of condensate. The film creates a larger resistance to the heat transfer and therefore this process is less efficient. However, in designing and testing a condenser, filmwise condensation is desired as this is the most likely mode to occur. The high efficiency and randomness of dropwise condensation are not predictable and could lead to over-speculation of the condenser's capabilities. Designing for filmwise condensation is conservative and leaves a margin for error [Ref. 1].

C. BASIC HEAT-TRANSFER EQUATION

The basic heat-transfer equation used to describe the relationship between temperature difference and heat-transfer rate in a heat exchanger is:

$$Q = UA(LMTD) \tag{1.1}$$

where

Q = heat-transfer rate,

U = overall heat-transfer coefficient,

A = surface area for heat transfer consistent with U, and

LMTD = log-mean-temperature difference.

In a condenser, the value for the log-mean-temperature difference (LMTD) is dependent on the characteristics of the vapor/condensate and cooling water flow. The limits of this parameter are set primarily by the saturation temperature of the vapor and the temperature of the cooling water sink.

$$LMTD = \frac{(T_2 - T_1)}{\ln\left[\frac{T_{sat} - T_1}{T_{sat} - T_2}\right]}, \qquad (1.2)$$

where

T_1 = cooling water inlet temperature,

T_2 = cooling water outlet temperature, and

T_{sat} = vapor saturation temperature.

The overall heat-transfer coefficient (U) is dependent on cleanliness, construction, and composition of the condenser tubes, as well as the fluid properties of the condensate and the cooling water. It is inversely proportional to the resistance to heat transfer. The area (A), consistent with the coefficient, is usually the outside area of the tubes. This area can be increased by the addition of fins. However, as pointed out by Wanniarachchi, et al. [Ref. 2] and others [Ref. 3,4], the enhancement to heat transfer observed after adding fins is caused not only by the increased area but also by the thinning of condensate film due to surface-tension forces. The change in film thickness affects the resistance to heat transfer and therefore affects the overall heat-transfer coefficient. On the other hand, surface tension forces cause a thick condensate film to be present between the fins over the lower portion

of the tube. This tends to create a poorer performance on the lower portion of the tube. Despite this, finned tubes have been demonstrated to provide considerable enhancement over smooth tubes for various fluids, including steam [Refs. 2, 3, 5]. By considering the LMTD to be almost constant, Equation 1.1 clearly states that the optimum value for heat transfer occurs at the optimum value of the product of the surface area and the overall heat-transfer coefficient.

D. RESEARCH AT THE NAVAL POSTGRADUATE SCHOOL

A systematic study to determine the effects of fin parameters, such as fin spacing, height, and shape, tube diameter and vapor velocity on condensation heat-transfer enhancement, began in June 1982 with the building of a test apparatus. Krohn [Ref. 6] designed and built the experimental apparatus to study enhanced condensation heat transfer on horizontal tubes. His apparatus, as modified, is described in Chapter III of this thesis. Graber [Ref. 7] completed the instrumentation and calibration for the apparatus and took preliminary data on a smooth tube. The original smooth tube had thermocouples embedded in the tube wall to directly measure wall temperature. This tube was used to generate a correlation for the inside heat-transfer coefficient which, in turn, was used to infer the outside heat-transfer coefficient by subtracting the inside and wall resistances from the overall resistance (Equation 4.17). In December 1983, Poole [Ref. 8] demonstrated the use of the modified Wilson plot technique that compared favorably with the direct method involving wall temperature measurements. The modified Wilson plot technique is described in Chapter IV of this

thesis. Poole experienced difficulties in obtaining complete filmwise condensation on a copper tube with steam as a working fluid. He had partial success in obtaining filmwise condensation by oxidizing the tubes with a special solution consisting of equal amounts of sodium hydroxide and ethyl alcohol heated to about 80° C. The oxidation left a very thin coating on the tube with negligible thermal resistance. Although Poole had troubles in maintaining complete filmwise condensation, he concluded that the optimum spacing for steam condensation on a horizontal tube with rectangular fins is around 1.5 mm. Poole also found that the enhancement of the finned tube over the smooth tube was greater than the enhancement in surface area alone.

Georgiadis [Ref. 5], in September 1984, improved the tube cleaning and oxidizing procedures and verified the optimum fin spacing for steam as 1.5 mm for rectangular finned tubes with various fin thicknesses and heights. He found that the heat-transfer enhancement does not strongly depend on fin thickness, though a thickness of 0.75 to 1.0 mm thickness was slightly better than the average. Although increased fin height improved enhancement, increasing fin height above 1.0 mm increased the heat-transfer enhancement less than the percentage surface area gained. Flook [Ref. 9] tested tubes with triangular, trapezoidal, parabolic, and rectangular shape fins. The parabolic tubes had superior heat-transfer performance. Flook also tested for the effect of tube material and vapor velocity. He found that an increase in vapor velocity from 2 to 8 m/s increased the heat-transfer rates as much as ten percent. He compared the results of a stainless steel tube

with a copper tube and confirmed that materials with high thermal conductivities will enhance the heat-transfer performance.

In March 1986, Mitrou [Ref. 10] tested wire-wrapped tubes and tubes with rectangular, trapezoidal, triangular, and parabolic shape fins. The parabolic fins had the best heat-transfer performance. Mitrou confirmed the effects of thermal conductivity discussed by Flook by testing tubes made out of copper, aluminum, copper-nickel, and stainless steel. Cakan [Ref. 11], in December of 1986, continued testing with steam and attempted to improve the vapor-side heat-transfer coefficient by attaching a porous drainage strip to the underside of the finned tube. The drainage strip was designed to remove the thick condensate film on the lower portion of the tube and thus enhance the performance of the lower portion. Cakan found that the use of drainage strips significantly enhanced the vapor-side coefficient.

In June 1987, Zebrowski [Ref. 12] was the first student to test a fluid other than steam. R-113 was selected because of its low surface tension. Oxidizing the tube was not required to maintain complete filmwise condensation for R-113. Zebrowski's research resulted in an optimum fin spacing between 0.25 and 0.5 mm. He showed that the Beatty-Katz relationship for the outside heat-transfer coefficient agreed with his experimental results to within ±10 percent for interfin spacings greater than 1.0 mm. As the interfin spacing was decreased from 1.0 mm, the Beatty-Katz relationship overpredicted experimental results. Zebrowski concluded that this overprediction was caused by condensate retention on the lower portion of the tube.

Zebrowski also measured the local vapor-side heat transfer coefficient for two finned tubes. This was accomplished by systematically insulating the upper portions of the tube and using the modified Wilson plot technique. He found that the local enhancement at the top of the tube was approximately twice the average enhancement. Lester [Ref. 13], in September 1987, with steam as the working fluid, tested for the local vapor-side coefficient around a finned tube. As with Zebrowski, he concluded that at the top of the tube, the local coefficient was approximately twice the average value around the tube.

Table 1.1 shows a summary of the NPS research program. All of the previous research was for tubes with a root diameter of 19.05 mm. Since tube diameter may play a significant role in determining the condensate retention angle and heat and fluid flow processes, it is important that this aspect of the problem be studied. Also, a fluid with intermediate surface tension properties, such as ethylene glycol, should be tested to further study the effect of fluid properties on the condensation process.

E. OBJECTIVES

The main objectives of this thesis were:

1. to measure the effect of root diameter on the enhancement of finned tubes, and
2. to modify the apparatus to enable the use of ethylene glycol as a working fluid.

TABLE 1.1

SUMMARY OF NPS RESEARCH PROGRAM

DATE	STUDENT	FLUID	ACCOMPLISHMENTS
Jun 82	Krohn	–	• Designed and built the experimental apparatus to study enhanced condensation heat transfer on horizontal tubes.
Dec 82	Graber	Steam	• Completed instrumentation and calibration of apparatus. • Used smooth tube with embedded thermocouples to directly measure wall temperature.
Sep 84	Georgiadis	Steam	• Improved cleaning and oxidizing procedures. • Found optimum fin spacing for rectangular fin to be 1.5 mm. • Found heat-transfer enhancements do not strongly depend on fin thickness. • Found increasing fin height above 1.0 mm increased heat-transfer enhancements less than the percentage of surface area gained.
Dec 84	Flook	Steam	• Found parabolic finned tubes had superior performance to rectangular, trapezoidal, and triangular finned tubes. • Found a vapor velocity increase from 2 to 8 m/s can increase heat-transfer enhancement up to 10 percent. • Found materials with high thermal conductivity will enhance the heat-transfer performance.
Mar 86	Mitrou	Steam	• Tested wire-wrapped tubes. • Found parabolic fins had best heat-transfer performance

Dec 86	Cakan	Steam	• Found enhancement can be significantly improved by attaching a porous drainage strip on the underside of a finned tube.
Jun 87	Zebrowski	R-113	• Found the optimum fin spacing for R-113 to be between 0.25 and 0.5 mm. • Local enhancement at top of tube was approximately twice the average enhancement.
Sep 87	Lester	Steam	• Found local enhancement at top of tube was approximately twice the average enhancement.

II. LITERATURE SURVEY

A. INTRODUCTION

Until recently, the use of horizontal low integral-fin tubes for heat transfer with high surface tension working fluids (i.e., water) was considered impractical. A visual inspection of the of the horizontal tube revealed a thick film of retained condensate on the lower portion of the tube. Owing to this thick film, the heat-transfer performance in this lower portion of the tube was expected to be negligible. However, Wanniarachchi, et al. [Ref. 14] and Yau, et al. [Ref. 4] have shown considerable enhancements even for fully flooded tubes. Therefore, a complete understanding of the actual physical phenomena that take place in the flooded portion is essential in predicting the heat-transfer performance of finned tubes undergoing filmwise condensation.

B. CONDENSATE RETENTION ANGLE

The condensate retention angle has been defined as the angle measured from the bottom of a horizontal finned tube to a point around the tube circumference where the condensate film between fins abruptly thins. This angle is graphically depicted in Figure 2.1. Condensate retention angle is dependent on fluid properties and fin geometry.

Katz, et al. [Ref. 15] were the first to investigate the condensate retention angle and to develop an equation for predicting its behavior.

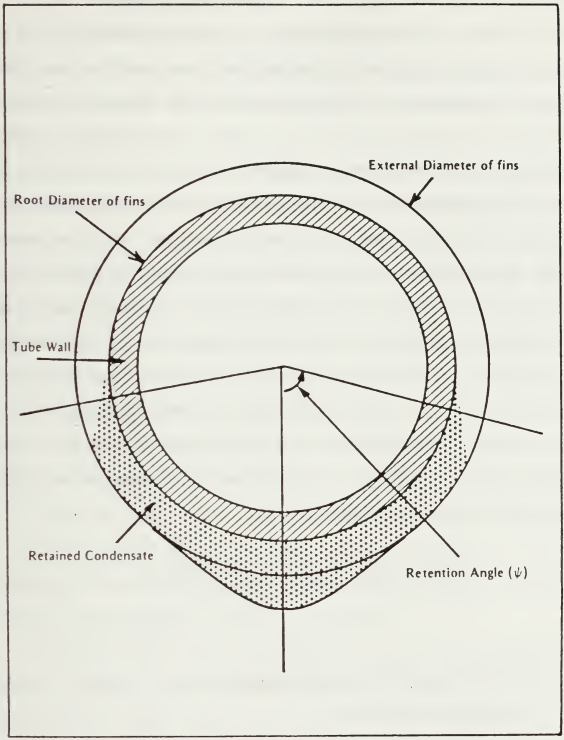

Figure 2.1 **Schematic of Condensate Retention Angle on Finned Tubes**

Their initial tests were conducted on two disks separated by a washer to simulate two adjacent fins. Later, tubes with fin densities of 276 to 984 fins per meter (fpm) and fin heights of 1.2 to 5.7 mm were tested. The amount of condensate retained on the tube and the retention angle were measured by weighing and by visual inspection with a cathetometer. The data were taken in a static condition (i.e., no condensation occurring) with water, aniline, acetone, and carbon tetrachloride. The surface tension for each of these fluids was measured by the pendant drop method and a capillary tube. Katz found that retention angle was dependent on fin geometry and fluid properties. The ratio of the surface tension to the difference of condensate and vapor densities was very significant and explained why retention angle varied from one fluid to another for a given tube. Since the vapor density is much smaller than the condensate density, it was ignored, thereby making the ratio of surface tension to condensate density the major contributor from the working fluid. Equation 2.1 shows the relationship developed by Katz, et al. [Ref. 15].

$$\frac{\Psi}{\sin\Psi} = \frac{\sigma}{\rho_l g}\left[\frac{4D_f - 2D_r - 2s}{\frac{\pi}{4}\left(D_f^2 - D_r^2\right)s}\right]\left(\frac{180}{980}\right), \qquad (2.1)$$

where

Ψ = condensate retention angle (degrees),

σ = surface tension (N/m),

g = gravitational constant (9.806 m/s^2),

ρ_l = condensate density (kg/m^3),

D_r = root diameter (m),

D_f = fin diameter (m), and

s = interfin spacing for rectangular fin(m).

This equation shows that, keeping the fin height and spacing constant, an increase in root diameter would result in a decrease in condensate retention angle.

Until an investigation by Rudy and Webb [Ref. 16] in 1981, the retention angle had been determined only under static conditions. Rudy and Webb measured liquid retention angles by visual sighting through a cathetometer. They measured the retention angle for water, R-11, and n-pentane under static conditions and their results compared favorably with the model developed by Katz, et al. (Equation 2.1). The retention angles for R-11 and n-pentane were also measured under dynamic conditions. Integral-fin tubes with 748, 1024, 1378 fpm, a "Thermoexcel-C"tube with 1429 fpm, and a pin-fin tube with 1378 fpm were examined under static and dynamic conditions. They confirmed the Katz, et al. [Ref. 15] conclusion that retention angle increased with the ratio of surface tension to condensate density, and concluded that the condensate retention angle was not significantly different under dynamic and static conditions.

In 1982, Rifert [Ref. 17] developed an equation to predict condensate retention angle by modeling the rise height between fins to capillary rise height along vertical plates. Again, retention angle was strongly influenced by the ratio of surface tension to condensate density. Equation 2.2, developed by Rifert, demonstrates that an

increase in root diameter will decrease the condensate retention angle

$$\Psi = \cos^{-1}\left[1 - \frac{2\sigma(P_w - p)}{\rho_l g D_f A_p}\right], \qquad (2.2)$$

where

A_p = profile area of fin (m^2),

P_w = wetted perimeter (m), and

p = fin pitch (m).

Rudy and Webb [Ref. 18] developed a general equation to predict retention angle for finned tubes of various fin geometries. Their working fluids of water, R-11, n-pentane, and acetone were used with finned tubes having fin densities of 748 to 1417 fpm. Their static test consisted of a finned tube being placed in a shallow pool of working fluid. The rise height of the working fluid in the interfin spaces was compared to an unrolled tube of the same fin geometry. The unrolled tube was fabricated by slicing a tube section and carefully peeling the tube open into a flat plate. The rise heights were the same. When the finned tube and the unrolled tube were removed from the shallow pool, the rise heights remained unchanged. From these observations, Rudy and Webb deduced that the retention angle was caused by a balance of surface tension forces and the weight of condensate. A simple force balance on the retained condensate led to the following equation:

$$\Psi = \cos^{-1}\left[1 - \frac{2\sigma(2e - t)}{D_f \rho_l g e s}\right], \qquad (2.3)$$

where

e = fin height (m), and

t = fin thickness for rectangular fin (m).

Rudy and Webb found that Equation 2.3 predicted condensate retention angle to within ±10 percent. Again, increasing the root diameter would lower the condensate retention angle.

Honda, et al. [Ref. 19] did a photographic study on dynamic and static condensate retention angles for methanol and R-113. They confirmed the conclusion of Rudy and Webb that static and dynamic retention angles were approximately the same. They experimented on finned tubes with and without porous drainage strips. Their measurements with no strips were in agreement with previous experimental data, and they developed the following equation:

$$\Psi = \cos^{-1}\left[1 - \frac{4\sigma\cos\beta}{D_f \rho_l g s}\right], \qquad (2.4)$$

where

β = fin-tip half angle.

In 1985, Rudy and Webb [Ref. 20] extended their prediction of condensate retention angle for various fin geometries by modifying Equation 2.3. They tested finned tubes with fin densities of 748 to 1378 fpm, one spine fin tube with 1378 fpm, and a "Thermoexcel-C" tube. They used R-11, water, and n-pentane as the working fluids. Again, Rudy and Webb concluded that the retention angle increases with the ratio of surface tension to condensate density and fin height

but decreases as tube diameter increases. They developed the following expression for a trapezoidal shape fin shown in Figure 2.2.

$$\Psi = \cos^{-1}\left[1 - \frac{2\sigma(t_t + 2e - t_b)}{D_f \rho_l g(t_t e - s_b e - e t_b)}\right], \qquad (2.5)$$

where

t_t = fin thickness at tip (m),

t_b = fin thickness at base (m), and

s_b = interfin spacing at base (m).

For a rectangular-shape fin, Equation 2.5 reduces to the following:

$$\Psi = \cos^{-1}\left[1 - \frac{4\sigma}{D_f \rho_l g s}\right], \qquad (2.6)$$

This equation is identical to Equation 2.4 of Honda when $\beta = 0$ degrees.

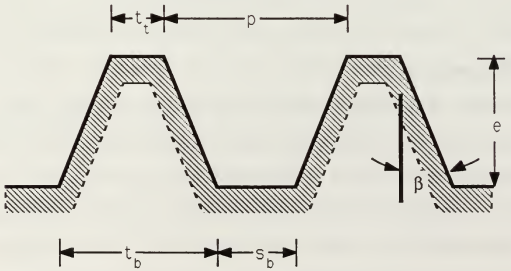

Figure 2.2 **Trapezoidal Fin Used by Rudy and Webb** [Ref. 20]

Once again, Equations 2.5 and 2.6 predict that condensate retention angle will decrease with increasing tube diameter. Rudy and Webb completed static retention angle tests on 19 mm and 25 mm diameter tubes with fin densities of 1024 fpm. They observed that the rise heights were equal and therefore the larger-diameter tube retained less condensate and had a smaller retention angle.

Masuda and Rose [Ref. 21] found that condensate was retained not only in the flooded portion of the tube. Their photographic study revealed that condensate was also retained at the base of the fin in the upper portion of the tube usually referred to as the unflooded portion. The film thickness around the base decreased with circumferential position around the tube. They therefore postulated that more surface area of the finned tube was insulated by the condensate than previously expected. Masuda and Rose [Ref. 21] concentrated their research on the profile of the condensate in the interfin spacing. They defined four separate retention conditions based on the meniscus profile in the interfin spaces and along the sides of the fin. These retention conditions are listed below and shown pictorially in Figure 2.3.

1. "...the interfin space is just filled by the meniscus but the fin flanks are not wholly wetted." [Ref. 21] (Figure 2.3 b(2))

2. "...where the whole of the flank is just wetted and for which the liquid film at the center of the interfin spacing has finite thickness." [Ref. 21] (Figure 2.3 b(3), defined as fully flooded)

3. "...when the fin flank is just completely wetted but the interfin space is not wholly wetted." [Ref. 21] (Figure 2.3 c(2))

4. "...the whole of the interfin space is just wetted and for which the contact angle at the fin tip is non-zero." [Ref. 21] (Figure 2.3 c(3))

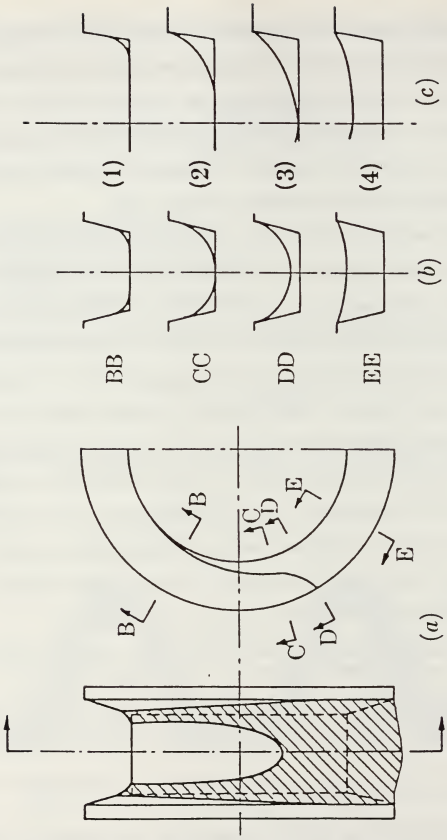

Figure 2.3 **Flooding Conditions Proposed by Masuda and Rose** [Ref. 21]

Masuda and Rose developed separate expressions for each listed flooding condition. Condition three was considered the fully flooded condition and, in this situation, their expression reduces to Equation 2.6 for rectangular fins.

Honda, et al. [Ref. 22], in 1987, developed two equations for the prediction of condensate retention angle. One expression for retention angle was used when the fin spacing exceeded twice the fin height and the other when the fin spacing was less than twice the fin height. The latter case, for rectangular finned tubes, reduces to Equation 2.6.

C. HEAT-TRANSFER PERFORMANCE ON FINNED TUBES

In 1948, Beatty and Katz [Ref. 23] were the first to develop a model to predict the outside condensing heat-transfer coefficient for a horizontal finned tube. They divided the finned tube into two geometric regions. The fin flank was considered to be a vertical plate and the interfin spacing to be a smooth horizontal tube. By combining the equations of Nusselt for vertical plates and smooth horizontal tubes, Beatty and Katz expressed the outside heat-transfer coefficient as shown in Equation 2.7.

$$h_{BK} = 0.689F^{0.25}\left[\frac{A_r}{A_o}\left(\frac{1}{D_r^{0.25}}\right) + 1.3\eta_f\frac{A_f}{A_o}\frac{1}{L^{0.25}}\right], \qquad (2.7)$$

where

$$F = \left[\frac{k_l^3\rho_l g h_{fg}}{\mu_l \Delta T_{vs}}\right], \qquad (2.8)$$

and

$$L_e = \pi \left[\frac{D_f^2 - D_r^2}{4 D_f} \right] \tag{2.9}$$

h_{BK} = Beatty-Katz outside heat-transfer coefficient($W/m^2 \cdot K$),

h_{fg} = specific enthalpy of vaporization (J/kg),

k_l = condensate thermal conductivity ($W/m \cdot K$),

μ_l = condensate dynamic viscosity (kg/m·s),

η_f = fin efficiency,

ΔT_{vs} = temperature drop across the condensate film (K),

A_r = surface area of smooth tube (m^2),

A_f = surface area of fin (m^2), and

A_o = total external surface area, $A_r + \eta_f A_f$, (m^2).

The coefficient of 0.689 is five percent less than the expected value of 0.728 from the Nusselt equation for a smooth horizontal tube. This coefficient resulted from tests carried out on six single horizontal finned tubes. These tubes had fin densities of up to 630 fpm. Their working fluids included methyl chloride, sulfur dioxide, refrigerant-22, propane, n-butane, and n-pentane. Surface tension for these fluids varied from 0.005 to 0.025 N/m. They found that the computed results from Equation 2.7 and experimental data agreed within ten percent. Notice that Equation 2.7 shows that the heat-transfer coefficient decreases with increasing tube diameter.

Although the use of Nusselt's equations was ingenious, those equations forced Beatty and Katz to apply Nusselt's assumptions to

their model. The most important assumption was that gravity forces alone controlled condensate drainage. No surface tension forces existed and no condensate was retained between fins. Because Beatty and Katz [Ref. 23] only tested tubes with low fin densities and used relatively low surface tension working fluids, their equation seemed promising. Rudy and Webb [Ref. 16] found that the Beatty and Katz model overpredicted the results for fluids with a higher surface tension to condensate density ratio. They attempted to use the Beatty and Katz relationship for only the unflooded region, which led to Equation 2.10.

$$h^{\cdot}_{BK} = \left(\frac{180 - \Psi}{180}\right) h_{BK} \,. \tag{2.10}$$

where h_{BK} is given by Equation 2.7 and

$h^{\cdot}_{BK}$ = modified Beatty-Katz condensing coefficient ($W/m^2 \cdot K$).

This was the first research to include the effect of condensate retention in heat transfer. They reasoned that surface tension forces caused the retention of the condensate on the lower portion of the tube to act as an insulator. This equation resulted in 10- to 50-percent underpredictions for R-11, n-pentane, and water.

Owen, et al. [Ref. 24], in 1983, concluded that the margin of error in the Rudy and Webb Equation resulted from the assumption of no heat transfer in the flooded region. Therefore, to improve this model, Owen, et al. allowed for one-dimensional heat conduction through the fins and condensate film in the flooded region. The condensate thickness was presumed to be equal to the fin height in the flooded region.

This model, however, showed only a slight improvement over the Rudy and Webb model.

It became apparent that condensation on a finned tube was a very complex phenomenon with a number of controlling parameters not considered in previous models. Variables not considered were three-dimensional condensate flow, surface tension forces, wall conduction effects, condensate film thickness variations, and vapor velocities [Ref. 25]. Previous models considered only the insulating effect of the condensate film in the flooded region. Gregorig [Ref. 26], as early as in 1954, proved that surface tension also produces pressure gradients that thin the condensate film around the fin tips and along the fin sides.

In 1987, Webb, et al. [Ref. 27] re-examined the Beatty-Katz model and pointed out that on finned tubes surface tension, not gravity, was the prime mover of condensate. Therefore, the Nusselt analysis was not valid for finned tubes. They therefore divided the finned tube into two regions: the flooded and the unflooded portions. Equation 2.11 was used to compute the average outside heat-transfer coefficient

$$h\eta = \left(\frac{180-\Psi}{180}\right)\left[h_h \frac{A_r}{A} + h_f \eta_f \frac{A_f}{A}\right] + \left(\frac{\Psi}{180}\right) h_b \,, \qquad (2.11)$$

where

h = condensing coefficient based on A_{df} ($W/m^2 \cdot K$),

h_f = condensing coefficient of the fin ($W/m^2 \cdot K$),

h_h = condensing coefficient for smooth horizontal tube ($W/m^2 \cdot K$),

h_b = condensing coefficient for flooded portion ($W/m^2 \cdot K$),

A_{df} $= \pi D_f L$ (m^2),

L = length of tube (m), and

η = surface efficiency, $(1 - (1 - \eta_f) A_r/(A_r+A_f))$.

The condensing coefficient for the fin (h_f) was determined by assuming that surface tension forces induced pressure gradients along the condensate film surface. They assumed a linear pressure gradient from fin tip to fin root. A heat balance on the condensate yielded the average heat-transfer coefficient for the fin. To compute the heat-transfer coefficient for the horizontal smooth tube portion (h_h) in the interfin spaces, an iterative process which would take into account the additional condensate from the fin flanks was used. The condensing coefficient in the flooded region (h_b) was derived by use of two-dimensional conduction of the fin-condensate composite structure. They found that in the flooded region, the heat-transfer rate only accounted for 0.2 percent of the total rate for R-11. For steam with a retention angle of 54 degrees, the heat transfer rate in the flooded region was only 1.6 percent of the total rate. These results suggested that the flooded portion of the tube could be practically ignored. Notice that these calculated results are in disagreement with the experimentally observed results mentioned earlier that even fully flooded tubes gave considerable enhancements. Therefore, it is possible that actual processes with fully flooded tubes are far more complex than can be explained by one- or two-dimensional heat conduction alone. By ignoring the heat transfer in the flooded portion, Webb, et al. [Ref. 27] pointed out the importance of the retention angle. By

decreasing the retention angle, the heat transfer would significantly increase as shown by Equation 2.11. With this model, Webb, et al. [Ref. 27] found that experimental and theoretical results for R-11 agreed to within ±25 percent. Disappointed with these results, Webb, et al. [Ref. 27] used the theory of Adamek [Ref. 28] to predict a new value for the condensing coefficient on the unflooded fin flanks. This latter method provided results within ±20 percent of their experimental data for R-11.

In 1987, Honda, et al. [Ref. 29] introduced a prediction model that accounted for surface-tension-induced pressure gradients, condensate retention angle, heat transfer through the flooded region, and fin geometry. The tube was divided into flooded and unflooded regions and the average Nusselt number and wall temperature were computed for each region.

$$Nu_d = \left[\frac{Nu_{du}\,\eta_u(1-\tilde{T}_{wu})(1-\Psi) + Nu_{df}\,\eta_f(1-\tilde{T}_{wf})\Psi}{(1-\tilde{T}_{wu})(1-\Psi)+(1-\tilde{T}_{wf})\Psi} \right], \qquad (2.12)$$

where the dimensionless temperature ($\tilde{T}$) and retention angle (Ψ) were expressed as:

$$\tilde{T} = \left[\frac{T - T_c}{T_s - T_c} \right], \qquad (2.13)$$

and

$$\Psi = \frac{\psi}{180} \qquad (2.14)$$

Nu_d = average Nusselt number for finned tube,

Nu_{du} = average Nusselt number for unflooded portion,

Nu_{df} = average Nusselt number for flooded portion,

T_c = average coolant temperature,

T_s = saturation temperature,

$\hat{T}_{wd}$ = dimensionless average wall temperature for flooded portion, and

$\hat{T}_{wu}$ = dimensionless average wall temperature for unflooded portion.

Equation 2.6 was used to solve for the condensate retention angle. In Equation 2.12, the retention angle plays a significant role in determining the heat transfer. The average Nusselt numbers were used in Equation 2.12 because Honda, et al. [Ref. 29] allowed the surface-tension-induced pressure gradients to change around the circumference of the tube. A ±20 percent error was found between this model and experimental results for 22 tubes and 11 fluids. Marto, et al. [Ref. 30] compared this model with their R-113 experimental results and found the model to be generally conservative with a ±20 percent error. The model did underpredict for very small fin spacings.

D. SUMMARY

From these previous findings, it is apparent that the condensate retention angle can be easily predicted. Equation 2.6 is the generally accepted expression for condensate retention angle. From this equation, it is easily seen that an increase in the tube root diameter will decrease the condensate retention angle. Although a great deal of

effort has been applied to develop an accurate heat-transfer prediction model, one does not exist. Marto, et al. [Ref. 30] found that the Honda, et al. [Ref. 29] model appears to be the best, showing an agreement to within ±20 percent of the experimental data. This percent error was far better over the entire range of fin spacings tested than obtained with the Webb, et al. [Ref. 27] and the Beatty-Katz [Ref. 23] models.

III. APPARATUS AND TUBES TESTED

A. DESCRIPTION OF APPARATUS

The test apparatus, as shown in Figure 3.1, consisted of a boiler, a test section, glass piping, and an auxiliary condenser with a purging system to remove non-condensing gases. The boiler was fabricated from a 0.3048 m (12 inch) diameter Pyrex glass section with ten 4-kW, 440-V, Watlow immersion heaters. Vapor flowed upward from the boiler into a 2.44 m-long section of 152 mm-diameter glass piping before making a 180-degree turn toward the test section 1.52 m below. The test section (see Figure 3.2) was fabricated from stainless steel with nylon and Teflon fittings to support the test tube and to connect cooling water. Cooling water to the test tube was pumped from a water sump and was varied by a throttle valve at the inlet of a flowmeter. A continuous flow of tap water was supplied to the water sump. A thermocouple, placed just above the test tube, and a manometer provided accurate vapor temperature and pressure readings, respectively. A view port in the test section allowed the condensation process to be observed and photographed. The auxiliary condenser consisted of a copper coil within Pyrex glass piping. Cooling water supply was tap water that was controlled by a throttle valve at the inlet of a flowmeter. Modifications made to the auxiliary condenser are discussed later in this chapter.

Figure 3.1 **Schematic of Test Apparatus**

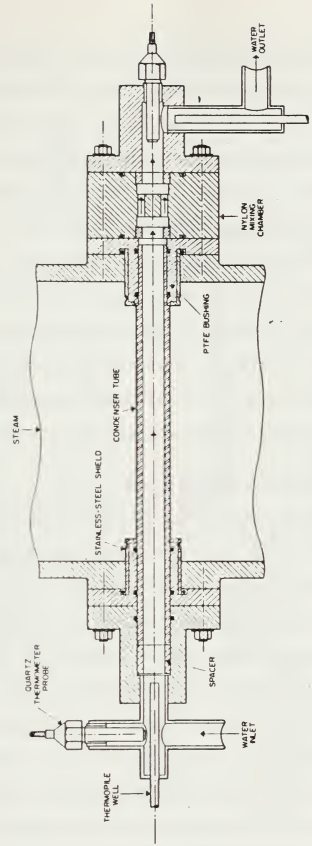

Figure 3.2 **Schematic of Test Section (Insert Removed)**

The purging system consisted of copper tubing, a small copper coil, a Plexiglas cylinder, and a vacuum pump. Gases drawn by the pump left the secondary condenser via the copper tubing and flowed into the copper coil. This coil was located in the water sump that provided cooling water to the test tube. The heat exchange in the coil condensed any residual working fluid vapor. The non-condensing gases and residual working fluid were collected in a small cylinder in the water sump. The liquid collected at the bottom of the cylinder was drained at the end of the data run. The non-condensing gases (usually air) were suctioned to the top of the container and drawn into the pump suction (Figure 3.3). A more detailed description of the apparatus has been provided in the references [Refs. 5, 8, 9, 11, 13].

B. MODIFICATIONS TO APPARATUS

Modifications were made to the original apparatus to improve system integrity and to meet the objectives of this thesis. Prior to these modifications, cooling water to the secondary condenser was contained in two helically wound coils made of 3/8-inch copper tubing. A 4-inch coil was located inside a 5 1/2-inch coil. Each coil was 18 inches in length. Preliminary tests with ethylene glycol at a saturation temperature of 128° C indicated that the water flow rate through these coils was not large enough. When proper water flow rate was provided to achieve a desired system pressure, slugs of liquid and steam were observed to be flowing out of the cooling coils, indicating that boiling of the water was occurring. The steam produced created

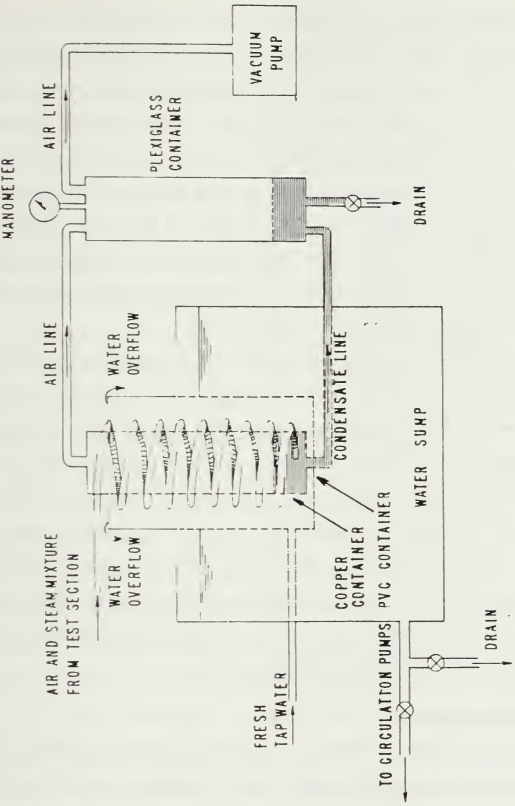

Figure 3.3 **Schematic of Vacuum System and Cooling Water Sump**

vapor-blocking inside the tubes, thus almost stopping the water flow intermittently. When this occurred, the system pressure started to increase. Once the tube was entirely blanketed with vapor, water rushed again, providing cooling. This cycle repeated while the system pressure experienced uncontrollable fluctuations. To avoid this problem, a new 5-inch diameter helical coil was therefore fabricated from 5/8-inch copper tubing. The new coil was 18 inches in length and tested satisfactorily for all three working fluids. The larger inner diameter of this tube was adequate in preventing any vapor blocking by allowing a larger cooling water mass flow rate.

Since the new configuration called for a single coil over two, a new base plate for the secondary condenser was needed. The fitting for the gravity drain condensate return line was 1/2 inch vice the 1-inch fitting out of the dual coil base plate. A single 1/2-inch stainless steel tube with a 90 degree bend was used for the drain line. Previously, the old drain line reduced from 1 inch to 1/2 inch by using two reducing fittings. This drain line was a constant source of vacuum leaks and its location in the system made repairs very difficult. The installation of the single 1/2-inch line improved system integrity by eliminating a possible source of vacuum leaks.

C. TUBES TESTED

One smooth tube, 18 tubes having rectangular section fins, and a special tube identical to the one used by Masuda, et al. [Ref. 3] of Queen Mary College, University of London, were to be tested with steam, R-113, and ethylene glycol as the working fluids. All tubes were

made of copper and the 18 finned tubes consisted of three families having different tube root diameters. The tube diameter was the characteristic common to each family. The tubes with the 12.7 mm diameter (also referred to as root diameter) were considered the small tubes, while the 19.05 mm and the 25 mm were medium and large tubes, respectively. Each tube matched one other tube in a different family with all geometric parameters, with the exception of the diameter. All tubes had a fin height of 1.0 mm and a fin thickness of 1.0 mm. The comparison tube will be referred to as the QMC tube. Tube parameters are listed in Table 3.1. Figure 3.4 shows a photograph of the small-diameter tube family. Figure 3.5 shows a photograph of tubes with a 1.5 mm fin spacing, while Figure 3.6 shows a photograph of the inserts used during this investigation.

Various problems were encountered while testing and will be discussed in Chapter V. Only preliminary data were taken for the small and QMC tube using ethylene glycol. After completing R-113 and ethylene glycol data, tube 10 was mistakenly modified by blasting its surface with glass beads in an attempt to remove the oxide film. Close inspection of the tube surface area revealed that the local geometry around the tips of the fins had been significantly altered. Therefore, a tube of the same dimensions was produced to replace tube 10. However, the new tube was manufactured at the NPS machine shop and its copper surface was slightly different than the original tube that was commercially manufactured.

TABLE 3.1

DIMENSIONS OF TUBES TESTED

Tube	D_r (mm)	D_i (mm)	s (mm)	t (mm)	e (mm)
Smooth tube					
1	19.05[a]	12.7	-	-	-
Small tubes					
2	12.7	9.53	0.25	1.0	1.0
3	12.7	9.53	0.5	1.0	1.0
4	12.7	9.53	1.0	1.0	1.0
5	12.7	9.53	1.5	1.0	1.0
6	12.7	9.53	2.0	1.0	1.0
7	12.7	9.53	4.0	1.0	1.0
Medium tubes					
8	19.05	12.7	0.25	1.0	1.0
9	19.05	12.7	0.5	1.0	1.0
10	19.05[b]	12.7	1.0	1.0	1.0
11	19.05	12.7	1.5	1.0	1.0
12	19.05	12.7	2.0	1.0	1.0
13	19.05	12.7	4.0	1.0	1.0
Large tubes					
14	25.0	12.7	0.25	1.0	1.0
15	25.0	12.7	0.5	1.0	1.0
16	25.0	12.7	1.0	1.0	1.0
17	25.0	12.7	1.5	1.0	1.0
18	25.0	12.7	2.0	1.0	1.0
19	25.0	12.7	4.0	1.0	1.0
GMC tube					
20	12.7	9.53	1	0.5	1.59

[a] Dr = Do for smooth tube
[b] Glass beaded tube

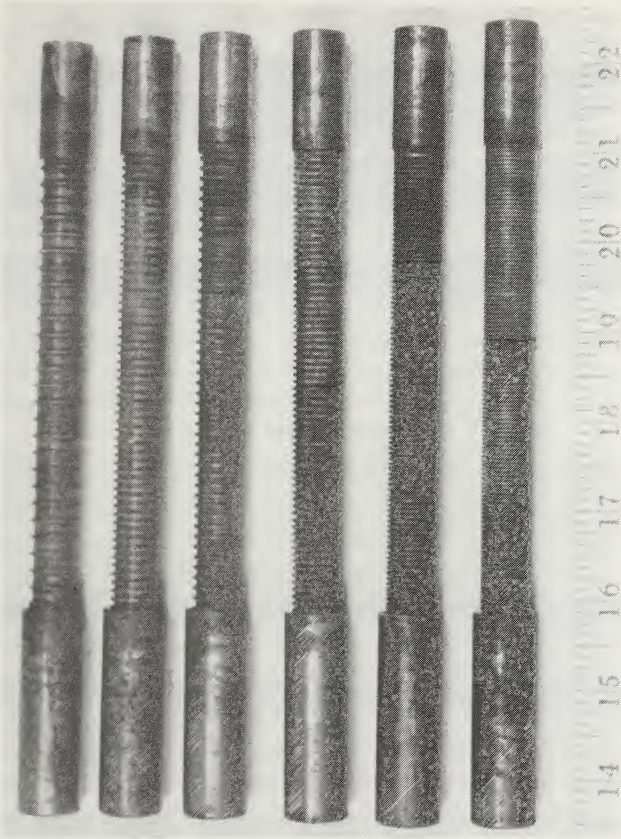

Figure 3.4 **Photograph of Small-Diameter Tube Family**

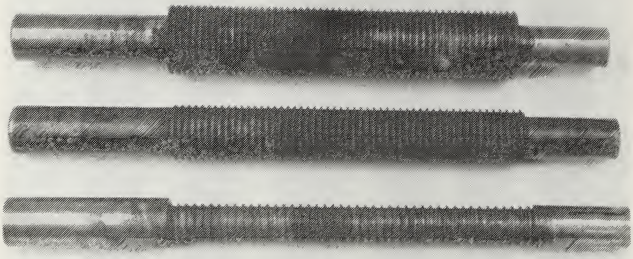

Figure 3.5 **Photograph of Tubes With 1.5 mm Spacing**

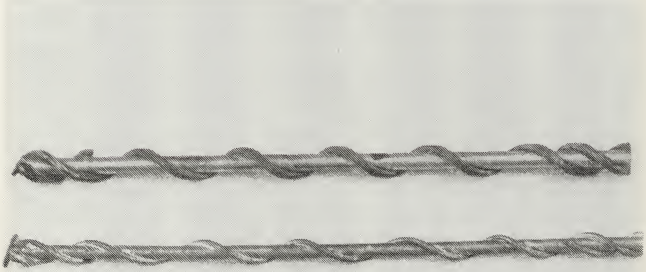

Figure 3.6 **Photograph of Inserts**

D. SYSTEM INTEGRITY

After completing the modifications to the apparatus, it was important to verify system integrity prior to taking data. System integrity is a term used to describe the air tightness of the closed-loop apparatus. For approximately three months, the system had remained idle prior to this research. For this reason, all the rubber gaskets were replaced. A vacuum test was conducted by using the vacuum system to bring the pressure in the apparatus down to approximately 20 mm of mercury. The apparatus was secured and the vacuum pump turned off. If the manometer indicated that the apparatus had maintained a vacuum within 2 mm in a 24-hour period, system integrity was considered good. This test was repeated between data runs at least once a week.

Initially, many leaks in the apparatus were found around the fittings of the condensate drain lines. Three valves and a second gasket were replaced. Some leaks were located by placing the system under vacuum to draw in Freon gases. Once the Freon gases were in the apparatus, nitrogen gas was used to slightly pressurize the apparatus. A Freon detector was then slowly moved around the outside of the apparatus to detect leaks. This method was successful in finding the last few leaks.

The presence of non-condensing gases during data taking was a good indication of a vacuum leak. The data reduction program would ask the operator if non-condensing gas concentration needed to be checked. The check compared the actual vapor temperature measured

by the thermocouple in the vapor space upstream of the test tube to the calculated saturation temperature for the apparatus pressure. Non-condensing gases were checked prior to the first data set accepted and the last data set accepted. If the check prior to the last data set showed the presence of non-condensing gases, the entire data run was discarded. A vacuum test was conducted after non-condensing gases were detected or if the data were suspect. Most vacuum leaks were caused by a bad gasket or valve on the secondary condenser or by the vacuum system being inadvertently left open.

IV. EXPERIMENTAL AND DATA REDUCTION PROCEDURES

A. EXPERIMENTAL PROCEDURES

Prior to testing, a soft brush and tap water were used to clean the interior and exterior of each tube. Distilled water was used for the final rinse. As proven by Zebrowski [Ref. 12], while testing R-113, an oxidizing coating was not needed to assure filmwise condensation. A preliminary test with ethylene glycol indicated that there was no difference between the results with and without a coating. For this reason, it was determined that the oxidizing coating was not required for filmwise condensation with ethylene glycol.

When the working fluid was steam, the tube had to be coated with a thin oxidation layer with negligible thermal resistance to ensure filmwise condensation. Equal volumes of sodium hydroxide and ethyl alcohol were mixed and heated to about 80° C to make an oxidizing solution. This solution was applied while the tube was suspended above a pool of boiling water. To establish a coating, this oxidizing solution was applied every ten minutes for one hour. When retesting a tube, the solution was applied every five minutes for 20 minutes. Once a tube was coated, it was rinsed with distilled water. Also, with steam, an insert was placed in the tube to enhance the internal heat-transfer coefficient. The reason for this procedure is explained later in this chapter. The insert was placed in the same position for every tube (see

Figure 3.6) Since the large- and medium-diameter tubes had the same inside diameter, the same insert was placed in them.

When the tube was ready for testing, it was installed in the test section. Installation took approximately five minutes. The tap water supply to the water sump was opened and the pumps were started. An initial flow rate of 20 percent was set and a visual inspection for leaks at the fittings was conducted. The boiler control panel was energized and the system was brought up to operating temperature by adjusting the boiler input power, adjusting cooling water flow to the secondary condenser, and operating the vacuum system. The procedures for placing this system in operation were outlined by Poole [Ref. 8].

The removal of non-condensing gases was vital to ensure reliable and consistent results. The Gibbs-Dalton ideal gas mixture relations, together with the measured vapor temperature and the temperature corresponding to the measured pressure, were used to compute the non-condensing gas (believed to be air) concentration. The computed non-condensing gas molar concentrations were found to be ±0.5 percent. This reveals a non-condensing gas concentration which is zero to within the accuracy of the measurements. Once a tube had been installed in the apparatus, the purge system was operated successfully to remove all non-condensing gases before storing any data. When testing with steam, the vacuum system was in operation with the inlet valve opened fully for low pressure and opened slightly for atmospheric pressure. Georgiadis [Ref. 5] found that operating the vacuum

pump did not alter experimental results but maintained filmwise condensation conditions longer.

The output of the vapor thermocouple, which was continuously displayed on the voltmeter, was used in obtaining and maintaining the system temperature (hence pressure). Once the operating temperature was established, sample data were taken to check for non-condensing gases and desired vapor velocity. For example, if the vapor velocity was below the desired value, the boiler power and the flow to the secondary condenser cooling water were increased. Table 4.1 shows a list of operating conditions for each fluid.

TABLE 4.1

OPERATING CONDITIONS

Fluid	Thermocouple (microvolts)	Temperature (°C)	Pressure (mm Hg)
R-113	1977	48	765
Steam	1977	48	85
Steam	4280	100	765
Ethylene Glycol	5400	128	62

For each data run, the steady-state condition was maintained for about 30 minutes before any taking of data. At each data point, the test-tube cooling water flow rate was manually entered. When R-113 was the working fluid, data were taken at cooling water velocities given by 20, 26, 35, 45, 54, 62, 70, 80, and 20 percent flow rates. For these tubes, the 80 percent flow rate resulted in a cooling water velocity of about 4.4 m/s. The same data points were taken for the

medium- and large-diameter tubes using steam as the working fluid. The insert in the small-diameter tube would not allow flow rates above 70 percent; therefore, for this tube with steam, the flow rates were adjusted to 20, 26, 33, 40, 47, 54, 61, 66, and 20 percent. The 66 percent flow rate resulted in a 6.5 m/s water velocity through the tubes. The coolant temperature rise decreases with increasing water velocity, thus increasing the uncertainties associated with this temperature measurement.

Preliminary tests with ethylene glycol indicated that sub-cooled boiling was occurring inside the tube. An attempt was made to lower the operating pressure of the system to decrease the vapor temperature. However, at very low operating pressures, the boiling of the ethylene glycol was very explosive and the system pressure fluctuations were excessive so that the operation was considered unsafe. A combination of decreasing operating pressure and using larger flow rates through the test tube was used to prevent the internal boiling. The operating pressure was lowered to 62.2 mm Hg, which resulted in a saturation temperature of 128° C. At this set point, the system still had small fluctuations in pressure due to some explosive boiling. The flow rates used for ethylene glycol were 30, 38, 45, 52, 60, 65, 70, 80, and 30 percent. The small-diameter tubes did not have sufficient cooling water capacity to prevent cooling water from boiling and therefore were not tested. Again, the coolant temperature rise decreases with increasing water velocity, thus increasing the uncertainties associated with this temperature measurement. Therefore,

owing to the larger velocities involved, the data for ethylene glycol are expected to be less reliable than for the other two fluids.

B. DATA REDUCTION PROCEDURES

1. Background

The total resistance to heat transfer from the vapor to the tube cooling water consists of the sum of the vapor-side, wall, and inside resistances, as shown in Figure 4.2.

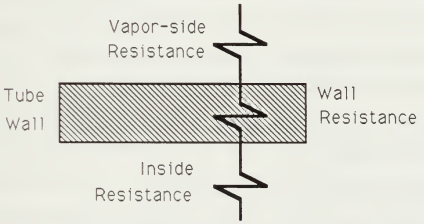

Figure 4.1 **Resistance to Heat Transfer**

The vapor-side and inside resistances were convective in nature, and therefore the resistances could be expressed by the reciprocal of the respective heat-transfer coefficient and surface area product.

$$R_i = \frac{1}{h_i A_i} , \tag{4.1}$$

and

$$R_v = \frac{1}{h_o A_o} , \tag{4.2}$$

where

$$A_i = \pi D_i (L + L_1 \eta_1 + L_2 \eta_2) , \tag{4.3}$$

and

$$A_o = \pi D_r L , \tag{4.4}$$

D_r = root diameter (m)

R_i = inside resistance ($m^2 \cdot K/W$),

R_v = vapor-side resistance ($m^2 \cdot K/W$),

h_i = inside heat-transfer coefficient ($W/m^2 \cdot K$),

h_o = outside heat-transfer coefficient ($W/m^2 \cdot K$),

A_i = effective inside area (m^2)[1],

A = outside area (m^2),

L = length of exposed tube (133 mm),

L_1 = length of inlet portion of tube in nylon bushing (m),

L_2 = length of outlet portion of tube in nylon bushing (m),

η_1 = fin efficiency for inlet portion of tube,

η_2 = fin efficiency for outlet portion of tube.

The wall resistance was easily computed from the thermal conductivity of copper and the inside and outside diameters.

---

[1]The axial heat conduction into the inlet and outlet insulated portions of the tube were accounted for by computing the associated fin efficiencies. For this purpose, the extended-fin assumption was used.

$$R_w = D_r \frac{\ln \frac{D_r}{D_i}}{2k_m}, \qquad (4.5)$$

R_w = wall resistance ($m^2 \cdot K/W$),

k_m = thermal conductivity of copper ($W/m \cdot K$).

This equation assumes that the heat flux was radial through the tube walls.

Combining Equations 4.1, 4.2, and 4.5, the overall thermal resistance can be expressed as:

$$\frac{1}{U_o A_o} = \frac{1}{h_o A_o} + \frac{1}{h_i A_i} + \frac{R_w}{A_o} \qquad (4.6)$$

In order to compute the overall heat-transfer coefficient, the heat-transfer rate must be found. The heat-transfer rate may be computed by measuring the inlet and outlet test tube cooling water temperatures and computing the properties of the cooling water at its average temperature. The test tube cooling water inlet and outlet temperatures were measured by quartz thermometers and a ten-junction thermopile. The quartz thermometer readings were used in the computation of the log-mean-temperature difference (Equation 1.2) and in the heat-transfer rate below:

$$Q = \dot{m} c_p \Delta T, \qquad (4.7)$$

where

$$\dot{m} = \rho_c A_c v, \tag{4.8}$$

$\dot{m}$ = mass flow rate (kg/s),

c_p = specific heat at constant pressure (J/kg · K),

ΔT = cooling water temperature rise (K),

ρ_c = test tube bulk cooling water density (kg/m^3),

A_c = cross-sectional area of test tube (m^2),

v = test tube average cooling water velocity (m/s).

Once the heat transfer rate is determined by Equation 4.7, the value can be substituted into Equation 1.2 to determine the overall heat-transfer coefficient. The determination of the inside and outside coefficients are the only two values still unknown in Equation 4.6.

2. Modified Wilson Plot Technique

In general, the outside resistance should be minimized if the measurements are performed only for the inside. Similarly, the inside resistance should be minimized if the primary concern is the outside heat-transfer coefficient. However, the modified Wilson plot technique provides both inside and outside coefficients simultaneously. With this method, in order to maximize accuracy, the inside and outside resistances should be made as equal as possible. Therefore, it was necessary to use an insert to boost the inside coefficient when steam was the working fluid.

The modified Wilson plot technique requires that the form of both inside and outside coefficients be known. During this study,

Sieder-Tate-type and Nusselt-type equations were used to represent the inside and outside, respectively.

$$h_i = C_i \frac{k_c}{D_i} Re^{0.8} Pr^{0.333} \left(\frac{\mu_c}{\mu_w}\right)^{0.14} = C_i \Omega , \qquad (4.9)$$

where

k_c = thermal conductivity of cooling water (W/m · K),

C_i = Sieder-Tate-type coefficient,

Re = Reynolds number,

Pr = Prandtl number,

μ_c = dynamic viscosity of cooling water at bulk temperature ($N \cdot s/m^2$),

μ_w = dynamic viscosity cooling water at inner wall temperature ($N \cdot s/m^2$),

and

$$h_o = \alpha \left[\frac{k_l^3 \rho_l^2 g h_{fg}}{\mu_l D_o \Delta T_f}\right]^{0.25} = \alpha F , \qquad (4.10)$$

where

α = dimensionless coefficient,

h_{fg} = specific enthalpy of vaporization (J/kg),

ΔT_{fg} = average temperature difference across condensate film (K),

μ_l = dynamic viscosity of condensate ($N \cdot s/m^2$).

By substituting the Nusselt- and the Sieder-Tate-type equations into Equation 4.6 and rearranging, the following is derived:

$$\left[\frac{1}{U} - R_w\right]F = \frac{A_o F}{C_i \Omega A_i} + \frac{1}{\alpha} \qquad (4.11)$$

This equation is in linear form and has two unknowns: C_i and α. By allowing:

$$Y = \left[\frac{1}{U_o} - R_w\right]F, \qquad (4.12)$$

$$X = \frac{A_o F}{A_i \Omega}, \qquad (4.13)$$

$$C_i = \frac{1}{m}, \qquad (4.14)$$

and

$$\alpha = \frac{1}{b}. \qquad (4.15)$$

Equation 4.11 reduces to:

$$Y = mX + b. \qquad (4.16)$$

Even though it is not readily evident, the calculation of Ω and F requires that C_i and α be known because of fluid property variations with temperature. Therefore, an iterative process was necessary to compute these values. To begin this process, a value of 2.5 was assumed for α and values of 0.071 and 0.028 were used for C_i with and without an insert, respectively. New values for C_i and α were calculated by performing a least-squares fit using Equation 4.16. This

process was repeated until consecutive values of both C_1 and α agreed within ±0.1 percent.

Once the Sieder-Tate-type coefficient was computed, the inside heat-transfer coefficient was determined using Equation 4.9. With the inside and overall heat-transfer coefficients computed, the outside coefficient was easily determined.

$$\frac{1}{h_o} = \frac{1}{U_o} - \left[\frac{A_o}{h_i A_i} + R_w \right] \tag{4.17}$$

Notice that any error in computing the inside coefficient will be carried over into the value of the outside coefficient.

Following the Nusselt theory, the experimental data can be expressed and be fitted using a least-squares analysis of the data with the following form:

$$q = a\Delta T^n \tag{4.18}$$

The heat flux can also be written as $h\Delta T$, resulting in the following:

$$h = a\Delta T^{n-1} \tag{4.19}$$

According to the Nusselt theory, n = 0.75. Therefore, n was set to 0.75 in this investigation so that the enhancement ratio (based on constant vapor-side temperature drop) can be expressed as:

$$\epsilon_{\Delta T} = \frac{h_f}{h_s} = \frac{a_f}{a_s} = \frac{\alpha_f F_f}{\alpha_s F_s} , \tag{4.20}$$

where the f and s refer to finned and smooth tubes, respectively. By keeping the average temperature drop across the condensate film the same for the finned and smooth tube, the values of F_f and F_s are equal. Therefore, Equation 4.20 becomes:

$$\epsilon_{\Delta T} = \frac{\alpha_f}{\alpha_s} \tag{4.21}$$

To obtain the enhancement ratio at constant heat flux, the following development was used:

$$q = h_f \Delta T_f = h_s \Delta T_s \,. \tag{4.22}$$

Therefore,

$$\epsilon_q = \left.\frac{h_f}{h_s}\right]_q = \left.\frac{\Delta T_s}{\Delta T_f}\right]_q \tag{4.23}$$

From Equation 4.18 with n = 0.75

$$a_f \Delta T_f^{0.75} = a_s \Delta T_s^{0.75} \tag{4.24}$$

therefore

$$\frac{\Delta T_s}{\Delta T_f} = \left[\frac{a_f}{a_s}\right]^{1.33} \tag{4.25}$$

and

$$\epsilon_q = \left[\frac{a_f}{a_s}\right]^{1.33} \tag{4.26}$$

From Equations 4.20 and 4.26, it is clear that

$$\epsilon_q = [\epsilon_{\Delta T}]^{1.33} \tag{4.27}$$

Notice that with the above development, both ϵ_q and $\epsilon_{\Delta T}$ are independent of q and ΔT.

As shown by Equation 4.10, the effect of tube diameter appears in the value of F, and therefore α is independent of the tube diameter and theoretically should not vary. Equation 4.11 shows α as the inverse of the y-intercept with values of X and Y dependent on F. Experimentally determined values of α for smooth tubes may differ slightly from one tube to another. However, only one smooth tube (having a diameter of 19.05 mm, Table 3.1) was available during this study and the α found for this tube (tube #1) was used in computing enhancements.

C. MODIFICATIONS TO PROGRAM

The program used by Zebrowski [Ref. 12] was modified for this investigation. The modifications incorporated are:

1. The tube diameters (both inside and outside) were made variables.
2. Functions that compute fluid properties were extended to include ethylene glycol.
3. Calibrations were included to account for the viscous dissipation from the insert and the mixing chamber for the small-diameter tubes.

The ethylene glycol used in this study was 99 percent pure with a range of 194° to 200° C for the normal boiling point. Therefore, it was

not possible to compute the non-condensing gas concentrations accurately from the experiential measurements described previously.

V. RESULTS AND DISCUSSION

A. INTRODUCTION

Experimental data were taken as described in Chapter IV. Some tubes were tested at least twice to show repeatability of the apparatus used during this investigation. If two tests did not result in outside heat-transfer coefficients within ±5 percent, a third set of data was taken on the same tube. Figures 5.1, 5.2, 5.3, and 5.4 show the repeatability of data for all three test fluids. As shown in Figure 5.1, data for R-113 show repeatability within ±3 percent for tubes 1 and 18. Similarly, Figure 5.2 shows repeatability for tube 11 with steam to be within ±7 percent. This repeatability was typical of all the medium- and large-diameter tubes with steam. However, poor repeatability with the small-diameter tubes (tube 5) with steam is shown in Figure 5.3. The variation is significantly larger at ±12 percent. As seen in Figure 5.4, two different runs of ethylene glycol with tube 19 yielded condensing heat-transfer coefficients which agree within ±5 percent.

Owing to time constraints, a method of recognizing good results without necessarily repeating all data runs needed to be devised. When taking data, the flow rate in the test tube was gradually increased from a minimum to a maximum percent and a last set of data was taken again at the minimum flow rate. It was felt that a comparison of the heat-transfer coefficient for the first and last data sets was a good

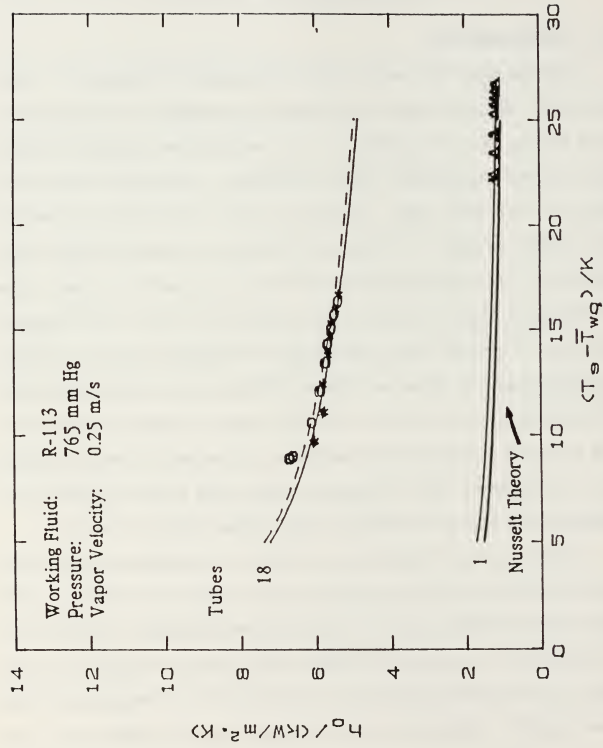

Figure 5.1 **Repeatability of R-113 Heat-Transfer Coefficients for Tubes 1 and 18**

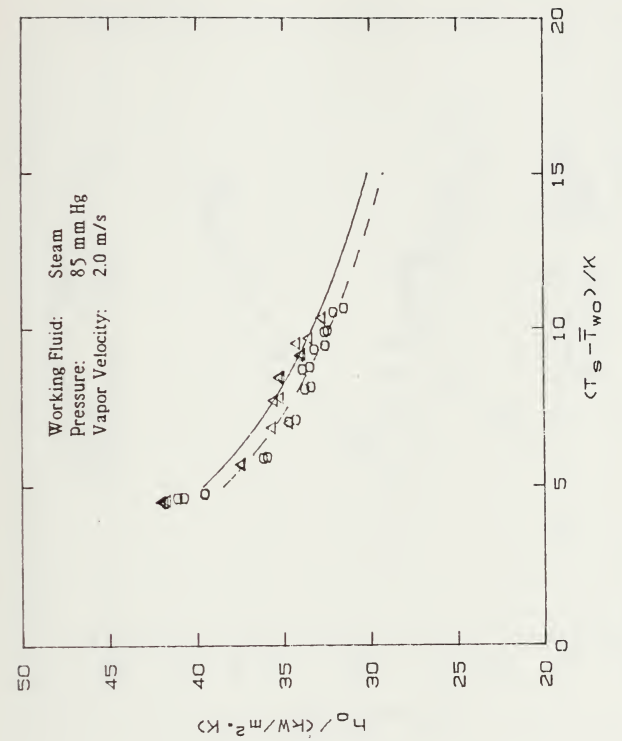

Figure 5.2 **Repeatability of Steam Heat-Transfer Coefficients for Tube 11**

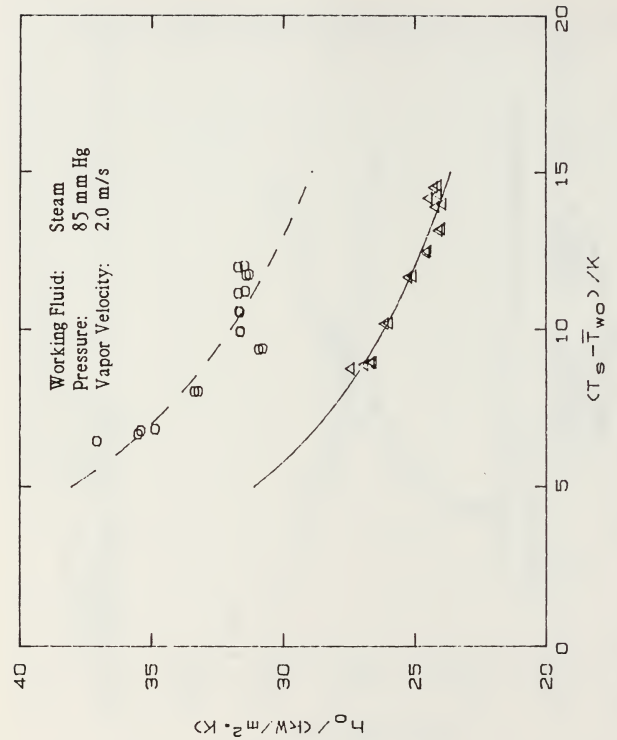

Figure 5.3 **Repeatability of Steam Heat-Transfer Coefficients for Tube 5**

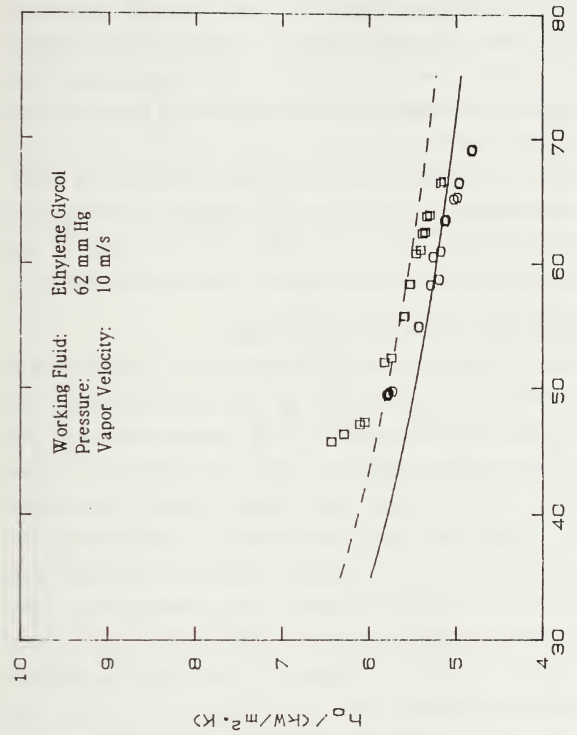

Figure 5.4 **Repeatability of Ethylene Glycol Heat-Transfer Coefficients for Tube 19**

indication of the quality of the data. If the comparison showed an increase in the coefficient from start to finish, dropwise condensation could have been responsible. Similarly, a decrease in the coefficient could have been caused by an in-leak of non-condensing gases (when operating at low pressure), and by the generation of gases within the boiler owing to the decomposition of the working fluid. As stated in Chapter IV, the modified Wilson plot technique computed the Sieder-Tate-type coefficient by using a linear least-squares fit to the data and taking the reciprocal of the slope. If the plot of the data did not resemble a good straight line (Figure 5.5), the data run was discarded.

B. INSIDE HEAT-TRANSFER COEFFICIENT

Table 5.1 lists the Sieder-Tate-type coefficients (C_i) computed for all tubes with each of the working fluids. As discussed earlier in Chapter IV, large- and medium-diameter tube families shared the same insert, while a different insert was used for the small tubes. Further, inserts were used only when steam was the working fluid. For this reason, C_i values were computed separately for the small-diameter tubes. As can be seen, the modified Wilson plot technique gives slightly different C_i values for different tubes. For example,for a given family of tubes, the inside diameter was identical and C_i should be the same. However, as shown in this table, C_i for steam (low pressure) varies between 0.048 and 0.051. This variation of six percent was within the expected uncertainty from the modified Wilson plot technique. Since the large and the medium tubes have identical internal

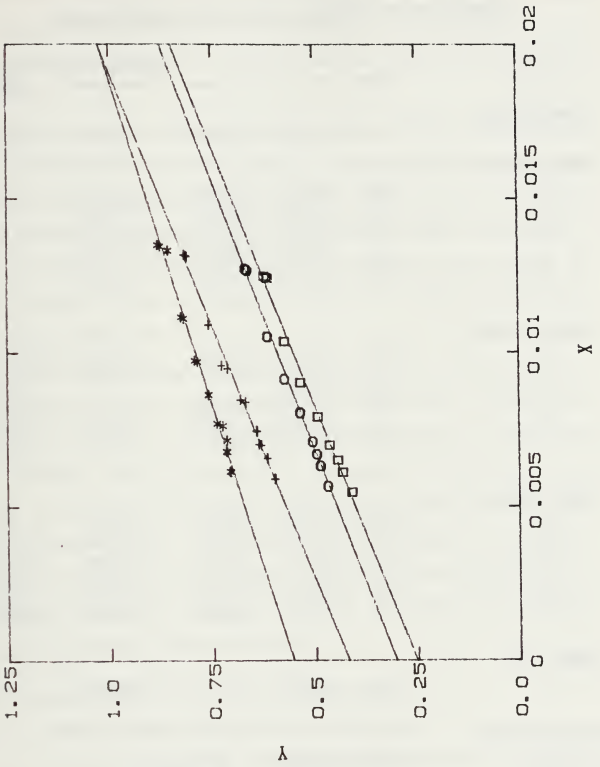

Figure 5.5 **Wilson Plot of Ethylene Glycol for Tubes 14, 15, 16, and 17**

TABLE 5.1

SUMMARY OF SIEDER-TATE-TYPE COEFFICIENTS

Tube	s (mm)	R-113	Working Fluid LP Steam	Working Fluid Atm Steam	Working Fluid Ethylene Glycol
Smooth tube					
1	–	0.0278	0.0679	0.0663	0.0318
Small tubes					
2	0.25	0.0279	0.0494	0.0509	–
3	0.5	0.0269	0.0505	0.0575	–
4	1.0	0.0281	0.0507	0.0513	–
5	1.5	0.0309	0.0481	0.0485	–
6	2.0	0.0395	0.0505	0.0482	–
7	4.0	0.0309	0.0505	0.0513	–
Medium tubes					
8	0.25	0.0341	0.0695	0.0689	0.0394
9	0.5	0.0258	0.0671	0.0642	0.0431
10	1.0	0.0286	–	–	0.0285
11	1.5	0.0282	0.0669	0.0677	0.0368
12	2.0	0.0273	0.0667	0.0671	0.0319
13	4.0	0.0274	0.091	0.0671	0.0299
Large tubes					
14	0.25	0.0359	0.0626	0.0668	0.0425
15	0.5	0.0279	0.0632	0.0624	0.0350
16	1.0	0.0317	0.0636	0.0684	0.0336
17	1.5	0.0303	0.0631	0.0687	0.0327
18	2.0	0.0301	0.0666	0.0679	0.0318
19	4.0	0.0302	0.0668	0.0678	0.035
QMC tube					
20	1.0	.0293	-	0.0513	-

Working Fluid		
R-113	0.030 ±0.002	(All tubes)
LP Steam	0.051 ±0.003	(Small tubes)
Atm Steam	0.066 ±0.002	(Medium and large tubes)
Ethylene Glycol	0.035 ±0.005	(Medium and large tubes)

geometries, theoretically they should have the same C_1 value. In order to obtain the outside heat-transfer coefficient in a consistent manner, the average C_1 values were computed and are shown at the bottom of Table 5.1.

For R-113, the average Sieder-Tate-type coefficient was computed to be 0.030 ±0.002. As seen in Table 5.1, for steam at atmospheric and low-pressure conditions, nearly the same Sieder-Tate-type coefficient was obtained. Coefficients for the medium and large tubes gave an average value of 0.066 ±0.002. The small-diameter tubes (with a different insert) gave an average value of 0.051 ±0.003 for the Sieder-Tate-type coefficient.

With ethylene glycol (no insert), the large and medium tubes gave an average Sieder-Tate-type coefficient of 0.035 ±0.005. Unfortunately, it was impossible to prevent subcooled boiling inside the small tubes with ethylene glycol. Notice that, as discussed by Masuda and Rose [Ref. 3], the extent of subcooled boiling changes with the water velocity. For this situation, it was not possible to represent the inside heat-transfer coefficient successfully by a single function as needed for the modified Wilson plot technique. Therefore, the testing of small tubes was discontinued for this working fluid.

C. OUTSIDE HEAT-TRANSFER COEFFICIENT

1. Repeatability with Previous NPS Data

Figure 5.6 shows the repeatability of the present outside heat-transfer coefficient for R-113 as compared with those of Zebrowski

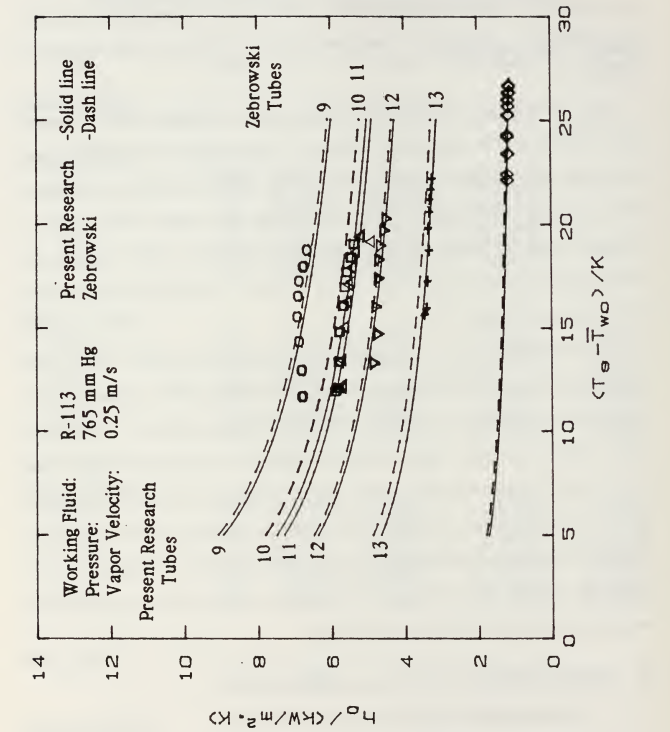

Figure 5.6 **Comparison of the Present R-113 Data and Zebrowski** [Ref. 12]

[Ref. 12]. This figure shows excellent repeatability, within ±3 percent for five of the medium tubes (tubes 1, 9, 10, 11, 12, and 13). Similarly, Figures 5.7 and 5.8 show repeatability for steam under low-pressure and atmospheric conditions, respectively, with those of Lester [Ref. 13]. It is evident that the maximum disagreement in the outside coefficient is about ±6 percent. Figures 5.9 and 5.10 demonstrate repeatability with results from Georgiadis [Ref. 5] with steam as the working fluid. This comparison shows a disagreement of up to ten percent in the outside heat-transfer coefficient.

Notice that on these figures, and all other similar figures, curves through the data are drawn. These curves represent a least-squares fit according to the equation:

$$q = a\Delta T^{0.75} \tag{5.1}$$

2. Outside Heat-Transfer Coefficient for R-113

Figures 5.11 through 5.13 show the variation of the outside heat-transfer coefficient for R-113 versus the vapor-side temperature drop for the small, medium and large tubes. On each figure, the curves are identified by the tube number (see Table 3.1 for the corresponding fin spacings). Notice that the relative position of each tube remains the same, regardless of the tube diameter, with the exception of the 0.25 mm fin spacing tubes (tubes 2 and 8). As shown by the uncertainty bands in Figure 5.11, the uncertainty of the data decreases with the

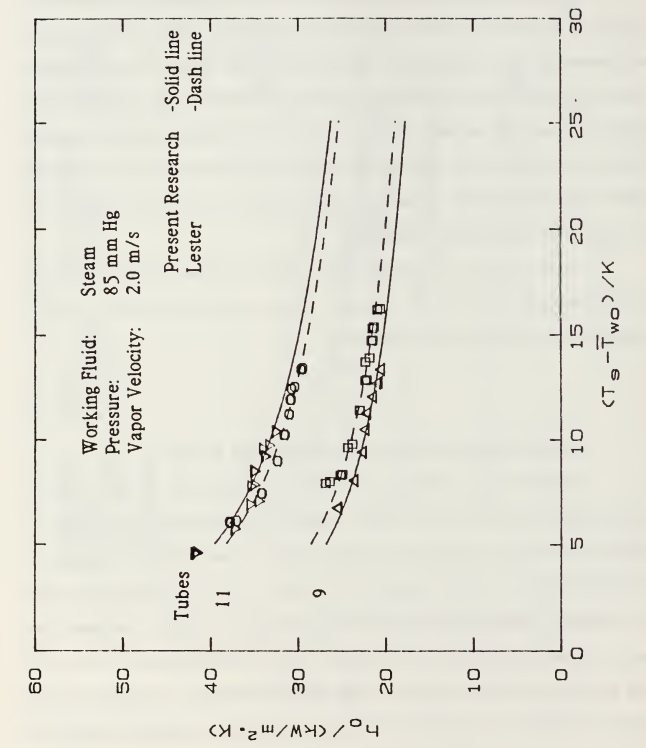

Figure 5.7 **Comparison of the Present Low-Pressure Steam Data and Lester** [Ref. 13]

Figure 5.8 **Comparison of the Present Atmospheric Steam Data and Lester** [Ref. 13]

Figure 5.9 **Comparison of the Present Low-Pressure Steam Data and Georgiadis** [Ref. 5]

Figure 5.10 **Comparison of the Present Atmospheric Steam Data and Georgiadis** [Ref. 5]

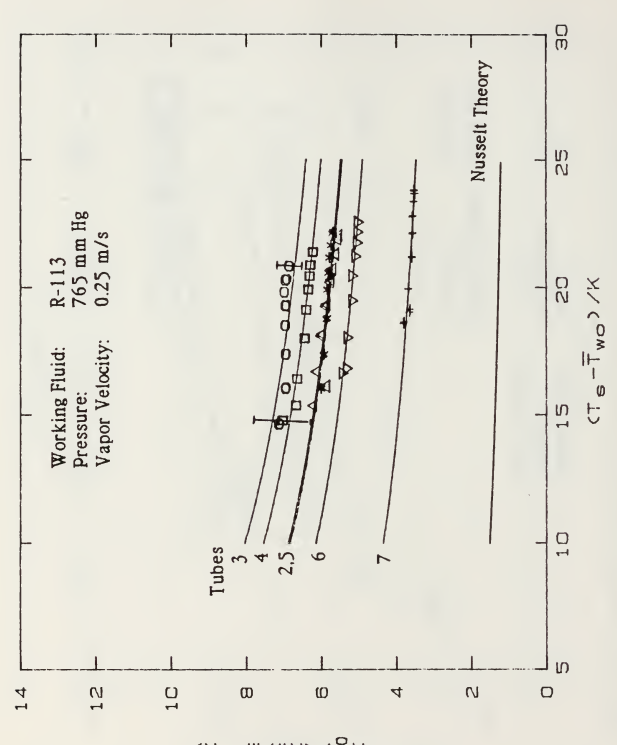

Figure 5.11 **R-113 Heat-Transfer Coefficients for Small-Diameter Tubes**

Figure 5.12 **R-113 Heat-Transfer Coefficients for Medium-Diameter Tubes**

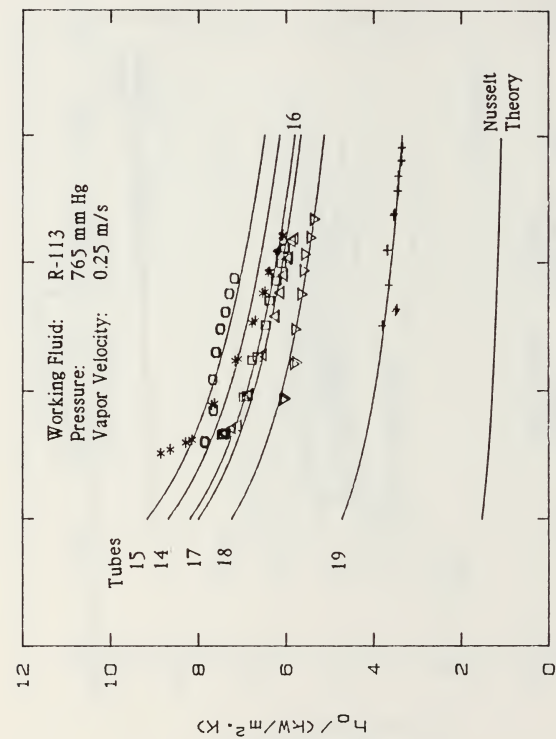

Figure 5.13 **R-113 Heat-Transfer Coefficients for Large-Diameter Tubes**

increasing vapor temperature drop. Increasing the cooling water flow rates increases the temperature drop, and thereby diminishes the uncertainties. This is true for all fluids tested.

The data shown in these three figures are repeated in Table 5.2 in the form of the vapor-side enhancement ratios, $\epsilon_{\Delta T}$. For comparison purposes, this table also lists the area enhancement and the condensate retention angle for each tube. The area enhancement is the ratio of the total surface area of the finned tube to the smooth tube. It is evident that the heat-transfer enhancement ratio generally increases with decreasing fin spacing (except for the 0.25 mm spacing). This trend is easily explained by the increasing area enhancement with decreasing fin spacing. However, as discussed in Chapter II, a decreased fin spacing also has a deleterious effect owing to the increased condensate retention angle (see Table 5.2). These retention angles were computed from Equation 2.6. Information given in Table 5.2 is also shown graphically in Figure 5.14. This figure shows that, for a given fin spacing, the large-diameter tube gave the best performance while the medium-diameter tube gave the poorest, with the exception of the 0.25 fin spacing. This figure also shows the uncertainty bands for enhancements predicted (see Appendix B for details) for typical R-113 data. As seen in Figure 5.14, the enhancements for each family lie within or very close to the uncertainty band. Although the uncertainty casts doubt on the relative position of the enhancements displayed on Figure 5.14, it is important to recall the excellent repeatability with

TABLE 5.2

SUMMARY OF R-113

Tubes	Fin Spacing (mm)	Area Enhancement	Retention Angle[1] (degrees)	Heat Transfer Enhancement ($\epsilon_{\Delta T}$)
Small tubes				
2	0.25	2.85	180	4.5
3	0.5	2.54	180	5.2
4	1.0	2.15	156	4.8
5	1.5	1.93	106	4.5
6	2.0	1.77	87	4.0
7	4.0	1.46	59	2.8
Medium Tubes				
8	0.25	2.77	79	4.7
9	0.5	2.47	54	5.2
10	1.0	2.10	37	4.4
11	1.5	1.88	30	4.4
12	2.0	1.74	26	3.7
13	4.0	1.44	18	2.7
Large Tubes				
14	0.25	2.73	69	5.3
15	0.5	2.44	47	5.6
16	1.0	2.08	33	5.0
17	1.5	1.86	27	4.9
18	2.0	1.72	23	4.5
19	4.0	1.43	16	2.9
QMC Tube				
20	1.0	3.47	43	6.3

[1] Calculated using Equation 2.6.

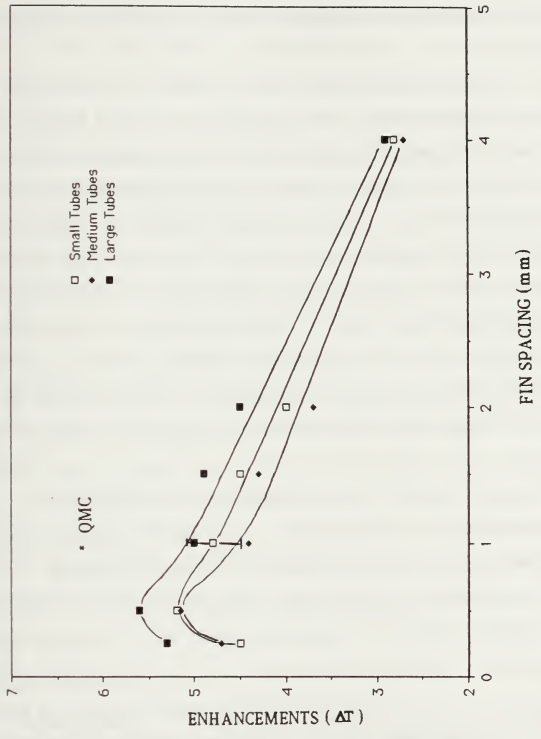

Figure 5.14 **Enhancements for R-113**

the R-113 data. Notice that among the tubes tested, the tube diameter has no effect on the optimum fin spacing, which is between 0.25 mm and 0.50 mm, but it does influence the magnitude of the enhancement ratio.

For the small-diameter tubes (Figure 5.11 and Table 5.2), tube 2 (0.25 mm spacing) was outperformed by tube 4 (1.0 mm spacing). As the diameter is increased from one tube family to another, the enhancement for the 0.25 mm tube overtakes the enhancement of the 1.0 mm tube. In the medium-diameter tubes, the 0.25 mm tube (tube8) performs slightly better than the 1.0 mm (tube 10). This trend continues into the large-diameter family, where tube 14 (0.25 mm spacing) outperformed tube 16 (1.0 mm spacing) by a larger magnitude. As seen in Table 5.2, the trend is consistent with the decreasing condensate retention angle. Comparing the retention angles for the small to large tubes reveal that the condensate retention angle decreases by 30 degrees for the 0.25 mm and only 20 degrees for the 1.0 mm tube. Therefore, as the diameter increases from small to large, the unflooded area for tubes with a 0.25 mm fin spacing increases much more than that for the tubes with a 1.0 mm fin spacing.

Tests with the GMC tube resulted in an enhancement ratio (for constant vapor-side temperature drop) of 6.3. As summarized graphically by Masuda and Rose [Ref. 3], the 1.0 mm GMC tube as tested by Yau, et al. [Ref. 4], with a 0.7 m/s vapor velocity, had approximately an enhancement of 6.4. Thus, the agreement between these two independent investigations is excellent.

3. Outside Heat-Transfer Coefficient for Steam

Figures 5.15 through 5.20 show the variation of the outside heat-transfer coefficient for steam for the small-, medium-, and large-diameter tubes. These figures were constructed in the same manner as those for R-113. Notice, as with R-113, the uncertainty is much greater for the low flow rates (Figure 5.18). As the difference between the vapor temperature and outside wall temperature decreases, the uncertainty increases. The large-diameter tubes have the greatest uncertainties (see Appendix B) due to the very low temperature difference. Owing to this low temperature difference and associated large uncertainty, the reprocessed data for the large-diameter tubes with an average C_1, listed in Table 5.1, was not well-correlated by Equation 5.1, which uses an exponent of 0.75 on the vapor to wall temperature difference.[1] A summary of the vapor-side enhancements, retention angles, and the area enhancements are located in Tables 5.3 and 5.4.

Enhancement versus fin spacing for steam at low-pressure conditions is shown in Figure 5.21. Using Equation 2.6, the fin spacing at which each tube diameter becomes fully flooded was computed and indicated on the figure by a vertical line. Notice that the

[1] A least squares fit of the data using Equation 5.1 but allowing a different exponent yielded exponents of 0.45 and 0.61 for the large diameter tubes at low-pressure and atmosphere conditions, respectively.

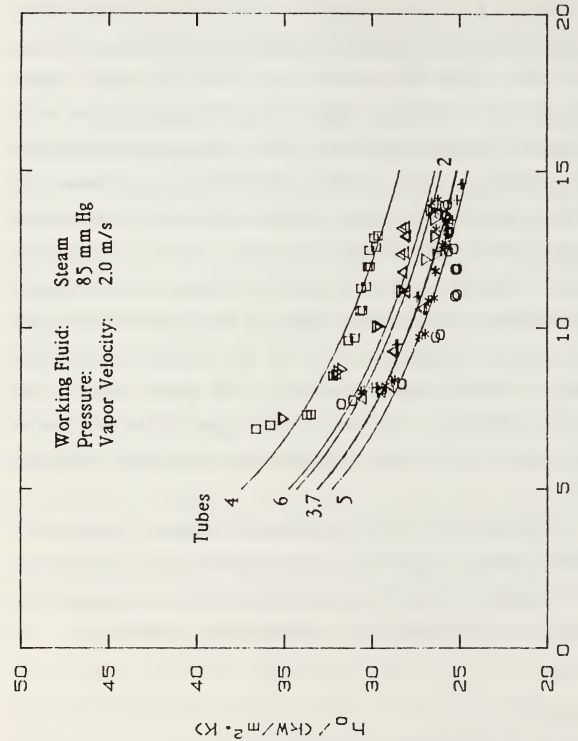

Figure 5.15 **Steam Heat-Transfer Coefficients for Small-Diameter Tubes at Low-Pressure Conditions**

Figure 5.16 **Steam Heat-Transfer Coefficients for Medium-Diameter Tubes at Low-Pressure Conditions**

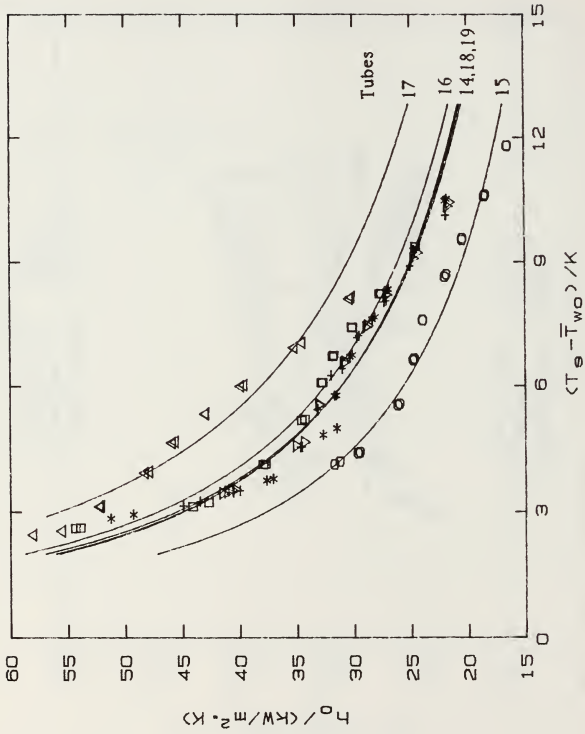

Figure 5.17 **Steam Heat-Transfer Coefficients for Large-Diameter Tubes at Low-Pressure Conditions**

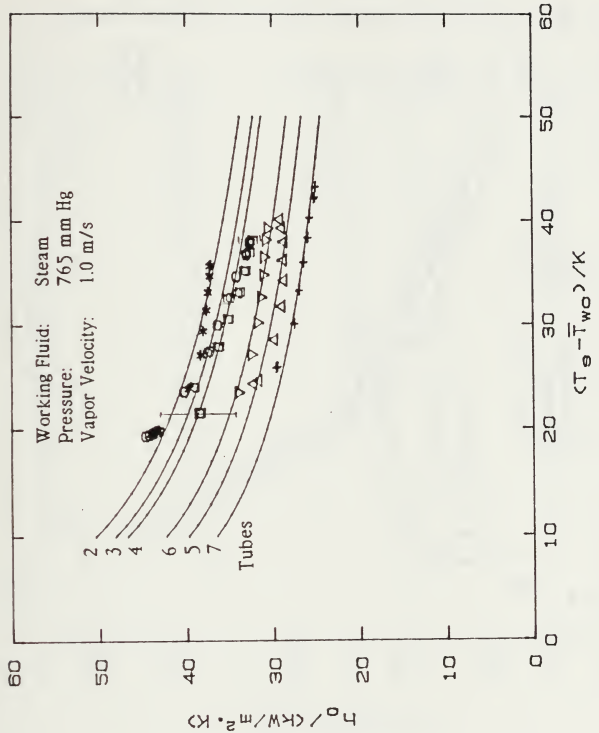

Figure 5.18 **Steam Heat-Transfer Coefficients for Small-Diameter Tubes at Atmospheric Conditions**

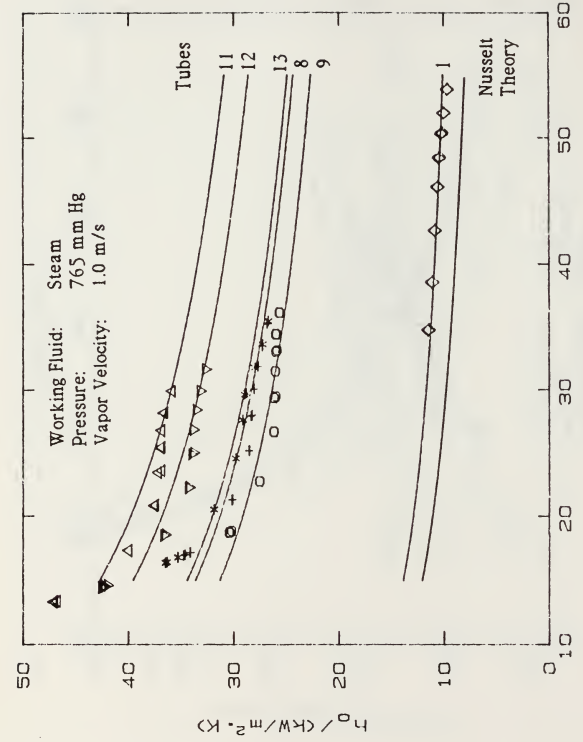

Figure 5.19 **Steam Heat-Transfer Coefficients for Medium-Diameter Tubes at Atmospheric Conditions**

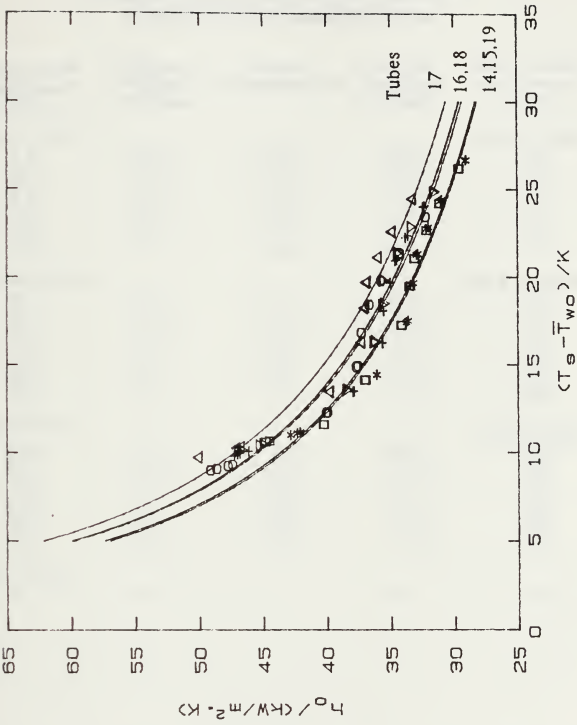

Figure 5.20 **Steam Heat-Transfer Coefficients for Large-Diameter Tubes at Atmospheric Conditions**

TABLE 5.3

SUMMARY OF STEAM ENHANCEMENTS AT LOW-PRESSURE CONDITIONS

Tubes	Fin Spacing (mm)	Area Enhancement	Retention Angle[1] (degrees)	Heat Transfer Enhancement ($\epsilon_{\Delta T}$)
Small tubes				
2	0.25	2.85	180	2.1
3	0.5	2.54	180	2.0
4	1.0	2.15	156	2.3
5	1.5	1.93	106	2.0
6	2.0	1.77	87	2.2
7	4.0	1.46	59	2.1
Medium Tubes				
8	0.25	2.77	180	1.9
9	0.5	2.47	180	1.8
10	1.0	2.10	109	–
11	1.5	1.88	84	2.6
12	2.0	1.74	71	2.5
13	4.0	1.44	48	2.4
Large Tubes				
14	0.25	2.73	180	2.2
15	0.5	2.44	180	1.8
16	1.0	2.08	92	2.5
17	1.5	1.86	72	3.0
18	2.0	1.72	61	2.5
19	4.0	1.43	42	2.5

[1] Calculated using Equation 2.6.

TABLE 5.4

SUMMARY OF STEAM ENHANCEMENTS AT ATMOSPHERIC CONDITIONS

Tubes	Fin Spacing (mm)	Area Enhancement	Retention Angle[1] (degrees)	Heat Transfer Enhancement ($\epsilon_{\Delta T}$)
Small tubes				
2	0.25	2.85	180	3.1
3	0.5	2.54	180	2.8
4	1.0	2.15	134	2.4
5	1.5	1.93	97	2.3
6	2.0	1.77	81	2.5
7	4.0	1.46	55	2.2
Medium Tubes				
8	0.25	2.77	180	2.4
9	0.5	2.47	180	2.2
10	1.0	2.10	100	-
11	1.5	1.88	78	2.9
12	2.0	1.74	66	2.7
13	4.0	1.44	45	2.3
Large Tubes				
14	0.25	2.73	180	2.7
15	0.5	2.44	147	2.4
16	1.0	2.08	85	2.8
17	1.5	1.86	67	3.1
18	2.0	1.72	57	3.0
19	4.0	1.43	40	2.9
QMC Tubes				
20	1.0	3.47	124	3.6

[1] Calculated using Equation 2.6.

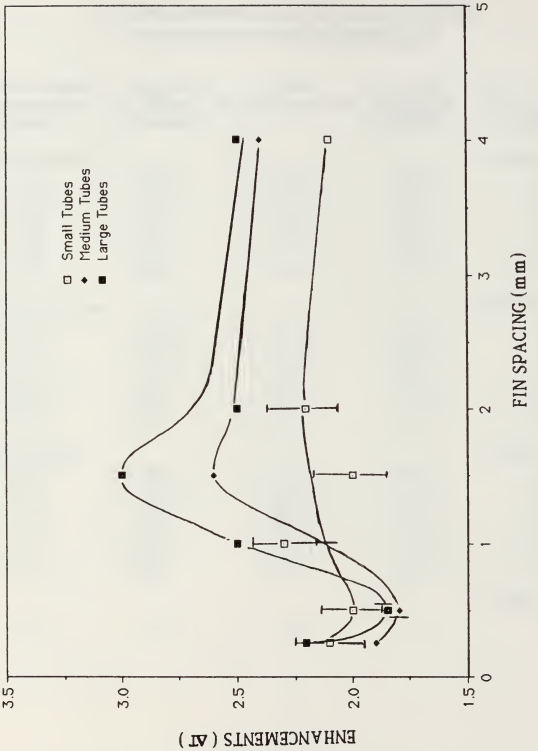

Figure 5.21 **Enhancements for Steam at Low-Pressure Conditions**

small-diameter tube becomes fully flooded at a spacing just under 1.0 mm. Medium- and large-diameter tubes become fully flooded at a spacing of approximately 0.5 mm. In the fully flooded region, enhancement was expected to increase as the fin spacing decreased. Once a tube is fully flooded, any further decrease in fin spacing should replace the flooding condensate with tube material and result in a greater performance. This trend is seen in the medium- and large-diameter tubes. Figure 5.21 indicates that, for small-diameter tubes, the enhancement in the fully flooded region appears to be more complicated than simply replacing condensate with tube material.

For partially flooded tubes, the change in diameter from medium to large did not affect the optimum fin spacing (1.5 mm). However, the small-diameter tube exhibited an optimum fin spacing close to 2.0 mm. Furthermore, for partially flooded tubes, Figure 5.21 shows that, for a given fin spacing, the large-diameter tube gave the best performance while the small-diameter tube gave the poorest performance.

Figure 5.22 displays the enhancement for steam at atmospheric conditions. Again, the vertical lines indicate the fin spacing at which the tube becomes fully flooded. Large increasing enhancements are shown to the left of the fully flooded lines (decreasing fin spacing). As with the low-pressure conditions, the optimum fin spacing is 1.5 mm for the medium- and large-diameter tubes, while a 2.0 mm optimum fin spacing is shown for the small-diameter tube. The

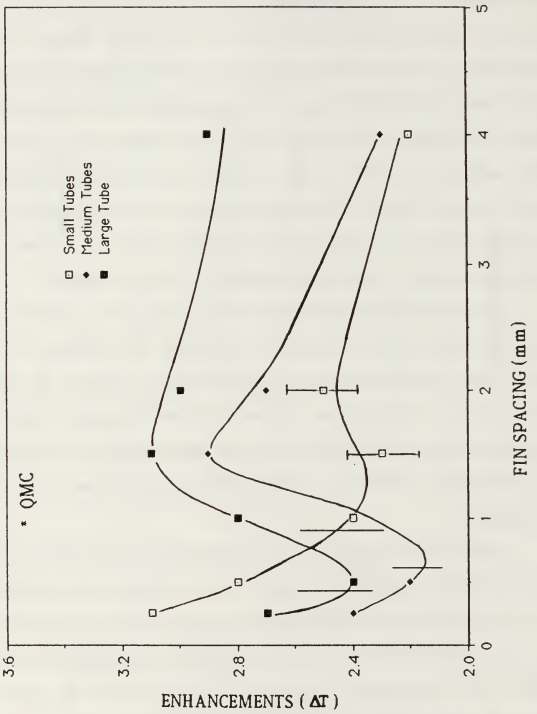

Figure 5.22 **Enhancements for Steam at Atmospheric Conditions**

optimum fin spacing for the medium-diameter tube, in both low-pressure and atmospheric conditions, agrees with Georgiadis. The order of enhancement from least to greatest is small, medium, and large.

The QMC tube is shown in Figure 5.22 to have an enhancement of 3.5. This is far larger than the measured enhancement of only 2.2 obtained at Queen Mary College [Ref. 3]. Marto [Ref. 30] pointed out in his review paper that there was an unexpected inconsistency between the NPS obtained data and the Queen Mary College obtained data for R-113 and steam. He found that for R-113, Queen Mary College data [Ref. 3] were higher than the NPS data (Zebrowski [Ref. 12]). As pointed out earlier in this thesis, for R-113, the present results with the QMC tube (this investigation) are in excellent agreement with the data obtained at Queen Mary College. Marto [Ref. 30] also pointed out that for the steam at atmospheric pressure, the data taken at Queen Mary College were less than the data taken a NPS. However, for steam, the result of this thesis for the enhancement of the QMC tube was much larger than the data for the NPS tubes. This indicates a consistent trend for R-113 and steam when comparing the performance of tubes 4 and 20. The reasons for the inconsistent trend of the Queen Mary College data are not known at present. Further investigation and communication is needed to solve this discrepancy.

4. Outside Heat-Transfer Coefficient for Ethylene Glycol

Figures 5.23 through 5.24 display the variation of the outside heat-transfer coefficient with the vapor-side temperature drop for the medium- and large-diameter tubes. These figures were constructed in the same manner as the R-113 figures. The relative position of each tube remained unchanged for each diameter. The uncertainties for the ethylene glycol are associated with the standard deviation of experimental values of C_1. Even though the uncertainty of the ethylene glycol data is as high as the large-diameter steam data, Figures 5.23 and 5.24 show good agreement with the least squares fit of Equation 5.1. As shown in Figures 5.23 and 5.24, the medium tube slightly outperformed the large tube. This is contradictory to the trends of R-113 and steam. As shown in Figure 5.25, the difference in enhancement between the medium- and large-diameter tubes is within the uncertainty band, and, therefore, the large-diameter tubes could possibly have the better enhancement. In either case, the performance of the two tube families is approximately the same. A summary of the vapor-side enhancements, retention angles, and area enhancements is located in Table 5.5. The change in diameter from medium to large did not affect the optimum fin spacing of 1.0 mm for the tubes tested. This optimum fin spacing agrees with Masuda and Rose [Ref. 3].

D. SUMMARY OF RESULTS

The literature discussed in Chapter II indicated that an increase in root diameter will decrease the condensate retention angle, and,

Figure 5.23 **Ethylene Glycol Heat-Transfer Coefficients for Medium-Diameter Tubes**

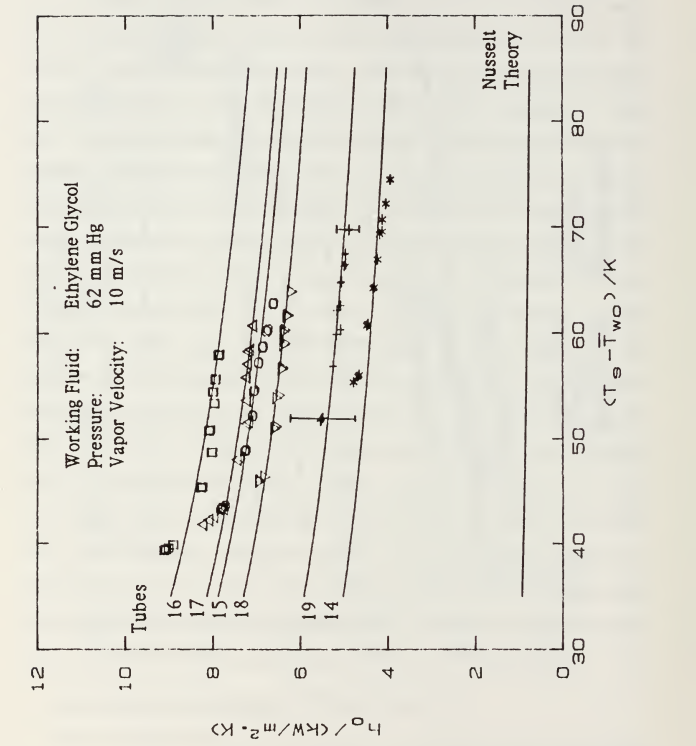

Figure 5.24 **Ethylene Glycol Heat-Transfer Coefficients for Large-Diameter Tubes**

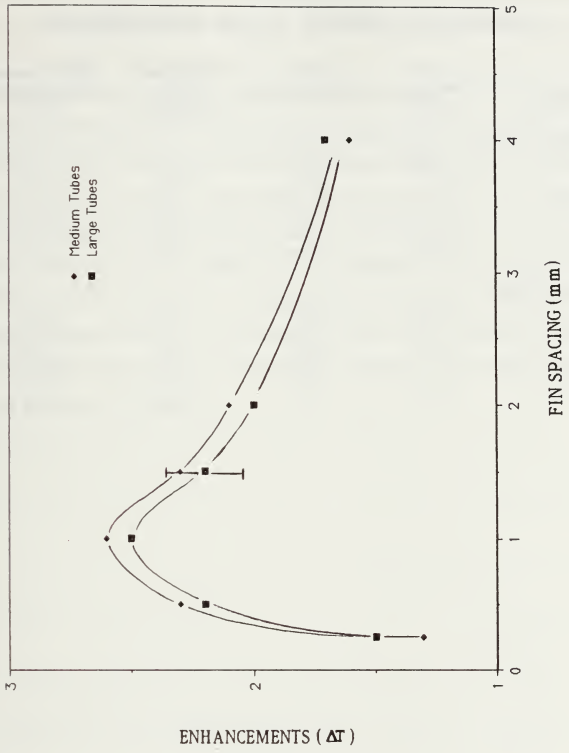

Figure 5.25 **Enhancements for Ethylene Glycol**

TABLE 5.5

SUMMARY OF ETHYLENE GLYCOL ENHANCEMENTS

Tubes	Fin Spacing (mm)	Area Enhancement	Retention Angle[1] (degrees)	Heat Transfer Enhancement ($\epsilon_{\Delta T}$)
Medium Tubes				
8	0.25	2.77	180	1.3
9	0.5	2.47	102	2.3
10	1.0	2.10	66	2.6
11	1.5	1.88	53	2.3
12	2.0	1.74	46	2.1
13	4.0	1.44	32	1.6
Large Tubes				
14	0.25	2.73	151	1.5
15	0.5	2.44	86	2.2
16	1.0	2.08	58	2.5
17	1.5	1.86	47	2.3
18	2.0	1.72	40	2.0
19	4.0	1.43	28	1.7

[1] Calculated using Equation 2.6.

therefore, a clear trend of increasing enhancement from small- to large-diameter tubes was expected. R-113 had similar enhancements for the small- and medium-diameter tubes, while the ethylene glycol had similar enhancements for the medium and large. The possibility of competing effects exists with a change in root diameter. For the large-diameter tubes, condensate must flow along a longer path length from the top to the bottom of the tube. This longer path length yields a larger average film thickness in the unflooded portion of the tube when compared with a small tube. This degrades the performance in the unflooded portion of the large-diameter tube when compared to a small-diameter tube. The significance of this effect depends on fluid properties such as thermal conductivity, viscosity, and surface tension and warrants further study.

VI. CONCLUSIONS AND RECOMMENDATIONS

A. CONCLUSIONS

1. Within the range of diameters tested, the effect of root diameter on the vapor- side coefficient was small. Results indicate that two or more competing mechanisms may exist while increasing the root diameter.

2. With the exception of the small-diameter tubes with steam, the optimum fin spacing was near 0.5, 1.0, and 1.5 mm for R-113, ethylene glycol, and steam respectively.

3. The optimum fin spacing for the small-diameter tube with steam was approximately 2.0 mm.

4. With the exception of the small-diameter tube with steam, a change in diameter did not effect the optimum fin spacing for each test fluid.

5. The data presented with this investigation supports the findings of past research at NPS. Variations from previous data for R-113 and steam were within ±3 percent and ±10 percent, respectively.

6. The comparison of the enhancements for the QMC tube was outstanding for R-113, while the steam comparison exhibited a large discrepancy.

B. RECOMMENDATIONS

1. Retest the families of tubes to verify trends observed for ethylene glycol.

2. Manufacture a new tube with the same dimensions as tube 10 using the same company that manufactured the original tubes.

3. Manufacture smooth tubes of small and large diameters. Compare the values obtained of α for these small and large smooth tubes with the value of α for the medium tube.

4. Manufacture additional tubes to include more fin spacings, especially in the vicinity of the fully flooded condition.

5. Operate the apparatus with methanol or ethanol as working fluids. In addition to having low boiling temperatures and good wetting characteristics, these fluids have approximately the same surface-tension to density ratio as ethylene glycol.

6. Increase the cooling water flow rates through the test tube to minimize uncertainties in vapor-side heat-transfer coefficients.

7. Modify the apparatus with a controller for the auxiliary condenser cooling water. Once the equilibrium set temperature is obtained, the controller can be placed in operation to maintain the set temperature.

8 Provide a cooling water sump and pump for the auxiliary condenser. The present tap water system is very susceptible to pressure fluctuations in the building.

APPENDIX A

RAW DATA

Table A.1 contains names of raw data files with corresponding tube number. Actual raw data files follow table.

TABLE A.1

SUMMARY OF RAW DATA FILES

Tube	Working Fluid R-113	LP Steam	Atm Steam	Ethylene Glycol
Smooth tube				
1	RMTH1	M1STV117	SMTHSTA65	M1EGV37
Small tubes				
2	S1RA13	S1STV104	S1STA105	-
3	S2RA123	S2STV98	S2STA99	-
4	S3RA15	S3STV95	S3STA96	-
5	S4RA17	S4STV74	S4STA100	-
6	S5RA18	S5STV93	S5STA94	-
7	S6RA19	S6STV89	S6STA91	
Medium tubes				
8	M1RA117	M1ASTV87	M1ASTA88	M1AEGV45
9	M4RA01	M4STV84	M4STA85	M4EGV39
10	M5RA02A	-	-	M5EGV34
11	M6RA03A	M6STV54	M6STA55	M6EGV40
12	M7RA04	M7STV80	M7STA81	M7EGV41
13	M8RA05	M8STV77	M8STA78	M8EGV42
Large tubes				
14	L1RA08	L1STV72	L1STA73	L1EG53
15	L2RA11	L2STV70	L2STA71	L2EG46
16	L3RA12	L3STV68	L3STA69	L3EG51
17	L4RA07	L4STV67	L4STA66	L4EG50
18	L5RA09	L5STV61	L5STA62	L5EG48
19	L6RA130	L6STV56	L6STA57	L6EG47
QMC tube				
20	QIRA20	-	QSTA106	-

File Name: S1STU1@4
Pressure Condition: Vacuum
Steam Velocity: 2.0 (m/s)

Data #	Vw (m/s)	Tin (C)	Tout (C)	Ts (C)
1	2.05	22.56	24.67	48.44
2	2.05	22.59	24.66	48.43
3	2.64	22.38	24.19	48.47
4	2.64	22.39	24.18	48.50
5	3.31	22.24	23.81	48.47
6	3.31	22.24	23.80	48.49
7	3.98	22.13	23.52	48.43
8	3.98	22.13	23.52	48.44
9	4.65	22.05	23.29	48.50
10	4.65	22.05	23.28	48.44
11	5.32	21.98	23.11	48.48
12	5.32	21.98	23.12	48.38
13	5.98	21.92	22.97	48.48
14	5.98	21.92	22.97	48.43
15	6.48	21.88	22.83	48.42
16	6.48	21.89	22.87	48.44
17	2.05	22.58	24.71	48.44
18	2.05	22.58	24.71	48.42

File Name: S2STU88
Pressure Condition: Vacuum
Steam Velocity: 2.0 (m/s)

Data #	Vw (m/s)	Tin (C)	Tout (C)	Ts (C)
1	2.05	22.21	25.24	48.42
2	2.05	22.22	25.25	48.41
3	2.64	22.03	24.77	48.44
4	2.64	22.03	24.76	48.48
5	3.31	21.88	24.38	48.50
6	3.31	21.88	24.38	48.52
7	3.98	21.76	24.12	48.50
8	3.98	21.76	24.12	48.51
9	4.65	21.72	23.92	48.44
10	4.65	21.72	23.93	48.46
11	5.32	21.66	23.75	48.43
12	5.32	21.66	23.75	48.42
13	5.98	21.60	23.61	48.42
14	5.98	21.60	23.61	48.48
15	6.47	21.57	23.52	48.48
16	6.47	21.57	23.51	48.48
17	2.05	22.25	25.35	48.41
18	2.05	22.25	25.37	48.42

File Name: S3STV95
Pressure Condition: Vacuum
Steam Velocity: 2.0 (m/s)

Data #	Vw (m/s)	Tin (C)	Tout (C)	Ts (C)
1	2.06	23.41	25.54	48.40
2	2.06	23.42	25.56	48.47
3	2.64	23.21	25.08	48.47
4	2.64	23.21	25.07	48.48
5	3.31	23.06	24.68	48.43
6	3.31	23.06	24.69	48.40
7	3.98	22.96	24.40	48.42
8	3.98	22.96	24.40	48.43
9	4.65	22.88	24.19	48.45
10	4.65	22.88	24.19	48.45
11	5.32	22.82	24.00	48.43
12	5.32	22.82	24.01	48.46
13	5.99	22.76	23.85	48.47
14	5.99	22.76	23.85	48.43
15	6.47	22.73	23.75	48.43
16	6.47	22.73	23.75	48.46
17	2.06	23.43	25.60	48.42
18	2.06	23.43	25.61	48.40

File Name: S4STV74
Pressure Condition: Vacuum
Steam Velocity: 2.0 (m/s)

Data #	Vw (m/s)	Tin (C)	Tout (C)	Ts (C)
1	2.05	22.05	24.13	48.39
2	2.06	22.06	24.13	48.45
3	2.64	21.87	23.66	48.49
4	2.64	21.88	23.68	48.55
5	3.50	21.70	23.19	48.43
6	3.50	21.70	23.19	48.41
7	4.46	21.57	22.82	48.48
8	4.46	21.58	22.82	48.54
9	5.33	21.50	22.59	48.43
10	5.33	21.50	22.59	48.39
11	6.10	21.44	22.42	48.41
12	6.10	21.44	22.42	48.46
13	5.71	21.48	22.51	48.50
14	5.71	21.48	22.52	48.45
15	3.98	21.67	23.02	48.51
16	3.98	21.67	23.02	48.46
17	2.05	22.15	24.21	48.52
18	2.06	22.15	24.21	48.55

File Name: S5STV93
Pressure Condition: Vacuum
Steam Velocity: 2.0 (m/s)

Data #	Vw (m/s)	Tin (C)	Tout (C)	Ts (C)
1	2.06	23.15	25.21	48.48
2	2.06	23.15	25.20	48.45
3	2.64	22.94	24.72	48.45
4	2.64	22.94	24.73	48.47
5	3.31	22.80	24.36	48.48
6	3.31	22.80	24.36	48.50
7	3.98	22.69	24.08	48.51
8	3.98	22.69	24.07	48.52
9	4.65	22.61	23.87	48.48
10	4.65	22.61	23.87	48.48
11	5.32	22.55	23.70	48.43
12	5.32	22.55	23.69	48.50
13	5.99	22.49	23.54	48.53
14	5.99	22.49	23.55	48.45
15	6.47	22.45	23.45	48.44
16	6.47	22.45	23.45	48.49
17	2.06	23.16	25.23	48.43
18	2.06	23.16	25.25	48.46

File Name: S6STV89
Pressure Condition: Vacuum
Steam Velocity: 2.0 (m/s)

Data #	Vw (m/s)	Tin (C)	Tout (C)	Ts (C)
1	2.06	22.53	24.66	48.42
2	2.06	22.52	24.65	48.44
3	2.64	22.36	24.20	48.47
4	2.64	22.36	24.20	48.48
5	3.50	22.19	23.72	48.47
6	3.50	22.19	23.73	48.46
7	4.46	22.07	23.36	48.49
8	4.46	22.07	23.35	48.52
9	5.32	21.99	23.12	48.44
10	5.32	21.99	23.11	48.49
11	6.09	21.94	22.95	48.40
12	6.09	21.93	22.94	48.42
13	6.67	21.89	22.82	48.48
14	6.67	21.90	22.83	48.49
15	4.94	22.04	23.22	48.44
16	4.94	22.04	23.22	48.46
17	2.06	22.62	24.73	48.38
18	2.06	22.62	24.73	48.42

File Name: M1ASTV87
Pressure Condition: Vacuum
Steam Velocity: 2.0 (m/s)

Data #	Vw (m/s)	Tin (C)	Tout (C)	Ts (C)
1	1.16	22.74	25.00	48.48
2	1.16	22.74	25.00	48.44
3	1.48	22.53	24.51	48.41
4	1.48	22.53	24.51	48.44
5	1.97	22.34	24.04	48.47
6	1.97	22.34	24.04	48.48
7	2.51	22.21	23.70	48.49
8	2.51	22.21	23.70	48.45
9	2.99	22.13	23.47	48.43
10	2.99	22.13	23.47	48.43
11	3.43	22.07	23.31	48.46
12	3.43	22.07	23.31	48.47
13	3.86	22.03	23.17	48.48
14	3.86	22.03	23.17	48.42
15	4.40	21.97	23.02	48.44
16	4.40	21.97	23.02	48.48
17	1.16	22.75	25.06	48.43
18	1.16	22.75	25.06	48.42

File Name: M4STV84
Pressure Condition: Vacuum
Steam Velocity: 2.0 (m/s)

Data #	Vw (m/s)	Tin (C)	Tout (C)	Ts (C)
1	1.16	22.88	25.13	48.46
2	1.16	22.90	25.14	48.46
3	1.48	22.73	24.87	48.40
4	1.48	22.73	24.88	48.46
5	1.97	22.58	24.23	48.48
6	1.97	22.58	24.23	48.44
7	2.51	22.47	23.90	48.40
8	2.51	22.47	23.90	48.40
9	2.99	22.40	23.69	48.40
10	2.99	22.40	23.69	48.31
11	3.42	22.36	23.53	48.48
12	3.42	22.36	23.53	48.41
13	3.86	22.33	23.40	48.45
14	3.86	22.32	23.41	48.48
15	4.40	22.28	23.27	48.47
16	4.40	22.28	23.27	48.40
17	1.16	23.03	25.26	48.44
18	1.16	23.03	25.26	48.40

File Name: M6STV54
Pressure Condition: Vacuum
Steam Velocity: 2.0 (m/s)

Data #	Vw (m/s)	Tin (C)	Tout (C)	Ts (C)
1	1.15	23.12	25.59	48.40
2	1.15	23.12	25.59	48.43
3	1.48	22.92	25.10	48.39
4	1.48	22.92	25.10	48.44
5	1.97	22.73	24.61	48.45
6	1.97	22.73	24.62	48.41
7	2.51	22.59	24.26	48.37
8	2.51	22.59	24.26	48.43
9	2.99	22.51	24.03	48.47
10	2.99	22.51	24.03	48.51
11	3.42	22.44	23.84	48.42
12	3.42	22.44	23.84	48.48
13	3.86	22.39	23.70	48.33
14	3.86	22.38	23.70	48.45
15	4.38	22.34	23.54	48.41
16	4.38	22.34	23.54	48.47
17	4.16	23.09	25.58	48.53
18	4.16	23.09	25.57	48.43

File Name: M7STV80
Pressure Condition: Vacuum
Steam Velocity: 2.0 (m/s)

Data #	Vw (m/s)	Tin (C)	Tout (C)	Ts (C)
1	1.16	22.98	25.44	48.49
2	1.16	22.98	25.45	48.53
3	1.48	22.77	24.93	48.40
4	1.48	22.77	24.92	48.40
5	1.97	22.59	24.45	48.51
6	1.97	22.59	24.45	48.48
7	2.51	22.46	24.10	48.41
8	2.51	22.46	24.10	48.36
9	2.99	22.38	23.87	48.44
10	2.99	22.38	23.86	48.43
11	3.42	22.32	23.70	48.43
12	3.42	22.32	23.69	48.43
13	3.86	22.28	23.55	48.40
14	3.86	22.28	23.55	48.40
15	4.40	22.22	23.40	48.45
16	4.40	22.22	23.39	48.39
17	4.16	23.00	25.44	48.43
18	4.16	23.00	25.44	48.48

File Name: M8STV77
Pressure Condition: Vacuum
Steam Velocity: 2.0 (m/s)

Data #	Vw (m/s)	Tin (C)	Tout (C)	Ts (C)
1	1.16	23.11	25.55	48.37
2	1.16	23.11	25.56	48.54
3	1.48	22.90	25.04	48.41
4	1.48	22.90	25.04	48.40
5	1.97	22.71	24.56	48.48
6	1.97	22.71	24.56	48.49
7	2.51	22.58	24.18	48.52
8	2.51	22.58	24.18	48.45
9	2.99	22.49	23.94	48.46
10	2.99	22.49	23.94	48.49
11	3.42	22.43	23.74	48.43
12	3.42	22.43	23.75	48.46
13	3.86	22.38	23.60	48.51
14	3.86	22.38	23.59	48.48
15	4.39	22.33	23.43	48.44
16	4.39	22.33	23.43	48.44
17	1.16	23.08	25.46	48.46
18	1.16	23.08	25.46	48.45

File Name: M1STV103
Pressure Condition: Vacuum
Steam Velocity: 2.0 (m/s)

Data #	Vw (m/s)	Tin (C)	Tout (C)	Ts (C)
1	1.16	23.11	24.87	48.49
2	1.16	23.12	24.88	48.44
3	1.48	22.93	24.41	48.40
4	1.48	22.93	24.41	48.44
5	1.86	22.79	24.06	48.48
6	1.86	22.79	24.07	48.46
7	2.24	22.69	23.81	48.44
8	2.24	22.69	23.81	48.44
9	2.61	22.62	23.62	48.47
10	2.61	22.62	23.62	48.48
11	2.99	22.56	23.46	48.38
12	2.99	22.56	23.46	48.40
13	3.37	22.51	23.33	48.53
14	3.37	22.51	23.34	48.43
15	3.64	22.48	23.26	48.45
16	3.64	22.47	23.25	48.44
17	1.16	23.16	24.91	48.51
18	1.16	23.16	24.92	48.45

File Name: L55TV61
Pressure Condition: Vacuum
Steam Velocity: 2.0 (m/s)

Data #	Vw (m/s)	Tin (C)	Tout (C)	Ts (C)
1	1.16	23.04	25.50	48.54
2	1.16	23.04	25.51	48.46
3	1.48	22.85	25.01	48.41
4	1.48	22.84	25.01	48.48
5	1.97	22.67	24.56	48.42
6	1.97	22.68	24.57	48.43
7	2.51	22.55	24.21	48.48
8	2.51	22.54	24.21	48.46
9	2.99	22.47	23.98	48.39
10	2.99	22.47	23.98	48.45
11	3.42	22.41	23.82	48.48
12	3.42	22.41	23.82	48.40
13	3.86	22.36	23.67	48.48
14	3.86	22.36	23.67	48.34
15	4.39	22.31	23.51	48.44
16	4.39	22.31	23.51	48.52
17	1.16	23.07	25.53	48.42
18	1.16	23.06	25.53	48.46

File Name: L55TV55
Pressure Condition: Vacuum
Steam Velocity: 2.0 (m/s)

Data #	Vw (m/s)	Tin (C)	Tout (C)	Ts (C)
1	1.16	22.45	25.65	48.51
2	1.16	22.45	25.67	48.48
3	1.48	22.27	25.40	48.45
4	1.48	22.27	25.39	48.41
5	1.97	22.10	24.96	48.39
6	1.97	22.10	24.96	48.40
7	2.51	22.98	24.62	48.41
8	2.51	22.98	24.63	48.37
9	2.99	22.91	24.41	48.44
10	2.99	22.92	24.42	48.50
11	3.42	22.87	24.25	48.43
12	3.42	22.87	24.26	48.48
13	3.85	22.82	24.12	48.46
14	3.85	22.83	24.12	48.44
15	4.39	22.79	23.98	48.42
16	4.35	22.79	23.98	48.48
17	1.16	23.58	25.01	48.48
18	1.15	23.58	26.02	48.44

File Name: L3STV68
Pressure Condition: Vacuum
Steam Velocity: 2.0 (m/s)

Data #	Vw (m/s)	Tin (C)	Tout (C)	Ts (C)
1	1.16	23.37	25.74	48.44
2	1.16	23.37	25.75	48.39
3	1.48	23.16	25.28	48.43
4	1.48	23.17	25.28	48.48
5	1.97	22.98	24.82	48.46
6	1.97	22.98	24.82	48.45
7	2.51	22.85	24.49	48.48
8	2.51	22.85	24.49	48.52
9	2.99	22.77	24.27	48.48
10	2.99	22.77	24.27	48.44
11	3.42	22.71	24.12	48.48
12	3.42	22.71	24.12	48.54
13	3.85	22.66	23.97	48.41
14	3.85	22.66	23.98	48.49
15	4.39	22.61	23.83	48.50
16	4.39	22.61	23.84	48.54
17	1.16	23.38	25.82	48.46
18	1.16	23.38	25.81	48.43

File Name: L4STV67
Pressure Condition: Vacuum
Steam Velocity: 2.0 (m/s)

Data #	Vw (m/s)	Tin (C)	Tout (C)	Ts (C)
1	1.16	23.28	25.72	48.43
2	1.16	23.28	25.74	48.49
3	1.48	23.09	25.30	48.48
4	1.48	23.09	25.30	48.49
5	1.97	22.91	24.85	48.45
6	1.97	22.91	24.85	48.46
7	2.51	22.78	24.53	48.45
8	2.51	22.79	24.53	48.46
9	2.99	22.70	24.31	48.42
10	2.99	22.70	24.31	48.45
11	3.42	22.65	24.15	48.43
12	3.42	22.66	24.16	48.43
13	3.85	22.61	24.01	48.42
14	3.85	22.61	24.01	48.49
15	4.39	22.56	23.85	48.45
16	4.39	22.56	23.85	48.49
17	1.16	23.33	25.84	48.41
18	1.16	23.33	25.84	48.50

File Name: L1STV72
Pressure Condition: Vacuum
Steam Velocity: 2.0 (m/s)

Data #	Vw (m/s)	Tin (C)	Tout (C)	Ts (C)
1	1.16	21.63	24.04	48.48
2	1.16	21.63	24.05	48.53
3	1.49	21.43	23.55	48.46
4	1.49	21.43	23.56	48.41
5	1.97	21.25	23.12	48.43
6	1.97	21.25	23.13	48.49
7	2.51	21.13	22.80	48.48
8	2.51	21.13	22.80	48.47
9	3.00	21.05	22.57	48.44
10	3.00	21.05	22.57	48.43
11	3.43	21.00	22.42	48.47
12	3.43	21.00	22.42	48.50
13	3.86	20.96	22.28	48.50
14	3.86	20.96	22.28	48.52
15	4.40	20.91	22.14	48.46
16	4.40	20.91	22.14	48.48
17	1.16	21.70	24.21	48.48
18	1.16	21.70	24.19	48.46

File Name: L2STV70
Pressure Condition: Vacuum
Steam Velocity: 2.0 (m/s)

Data #	Vw (m/s)	Tin (C)	Tout (C)	Ts (C)
1	1.16	23.37	25.61	48.54
2	1.16	22.36	25.62	48.54
3	1.46	23.19	25.15	48.43
4	1.48	23.19	25.15	48.46
5	1.97	23.02	24.72	48.49
6	1.97	23.02	24.72	48.45
7	2.51	22.91	24.41	48.45
8	2.51	22.91	24.41	48.49
9	2.99	22.83	24.18	48.49
10	2.99	22.83	24.18	48.45
11	3.42	22.78	24.02	48.44
12	3.42	22.78	24.03	48.52
13	3.85	22.74	23.89	48.49
14	3.85	22.74	23.89	48.49
15	4.39	22.69	23.75	48.51
16	4.39	22.69	23.75	48.51
17	1.16	23.48	25.74	48.45
18	1.16	23.48	25.74	48.52

File Name: S1STA105
Pressure Condition: Atmospheric
Steam Velocity: 1.0 (m/s)

Data #	Vw (m/s)	Tin (C)	Tout (C)	Ts (C)
1	2.06	22.75	30.21	100.01
2	2.06	22.76	30.24	100.00
3	2.64	22.57	28.98	100.02
4	2.64	22.57	28.99	100.01
5	3.31	22.43	28.03	100.03
6	3.31	22.43	28.03	100.01
7	3.98	22.33	27.35	100.00
8	3.98	22.33	27.35	100.00
9	4.65	22.25	26.78	100.01
10	4.65	22.25	26.79	100.03
11	5.32	22.19	26.34	100.00
12	5.32	22.19	26.34	100.01
13	6.00	22.14	25.97	100.00
14	6.00	22.14	25.97	100.01
15	6.48	22.10	25.73	100.04
16	6.48	22.10	25.74	100.05
17	2.06	22.82	30.32	99.99
18	2.06	22.81	30.28	100.02

File Name: S2STA93
Pressure Condition: Atmospheric
Steam Velocity: 1.0 (m/s)

Data #	Vw (m/s)	Tin (C)	Tout (C)	Ts (C)
1	2.06	23.43	30.88	100.04
2	2.06	23.44	30.90	99.98
3	2.64	23.25	29.68	100.03
4	2.64	23.26	29.67	100.00
5	3.31	23.11	28.62	100.05
6	3.31	23.12	28.64	100.03
7	3.98	23.02	27.91	99.99
8	3.98	23.02	27.90	100.02
9	4.65	22.95	27.30	100.00
10	4.65	22.95	27.33	100.05
11	5.32	22.90	26.86	99.98
12	5.32	22.90	26.85	100.03
13	5.99	22.85	26.44	100.01
14	5.99	22.85	26.43	100.02
15	6.47	22.82	26.19	100.03
16	6.47	22.82	26.20	99.99
17	2.06	23.54	31.00	100.00
18	2.06	23.54	31.03	100.05

File Name: S3STA96
Pressure Condition: Atmospheric
Steam Velocity: 1.0 (m/s)

Data #	Vw (m/s)	Tin (C)	Tout (C)	Ts (C)
1	2.06	23.37	30.81	99.97
2	2.06	23.39	30.82	100.02
3	2.64	23.21	29.57	99.97
4	2.64	23.21	29.55	99.97
5	3.31	23.08	28.54	100.03
6	3.31	23.08	28.53	100.00
7	3.98	22.99	27.80	100.00
8	3.98	22.99	27.81	100.04
9	4.65	22.93	27.23	99.99
10	4.65	22.93	27.24	99.96
11	5.32	22.88	26.79	100.04
12	5.32	22.88	26.77	100.00
13	5.99	22.83	26.40	100.02
14	5.99	22.83	26.40	99.99
15	6.47	22.80	26.16	99.99
16	6.47	22.80	26.16	100.01
17	2.06	23.51	30.68	100.01
18	2.06	23.51	30.70	100.01

File Name: S4STA100
Pressure Condition: Atmospheric
Steam Velocity: 1.0 (m/s)

Data #	Vw (m/s)	Tin (C)	Tout (C)	Ts (C)
1	2.06	23.17	29.93	99.96
2	2.06	23.17	29.93	100.00
3	2.64	23.01	28.78	99.98
4	2.64	23.00	28.77	100.01
5	3.31	22.87	27.84	100.01
6	3.31	22.86	27.84	100.01
7	3.98	22.78	27.19	100.03
8	3.98	22.78	27.20	100.04
9	4.65	22.71	26.71	99.99
10	4.65	22.72	26.70	100.00
11	5.32	22.66	26.29	99.98
12	5.32	22.66	26.30	100.04
13	5.99	22.63	25.99	100.01
14	5.99	22.63	25.99	100.01
15	6.47	22.60	25.79	100.02
16	6.47	22.60	25.79	100.00
17	2.06	23.30	30.09	100.02
18	2.06	23.30	30.10	100.05

File Name: S6STA94
Pressure Condition: Atmospheric
Steam Velocity: 1.0 (m/s)

Data #	Vw (m/s)	Tin (C)	Tout (C)	Ts (C)
1	2.06	23.13	30.06	99.99
2	2.06	23.13	30.06	100.00
3	2.64	22.94	28.91	100.01
4	2.64	22.94	28.91	100.03
5	3.31	22.80	27.99	99.99
6	3.31	22.80	27.99	99.99
7	3.98	22.70	27.30	99.99
8	3.98	22.70	27.30	100.05
9	4.65	22.62	26.77	100.00
10	4.65	22.62	26.77	100.00
11	5.32	22.56	26.35	100.01
12	5.32	22.56	26.34	99.97
13	5.99	22.51	25.98	100.00
14	5.99	22.51	25.98	100.00
15	6.47	22.47	25.75	100.00
16	6.47	22.47	25.75	99.98
17	2.06	23.19	30.11	99.98
18	2.06	23.19	30.12	100.02

File Name: S6STA91
Pressure Condition: Atmospheric
Steam Velocity: 1.0 (m/s)

Data #	Vw (m/s)	Tin (C)	Tout (C)	Ts (C)
1	2.06	22.54	29.16	100.04
2	2.06	22.55	29.18	99.96
3	2.64	22.36	27.97	99.98
4	2.64	22.36	27.97	99.99
5	3.31	22.22	27.06	100.01
6	3.31	22.22	27.06	100.00
7	3.98	22.13	26.39	100.00
8	3.98	22.13	26.39	99.98
9	4.65	22.05	25.86	100.00
10	4.65	22.05	25.86	100.03
11	5.33	22.00	25.45	100.00
12	5.33	22.00	25.45	100.01
13	6.00	21.95	25.07	100.01
14	6.00	21.95	25.08	99.99
15	6.48	21.92	24.86	100.00
16	6.48	21.92	24.87	99.98
17	2.06	22.58	29.21	99.99
18	2.06	22.57	29.20	99.97

File Name: M1ASTA88
Pressure Condition: Atmospheric
Steam Velocity: 1.0 (m/s)

Data #	Vw (m/s)	Tin (C)	Tout (C)	Ts (C)
1	1.16	22.73	30.49	99.96
2	1.16	22.73	30.49	99.98
3	1.48	22.53	29.19	100.01
4	1.48	22.53	29.19	100.03
5	1.97	22.34	27.95	100.00
6	1.97	22.34	27.95	99.99
7	2.51	22.21	27.06	100.00
8	2.51	22.21	27.06	100.02
9	3.00	22.12	26.47	99.99
10	3.00	22.12	26.46	99.99
11	3.43	22.07	26.01	99.95
12	3.43	22.07	26.01	99.98
13	3.86	22.02	25.64	100.01
14	3.86	22.02	25.64	100.01
15	4.40	21.97	25.27	99.99
16	4.40	21.97	25.27	100.01
17	1.16	22.77	30.47	99.98
18	1.16	22.77	30.48	100.00

File Name: M4STA85
Pressure Condition: Atmospheric
Steam Velocity: 1.0 (m/s)

Data #	Vw (m/s)	Tin (C)	Tout (C)	Ts (C)
1	1.16	23.07	30.47	100.05
2	1.16	23.07	30.46	99.94
3	1.48	22.88	29.24	100.06
4	1.48	22.88	29.24	100.04
5	1.97	22.70	28.05	100.02
6	1.97	22.70	28.05	100.04
7	2.51	22.58	27.20	99.98
8	2.51	22.57	27.19	99.98
9	2.99	22.50	26.64	99.97
10	2.99	22.50	26.64	100.01
11	3.43	22.44	26.24	100.01
12	3.43	22.44	26.25	99.93
13	3.86	22.40	25.93	100.02
14	3.86	22.40	25.92	100.01
15	4.40	22.35	25.56	100.01
16	4.40	22.35	25.57	100.00
17	1.16	23.10	30.51	99.96
18	1.16	23.10	30.51	100.01

File Name: M6STA55
Pressure Condition: Atmospheric
Steam Velocity: 1.0 (m/s)

Data #	Vw (m/s)	Tin (C)	Tout (C)	Ts (C)
1	1.16	23.17	31.33	100.01
2	1.16	23.17	31.33	100.00
3	1.48	22.98	30.02	99.98
4	1.48	22.98	30.03	100.06
5	1.97	22.80	28.80	99.94
6	1.97	22.79	28.79	99.91
7	2.51	22.67	27.93	99.95
8	2.51	22.67	27.92	99.98
9	2.99	22.60	27.35	99.98
10	2.99	22.60	27.35	100.01
11	3.42	22.55	26.92	99.95
12	3.42	22.55	26.92	99.96
13	3.86	22.51	26.57	99.99
14	3.86	22.51	26.57	99.99
15	4.40	22.46	26.18	99.95
16	4.40	22.46	26.18	99.94
17	1.16	23.25	31.39	99.96
18	1.16	23.25	31.41	99.99

File Name: M7STA81
Pressure Condition: Atmospheric
Steam Velocity: 1.0 (m/s)

Data #	Vw (m/s)	Tin (C)	Tout (C)	Ts (C)
1	1.16	23.02	31.03	99.97
2	1.16	23.03	31.05	100.03
3	1.48	22.84	29.74	100.01
4	1.48	22.84	29.74	100.02
5	1.97	22.68	28.53	99.96
6	1.97	22.68	28.53	99.99
7	2.51	22.56	27.66	100.00
8	2.51	22.56	27.66	99.95
9	2.99	22.48	27.07	100.00
10	2.99	22.48	27.08	100.04
11	3.43	22.43	26.65	99.95
12	3.43	22.43	26.65	99.96
13	3.86	22.38	26.30	99.97
14	3.86	22.38	26.30	99.93
15	4.40	22.33	25.92	100.00
16	4.40	22.33	25.92	100.01
17	1.16	23.13	31.12	100.02
18	1.16	23.13	31.13	100.03

File Name: M8STA78
Pressure Condition: Atmospheric
Steam Velocity: 1.0 (m/s)

Data #	Uw (m/s)	Tin (C)	Tout (C)	Ts (C)
1	1.16	23.07	30.69	99.98
2	1.16	23.07	30.70	99.99
3	1.48	22.86	29.40	99.99
4	1.48	22.86	29.40	100.01
5	1.97	22.68	28.20	99.98
6	1.97	22.68	28.20	99.98
7	2.51	22.55	27.32	99.99
8	2.51	22.55	27.33	99.99
9	2.99	22.45	26.74	99.94
10	2.99	22.46	26.74	99.97
11	3.43	22.39	26.31	99.99
12	3.43	22.39	26.31	99.96
13	3.86	22.34	25.95	99.99
14	3.86	22.34	25.95	100.03
15	4.40	22.29	25.58	100.00
16	4.40	22.29	25.58	99.98
17	1.16	23.08	30.74	99.97
18	1.16	23.08	30.73	100.02

File Name: SMTHSTA65
Pressure Condition: Atmospheric
Steam Velocity: 1.0 (m/s)

Data #	Uw (m/s)	Tin (C)	Tout (C)	Ts (C)
1	1.16	23.11	28.32	100.01
2	1.16	23.11	28.32	99.98
3	1.48	22.91	27.28	99.98
4	1.48	22.91	27.29	99.99
5	1.97	22.72	26.28	100.00
6	1.97	22.72	26.28	99.96
7	2.51	22.58	25.53	99.99
8	2.51	22.58	25.54	99.98
9	2.99	22.49	25.07	99.96
10	2.99	22.49	25.05	99.99
11	3.42	22.43	24.71	99.99
12	3.42	22.43	24.72	99.98
13	3.86	22.38	24.44	99.99
14	3.86	22.37	24.43	100.02
15	4.40	22.32	24.14	99.96
16	4.40	22.32	24.14	100.02
17	1.16	23.10	28.31	99.98
18	1.16	23.10	28.29	99.97

File Name: L1STA73
Pressure Condition: Atmospheric
Steam Velocity: 1.0 (m/s)

Data #	Vw (m/s)	Tin (C)	Tout (C)	Ts (C)
1	1.16	21.85	29.90	99.99
2	1.16	21.86	29.89	100.02
3	1.49	21.67	28.64	99.99
4	1.49	21.67	28.64	100.04
5	1.97	21.50	27.45	99.97
6	1.97	21.50	27.45	100.05
7	2.51	21.38	26.59	99.97
8	2.51	21.38	26.60	100.02
9	3.00	21.31	26.02	99.98
10	3.00	21.31	26.03	100.01
11	3.43	21.27	25.61	100.00
12	3.43	21.27	25.61	100.03
13	3.86	21.22	25.25	99.95
14	3.86	21.23	25.25	99.96
15	4.40	21.18	24.85	100.01
16	4.40	21.18	24.85	100.00
17	1.16	21.97	30.00	100.01
18	1.16	21.97	30.00	100.00

File Name: L2STA71
Pressure Condition: Atmospheric
Steam Velocity: 1.0 (m/s)

Data #	Vw (m/s)	Tin (C)	Tout (C)	Ts (C)
1	1.16	23.81	31.35	99.97
2	1.16	23.82	31.38	99.98
3	1.48	23.65	30.24	100.01
4	1.48	23.65	30.24	99.97
5	1.97	23.50	29.18	100.00
6	1.97	23.50	29.18	99.96
7	2.51	23.39	28.41	99.99
8	2.51	23.40	28.42	100.01
9	2.99	23.34	27.90	100.03
10	2.99	23.34	27.90	99.99
11	3.42	23.30	27.51	100.02
12	3.42	23.31	27.51	99.99
13	3.85	23.27	27.18	100.01
14	3.85	23.27	27.18	99.99
15	4.39	23.23	26.82	99.99
16	4.39	23.23	26.82	99.95
17	1.16	24.05	31.61	99.97
18	1.16	24.04	31.61	99.98

File Name: L3STA69
Pressure Condition: Atmospheric
Steam Velocity: 1.0 (m/s)

Data #	Vw (m/s)	Tin (C)	Tout (C)	Ts (C)
1	1.16	23.53	31.66	99.93
2	1.16	23.53	31.65	99.97
3	1.48	23.33	30.34	99.98
4	1.48	23.33	30.34	99.98
5	1.97	23.15	29.12	99.98
6	1.97	23.15	29.12	99.96
7	2.51	23.02	28.24	99.98
8	2.51	23.02	28.24	99.96
9	2.99	22.95	27.65	99.94
10	2.99	22.94	27.65	99.98
11	3.42	22.89	27.22	100.01
12	3.42	22.89	27.22	99.97
13	3.85	22.84	26.86	99.95
14	3.85	22.84	26.86	99.96
15	4.39	22.79	26.46	99.98
16	4.39	22.79	26.47	100.00
17	1.16	23.58	31.57	99.96
18	1.16	23.58	31.57	100.00

File Name: L4STA65
Pressure Condition: Atmospheric
Steam Velocity: 1.0 (m/s)

Data #	Vw (m/s)	Tin (C)	Tout (C)	Ts (C)
1	1.16	22.82	31.15	99.98
2	1.16	22.83	31.15	99.95
3	1.48	22.62	29.78	99.98
4	1.48	22.62	29.78	99.96
5	1.97	22.44	28.58	99.95
6	1.97	22.44	28.58	100.00
7	2.51	22.31	27.70	99.93
8	2.51	22.31	27.70	99.95
9	3.00	22.23	27.13	99.96
10	3.00	22.23	27.13	100.01
11	3.43	22.18	26.68	99.97
12	3.43	22.18	26.69	100.01
13	3.86	22.13	26.32	99.98
14	3.86	22.13	26.32	99.97
15	4.40	22.08	25.93	99.99
16	4.40	22.08	25.93	100.01
17	1.16	22.89	31.13	99.98
18	1.16	22.85	31.14	99.96

File Name: L5STA62
Pressure Condition: Atmospheric
Steam Velocity: 1.0 (m/s)

Data #	Vw (m/s)	Tin (C)	Tout (C)	Ts (C)
1	1.16	24.32	32.45	99.98
2	1.16	24.34	32.47	99.96
3	1.48	24.15	31.17	99.98
4	1.48	24.15	31.17	99.94
5	1.97	23.98	29.99	99.95
6	1.97	23.98	30.00	100.03
7	2.50	23.86	29.12	99.99
8	2.50	23.86	29.13	99.95
9	2.99	23.78	28.55	99.96
10	2.99	23.79	28.56	99.99
11	3.42	23.74	28.13	100.00
12	3.42	23.74	28.14	99.96
13	3.85	23.69	27.77	99.99
14	3.85	23.69	27.76	99.95
15	4.39	23.64	27.37	99.96
16	4.39	23.64	27.38	99.95
17	1.16	24.43	32.51	99.98
18	1.16	24.43	32.51	100.02

File Name: L6STA57
Pressure Condition: Atmospheric
Steam Velocity: 1.0 (m/s)

Data #	Vw (m/s)	Tin (C)	Tout (C)	Ts (C)
1	1.16	25.00	32.98	99.97
2	1.16	25.17	33.16	99.96
3	1.16	25.20	33.19	99.99
4	1.48	25.05	31.93	99.97
5	1.48	25.08	31.96	99.99
6	1.96	25.01	30.90	99.95
7	1.96	25.02	30.90	99.98
8	2.50	24.91	30.07	99.93
9	2.50	24.92	30.07	99.89
10	2.98	24.87	29.54	99.94
11	2.98	24.87	29.54	99.96
12	3.41	24.83	29.15	99.96
13	3.41	24.83	29.15	99.96
14	3.84	24.80	28.82	99.96
15	3.84	24.79	28.82	100.02
16	4.38	24.75	28.46	99.98
17	4.38	24.74	28.45	99.98
18	1.16	25.51	33.49	99.96

File Name: S1RA13
Pressure Condition: Atmospheric
Vapor Velocity: .25 (m/s)

Data #	Vw (m/s)	Tin (C)	Tout (C)	Ts (C)
1	2.07	21.15	21.98	48.48
2	2.07	21.15	21.98	48.49
3	2.64	20.93	21.63	48.48
4	2.64	20.93	21.63	48.50
5	3.51	20.75	21.30	48.44
6	3.51	20.75	21.30	48.46
7	4.47	20.64	21.09	48.52
8	4.47	20.64	21.09	48.52
9	5.34	20.57	20.95	48.42
10	5.34	20.57	20.95	48.40
11	6.10	20.52	20.85	48.49
12	6.10	20.52	20.85	48.47
13	6.87	20.48	20.77	48.48
14	6.87	20.48	20.77	48.49
15	7.84	20.44	20.68	48.45
16	7.84	20.44	20.68	48.50
17	2.07	21.18	22.01	48.50
18	2.07	21.19	22.02	48.48

File Name: S2RA22
Pressure Condition: Atmospheric
Vapor Velocity: .25 (m/s)

Data #	Vw (m/s)	Tin (C)	Tout (C)	Ts (C)
1	2.07	21.67	22.57	48.41
2	2.07	21.67	22.57	48.41
3	2.64	21.47	22.22	48.42
4	2.64	21.47	22.22	48.45
5	3.51	21.29	21.90	48.42
6	3.51	21.29	21.90	48.41
7	4.47	21.17	21.67	48.45
8	4.47	21.17	21.67	48.45
9	5.33	21.10	21.52	48.46
10	5.33	21.10	21.53	48.44
11	6.10	21.04	21.42	48.46
12	6.10	21.05	21.43	48.44
13	6.87	21.00	21.33	48.44
14	6.87	21.00	21.34	48.44
15	7.83	20.96	21.24	48.42
16	7.83	20.96	21.24	48.44
17	2.07	21.68	22.58	48.44
18	2.07	21.68	22.58	48.44

File Name: S3RA15
Pressure Condition: Atmospheric
Vapor Velocity: .25 (m/s)

Data #	Vw (m/s)	Tin (C)	Tout (C)	Ts (C)
1	2.07	21.57	22.46	48.44
2	2.07	21.57	22.46	48.46
3	2.64	21.37	22.11	48.51
4	2.64	21.37	22.11	48.50
5	3.51	21.20	21.78	48.58
6	3.51	21.20	21.78	48.60
7	4.47	21.08	21.56	48.57
8	4.47	21.08	21.56	48.55
9	5.33	21.01	21.41	48.53
10	5.33	21.01	21.41	48.57
11	6.10	20.96	21.31	48.52
12	6.10	20.96	21.31	48.52
13	6.87	20.92	21.23	48.48
14	6.87	20.92	21.23	48.48
15	7.83	20.88	21.14	48.47
16	7.83	20.88	21.14	48.44
17	2.07	21.64	22.52	48.94
18	2.07	21.64	22.53	48.99

File Name: S4RA17
Pressure Condition: Atmospheric
Vapor Velocity: .25 (m/s)

Data #	Vw (m/s)	Tin (C)	Tout (C)	Ts (C)
1	2.06	21.97	22.79	48.41
2	2.06	21.96	22.78	48.42
3	2.64	21.70	22.39	48.44
4	2.64	21.70	22.38	48.41
5	3.51	21.48	22.03	48.40
6	3.51	21.48	22.03	48.36
7	4.47	21.32	21.76	48.35
8	4.47	21.32	21.76	48.28
9	5.33	21.18	21.55	48.51
10	5.33	21.18	21.55	48.42
11	6.10	21.06	21.38	48.30
12	6.10	21.06	21.38	48.26
13	6.87	20.94	21.22	48.30
14	6.87	20.94	21.22	48.37
15	7.83	20.85	21.09	48.55
16	7.83	20.85	21.08	48.40
17	2.07	21.56	22.37	48.69
18	2.07	21.55	22.37	48.75

File Name: S5RA18
Pressure Condition: Atmospheric
Vapor Velocity: .25 (m/s)

Data #	Vw (m/s)	Tin (C)	Tout (C)	Ts (C)
1	2.07	21.22	22.00	48.48
2	2.07	21.22	22.00	48.48
3	2.64	21.01	21.66	48.54
4	2.64	21.01	21.66	48.53
5	3.51	20.82	21.33	48.48
6	3.51	20.82	21.33	48.51
7	4.47	20.71	21.12	48.42
8	4.47	20.71	21.12	48.43
9	5.34	20.63	20.97	48.43
10	5.34	20.63	20.97	48.46
11	6.10	20.58	20.87	48.43
12	6.10	20.58	20.87	48.43
13	6.87	20.54	20.79	48.40
14	6.87	20.54	20.80	48.44
15	7.83	20.50	20.71	48.36
16	7.83	20.50	20.71	48.36
17	2.07	21.24	22.02	48.61
18	2.07	21.24	22.02	48.59

File Name: S6RA18
Pressure Condition: Atmospheric
Vapor Velocity: .25 (m/s)

Data #	Vw (m/s)	Tin (C)	Tout (C)	Ts (C)
1	2.07	21.47	22.08	48.40
2	2.07	21.46	22.07	48.41
3	2.64	21.21	21.70	48.42
4	2.64	21.21	21.70	48.42
5	3.51	20.93	21.36	48.39
6	3.51	20.98	21.36	48.35
7	4.47	20.83	21.13	48.37
8	4.47	20.83	21.14	48.41
9	5.33	20.75	21.00	48.48
10	5.33	20.75	21.00	48.50
11	6.10	20.69	20.90	48.65
12	6.10	20.69	20.90	48.65
13	6.87	20.64	20.82	48.56
14	6.87	20.64	20.82	48.61
15	7.83	20.59	20.74	48.34
16	7.83	20.59	20.74	48.33
17	2.07	21.34	21.94	48.58
18	2.07	21.35	21.94	48.66

File Name: M8RA05
Pressure Condition: Atmospheric
Vapor Velocity: .25 (m/s)

Data #	Vw (m/s)	Tin (C)	Tout (C)	Ts (C)
1	1.16	20.51	21.22	48.65
2	1.16	20.51	21.22	48.60
3	1.49	20.30	20.89	48.56
4	1.49	20.30	20.89	48.58
5	1.98	20.11	20.59	48.54
6	1.98	20.11	20.59	48.55
7	2.52	20.00	20.39	48.48
8	2.52	20.00	20.40	48.52
9	3.00	19.93	20.28	48.50
10	3.00	19.94	20.28	48.47
11	3.44	19.89	20.20	48.52
12	3.44	19.89	20.20	48.51
13	3.87	19.92	20.20	48.57
14	3.87	19.93	20.20	48.56
15	4.41	19.90	20.15	48.56
16	4.41	19.90	20.15	48.55
17	1.16	20.70	21.40	48.48
18	1.16	20.70	21.41	48.46

File Name: M1ARA117
Pressure Condition: Atmospheric
Vapor Velocity: .25 (m/s)

Data #	Vw (m/s)	Tin (C)	Tout (C)	Ts (C)
1	1.16	21.91	22.60	48.42
2	1.16	21.91	22.61	48.45
3	1.49	21.71	22.30	48.43
4	1.49	21.71	22.30	48.44
5	1.97	21.53	21.99	48.46
6	1.97	21.52	22.00	48.48
7	2.51	21.40	21.79	48.48
8	2.51	21.40	21.79	48.44
9	3.00	21.32	21.66	48.43
10	3.00	21.32	21.66	48.43
11	3.43	21.26	21.56	48.44
12	3.43	21.26	21.56	48.42
13	3.86	21.21	21.48	48.43
14	3.86	21.21	21.49	48.42
15	4.40	21.16	21.41	48.43
16	4.40	21.16	21.41	48.44
17	1.16	21.88	22.62	48.40
18	1.16	21.88	22.61	48.37

File Name: M5RA03A
Pressure Condition: Atmospheric
Vapor Velocity: .25 (m/s)

Data #	Vw (m/s)	Tin (C)	Tout (C)	Ts (C)
1	1.16	20.37	21.28	48.54
2	1.16	20.37	21.28	48.54
3	1.49	20.16	20.94	48.53
4	1.49	20.16	20.95	48.51
5	1.98	19.96	20.60	48.39
6	1.98	19.96	20.61	48.39
7	2.52	19.83	20.37	48.34
8	2.52	19.83	20.37	48.32
9	3.01	19.74	20.22	48.40
10	3.01	19.74	20.22	48.46
11	3.44	19.69	20.12	48.51
12	3.44	19.69	20.12	48.54
13	3.87	19.64	20.04	48.56
14	3.87	19.64	20.04	48.55
15	4.41	19.60	19.95	48.56
16	4.41	19.60	19.95	48.56
17	1.16	20.36	21.28	48.52
18	1.16	20.36	21.28	48.60

File Name: M5RA04
Pressure Condition: Atmospheric
Vapor Velocity: .25 (m/s)

Data #	Vw (m/s)	Tin (C)	Tout (C)	Ts (C)
1	1.16	20.98	21.82	48.55
2	1.16	20.97	21.81	48.54
3	1.49	20.76	21.47	48.53
4	1.49	20.75	21.46	48.54
5	1.97	20.55	21.14	48.47
6	1.97	20.54	21.13	48.44
7	2.52	20.40	20.89	48.51
8	2.52	20.39	20.89	48.53
9	3.00	20.28	20.71	48.54
10	3.00	20.28	20.71	48.58
11	3.44	20.21	20.60	48.56
12	3.44	20.21	20.60	48.55
13	3.87	20.15	20.50	48.61
14	3.87	20.15	20.50	48.62
15	4.41	20.09	20.40	48.50
16	4.41	20.09	20.40	48.52
17	1.16	20.82	21.66	48.49
18	1.16	20.82	21.66	48.57

File Name: M4RA01
Pressure Condition: Atmospheric
Vapor Velocity: .25 (m/s)

Data #	Vw (m/s)	Tin (C)	Tout (C)	Ts (C)
1	1.17	19.16	20.18	48.47
2	1.17	19.16	20.18	48.47
3	1.49	18.94	19.83	48.45
4	1.49	18.94	19.83	48.44
5	1.98	18.75	19.50	48.34
6	1.98	18.74	19.49	48.33
7	2.52	18.61	19.25	48.31
8	2.52	18.61	19.25	48.30
9	3.01	18.53	19.10	48.39
10	3.01	18.53	19.10	48.39
11	3.45	18.47	18.99	48.37
12	3.45	18.47	18.99	48.39
13	3.88	18.43	18.90	48.34
14	3.88	18.43	18.90	48.32
15	4.42	18.39	18.81	48.36
16	4.42	18.38	18.81	48.39
17	1.17	19.16	20.19	48.51
18	1.17	19.16	20.19	48.48

File Name: M5RA02A
Pressure Condition: Atmospheric
Vapor Velocity: .25 (m/s)

Data #	Vw (m/s)	Tin (C)	Tout (C)	Ts (C)
1	1.17	19.62	20.58	48.32
2	1.17	19.62	20.57	48.51
3	1.49	19.40	20.21	48.29
4	1.49	19.40	20.22	48.29
5	1.98	19.21	19.88	48.31
6	1.98	19.20	19.87	48.38
7	2.52	19.08	19.65	48.33
8	2.52	19.08	19.65	48.48
9	3.01	19.00	19.50	48.28
10	3.01	19.00	19.49	48.28
11	3.44	18.95	19.40	48.39
12	3.44	18.95	19.40	48.51
13	3.88	18.90	19.31	48.61
14	3.88	18.90	19.31	48.53
15	4.42	18.86	19.22	48.25
16	4.42	18.86	19.23	48.22
17	1.17	19.63	20.59	48.52
18	1.17	19.63	20.59	48.44

File Name: RSMTH1
Pressure Condition: Atmospheric
Vapor Velocity: .25 (m/s)

Data #	Vw (m/s)	Tin (C)	Tout (C)	Ts (C)
1	1.17	19.74	20.07	48.31
2	1.17	19.73	20.06	48.22
3	1.49	19.51	19.78	48.50
4	1.49	19.50	19.78	48.55
5	1.98	19.30	19.51	48.45
6	1.98	19.30	19.51	48.32
7	2.52	19.14	19.31	48.60
8	2.52	19.13	19.31	48.57
9	3.01	19.04	19.19	48.50
10	3.01	19.04	19.19	48.48
11	3.44	18.98	19.11	48.46
12	3.44	18.98	19.11	48.42
13	3.88	18.92	19.04	48.47
14	3.88	18.93	19.04	48.47
15	3.88	18.92	19.04	48.43
16	4.42	18.87	18.97	48.45
17	4.42	18.87	18.97	48.52
18	1.17	19.64	19.98	48.58

File Name: RSMTH2
Pressure Condition: Atmospheric
Vapor Velocity: .25 (m/s)

Data #	Vw (m/s)	Tin (C)	Tout (C)	Ts (C)
1	1.17	19.83	20.17	48.35
2	1.17	19.83	20.17	48.39
3	1.49	19.60	19.87	48.44
4	1.49	19.60	19.87	48.45
5	1.98	19.39	19.61	48.44
6	1.98	19.39	19.60	48.43
7	2.52	19.25	19.42	48.43
8	2.52	19.25	19.42	48.46
9	3.01	19.15	19.31	48.42
10	3.01	19.16	19.31	48.48
11	3.44	19.09	19.23	48.45
12	3.44	19.09	19.22	48.44
13	3.88	19.04	19.16	48.45
14	3.88	19.04	19.16	48.45
15	4.42	19.00	19.10	48.48
16	4.42	18.99	19.10	48.45
17	1.17	19.75	20.09	48.38
18	1.17	19.75	20.09	48.35

File Name: L1RA08
Pressure Condition: Atmospheric
Vapor Velocity: .25 (m/s)

Data #	Vw (m/s)	Tin (C)	Tout (C)	Ts (C)
1	1.16	20.81	21.95	48.34
2	1.16	20.81	21.94	48.38
3	1.49	20.58	21.54	48.45
4	1.49	20.58	21.55	48.43
5	1.98	20.39	21.19	48.37
6	1.98	20.38	21.18	48.34
7	2.52	20.24	20.91	48.33
8	2.52	20.24	20.91	48.33
9	3.00	20.15	20.74	48.43
10	3.00	20.15	20.74	48.44
11	3.44	20.08	20.62	48.43
12	3.44	20.08	20.62	48.47
13	3.87	20.03	20.52	48.45
14	3.87	20.03	20.52	48.42
15	4.41	19.98	20.42	48.31
16	4.41	19.97	20.41	48.34
17	1.16	20.75	21.87	48.46
18	1.16	20.75	21.87	48.47

File Name: L2RA11
Pressure Condition: Atmospheric
Vapor Velocity: .25 (m/s)

Data #	Vw (m/s)	Tin (C)	Tout (C)	Ts (C)
1	1.16	21.89	22.96	48.45
2	1.16	21.89	22.96	48.55
3	1.49	21.69	22.63	48.62
4	1.49	21.69	22.63	48.62
5	1.97	21.51	22.31	48.54
6	1.97	21.51	22.31	48.56
7	2.51	21.40	22.09	48.43
8	2.51	21.40	22.08	48.43
9	3.00	21.32	21.94	48.50
10	3.00	21.32	21.93	48.46
11	3.43	21.27	21.83	48.39
12	3.43	21.27	21.83	48.37
13	3.86	21.23	21.74	48.56
14	3.86	21.23	21.75	48.60
15	4.40	21.19	21.65	48.39
16	4.40	21.19	21.65	48.41
17	1.16	21.94	23.01	48.43
18	1.16	21.95	23.01	48.45

File Name: L3RA12
Pressure Condition: Atmospheric
Vapor Velocity: .25 (m/s)

Date #	Vw (m/s)	Tin (C)	Tout (C)	Ts (C)
1	1.16	21.83	22.88	48.44
2	1.16	21.83	22.89	48.44
3	1.49	21.61	22.51	48.42
4	1.49	21.61	22.51	48.44
5	1.97	21.42	22.17	48.48
6	1.97	21.42	22.18	48.45
7	2.51	21.29	21.93	48.36
8	2.51	21.29	21.93	48.35
9	3.00	21.21	21.78	48.45
10	3.00	21.21	21.78	48.46
11	3.43	21.16	21.67	48.41
12	3.43	21.16	21.67	48.43
13	3.86	21.11	21.58	48.46
14	3.86	21.11	21.58	48.44
15	4.40	21.07	21.49	48.33
16	4.40	21.07	21.49	48.29
17	1.16	21.81	22.86	48.45
18	1.16	21.81	22.86	48.40

File Name: L4RA07
Pressure Condition: Atmospheric
Vapor Velocity: .25 (m/s)

Date #	Vw (m/s)	Tin (C)	Tout (C)	Ts (C)
1	1.16	21.82	22.87	48.44
2	1.16	21.81	22.86	48.43
3	1.49	21.59	22.49	48.42
4	1.49	21.58	22.49	48.40
5	1.97	21.39	22.13	48.36
6	1.97	21.39	22.14	48.40
7	2.51	21.23	21.86	48.51
8	2.51	21.23	21.86	48.55
9	3.00	21.13	21.69	48.48
10	3.00	21.13	21.68	48.44
11	3.43	21.06	21.57	48.39
12	3.43	21.06	21.56	48.39
13	3.86	21.00	21.46	48.38
14	3.86	21.00	21.46	48.35
15	4.40	20.94	21.36	48.35
16	4.40	20.94	21.35	48.42
17	1.16	21.66	22.70	48.46
18	1.16	21.65	22.70	48.46

File Name: L5RA09
Pressure Condition: Atmospheric
Vapor Velocity: .25 (m/s)

Data #	Vw (m/s)	Tin (C)	Tout (C)	Ts (C)
1	1.16	21.17	22.17	48.45
2	1.16	21.17	22.17	48.43
3	1.49	20.95	21.81	48.31
4	1.49	20.95	21.80	48.32
5	1.97	20.79	21.51	48.36
6	1.97	20.79	21.51	48.34
7	2.51	20.68	21.30	48.46
8	2.51	20.69	21.30	48.45
9	3.00	20.62	21.16	48.47
10	3.00	20.62	21.17	48.48
11	3.43	20.59	21.08	48.44
12	3.43	20.59	21.08	48.44
13	3.87	20.55	21.00	48.37
14	3.87	20.55	21.00	48.37
15	4.41	20.51	20.92	48.44
16	4.41	20.51	20.92	48.44
17	1.16	21.27	22.27	48.44
18	1.16	21.27	22.27	48.44

File Name: L6RA10
Pressure Condition: Atmospheric
Vapor Velocity: .25 (m/s)

Data #	Vw (m/s)	Tin (C)	Tout (C)	Ts (C)
1	1.16	21.16	21.99	48.41
2	1.16	21.15	21.98	48.44
3	1.49	20.92	21.62	48.44
4	1.49	20.91	21.61	48.48
5	1.97	20.70	21.27	48.36
6	1.97	20.70	21.27	48.34
7	2.51	20.58	21.06	48.40
8	2.51	20.58	21.06	48.35
9	3.00	20.53	20.95	48.36
10	3.00	20.53	20.95	48.36
11	3.43	20.50	20.87	48.41
12	3.43	20.50	20.88	48.42
13	3.87	20.49	20.83	48.48
14	3.87	20.49	20.83	48.51
15	4.41	20.46	20.76	48.48
16	4.41	20.46	20.76	48.48
17	1.16	21.24	22.06	48.40
18	1.16	21.24	22.06	48.40

File Name: M1AEGV45
Pressure Condition: Vacuum
Vapor Velocity: 10.0 (m/s)

Data #	Vw (m/s)	Tin (C)	Tout (C)	Ts (C)
1	1.70	22.12	24.63	127.86
2	1.70	22.12	24.65	127.88
3	2.13	22.00	24.06	127.92
4	2.13	22.00	24.07	127.91
5	2.51	21.92	23.71	127.93
6	2.51	21.92	23.71	127.90
7	2.89	21.87	23.44	127.87
8	2.89	21.87	23.45	127.88
9	3.32	21.82	23.21	127.97
10	3.32	21.82	23.21	127.96
11	3.59	21.79	23.08	127.94
12	3.59	21.79	23.09	127.98
13	3.86	21.77	22.98	127.93
14	3.86	21.77	22.98	127.91
15	4.40	21.73	22.79	127.91
16	4.40	21.73	22.79	127.90
17	1.70	22.17	24.68	127.96
18	1.70	22.17	24.68	127.94

File Name: M4EGV39
Pressure Condition: Vacuum
Vapor Velocity: 10.0 (m/s)

Data #	Vw (m/s)	Tin (C)	Tout (C)	Ts (C)
1	2.24	21.38	24.52	127.91
2	2.24	21.38	24.51	127.95
3	2.57	21.31	24.11	127.93
4	2.57	21.31	24.13	127.91
5	2.89	21.25	23.80	127.93
6	2.89	21.25	23.80	127.83
7	3.21	21.20	23.52	127.92
8	3.21	21.20	23.50	127.97
9	3.59	21.16	23.26	127.92
10	3.59	21.15	23.25	127.99
11	3.97	21.12	23.04	127.93
12	3.97	21.12	23.05	128.00
13	4.30	21.09	22.88	127.91
14	4.30	21.09	22.88	127.87
15	4.67	21.06	22.71	127.91
16	4.67	21.05	22.70	127.93
17	2.24	21.34	24.46	127.93
18	2.24	21.34	24.44	127.88

File Name: M5EGV34
Pressure Condition: Vacuum
Vapor Velocity: 10.0 (m/s)

Data #	Vw (m/s)	Tin (C)	Tout (C)	Ts (C)
1	2.79	20.46	23.23	127.79
2	2.79	20.45	23.22	127.79
3	3.11	20.40	22.96	127.78
4	3.11	20.40	22.97	127.84
5	3.44	20.36	22.75	127.81
6	3.44	20.36	22.74	127.85
7	3.76	20.33	22.55	127.80
8	3.76	20.33	22.56	127.79
9	4.19	20.29	22.34	127.80
10	4.19	20.29	22.34	127.78
11	4.63	20.26	22.15	127.79
12	4.63	20.26	22.15	127.82
13	5.06	20.23	21.99	127.84
14	5.06	20.23	21.99	127.82
15	5.38	20.21	21.87	127.80
16	5.38	20.21	21.89	127.81
17	2.79	20.45	23.24	127.75
18	2.79	20.45	23.24	127.78

File Name: M6EGV40
Pressure Condition: Vacuum
Vapor Velocity: 10.0 (m/s)

Data #	Vw (m/s)	Tin (C)	Tout (C)	Ts (C)
1	2.24	21.42	24.55	127.90
2	2.24	21.43	24.56	127.92
3	2.57	21.39	24.18	127.92
4	2.57	21.40	24.16	127.97
5	2.89	21.36	23.89	127.87
6	2.89	21.36	23.89	127.86
7	3.21	21.34	23.66	127.90
8	3.21	21.34	23.68	127.91
9	3.59	21.31	23.43	127.89
10	3.59	21.31	23.43	127.91
11	3.97	21.29	23.24	127.85
12	3.97	21.29	23.24	127.84
13	4.29	21.28	23.10	127.91
14	4.29	21.28	23.10	127.95
15	4.67	21.26	22.96	127.91
16	4.67	21.26	22.96	127.86
17	2.24	21.57	24.69	127.92
18	2.24	21.57	24.70	127.89

File Name: M7E6V41
Pressure Condition: Vacuum
Vapor Velocity: 10.0 (m/s)

Data #	Vw (m/s)	Tin (C)	Tout (C)	Ts (C)
1	2.24	21.51	24.35	128.00
2	2.24	21.51	24.36	127.97
3	2.57	21.45	24.00	127.97
4	2.57	21.45	24.01	128.03
5	2.89	21.40	23.72	127.96
6	2.89	21.40	23.73	127.99
7	3.21	21.35	23.49	127.96
8	3.21	21.35	23.50	127.99
9	3.59	21.31	23.26	128.01
10	3.59	21.31	23.27	127.99
11	3.97	21.28	23.06	127.98
12	3.97	21.28	23.08	127.99
13	4.29	21.25	22.92	127.93
14	4.29	21.25	22.92	127.97
15	4.67	21.22	22.79	128.00
16	4.67	21.22	22.79	127.95
17	2.24	21.52	24.39	127.97
18	2.24	21.52	24.39	127.97

File Name: M8E6V42
Pressure Condition: Vacuum
Vapor Velocity: 10.0 (m/s)

Data #	Vw (m/s)	Tin (C)	Tout (C)	Ts (C)
1	2.24	21.48	23.79	127.97
2	2.24	21.50	23.82	127.98
3	2.57	21.47	23.53	127.92
4	2.57	21.47	23.53	127.91
5	2.89	21.43	23.30	127.92
6	2.89	21.43	23.31	127.94
7	3.21	21.40	23.12	127.99
8	3.21	21.40	23.11	127.96
9	3.59	21.36	22.93	128.02
10	3.59	21.36	22.92	128.00
11	3.97	21.33	22.77	127.94
12	3.97	21.33	22.76	127.90
13	4.29	21.31	22.65	127.91
14	4.29	21.31	22.65	127.93
15	4.67	21.29	22.54	127.93
16	4.67	21.29	22.53	127.93
17	2.24	21.59	23.95	127.98
18	2.24	21.60	23.96	127.90

File Name: M1EGV37
Pressure Condition: Vacuum
Vapor Velocity: 10.0 (m/s)

Data #	Vw (m/s)	Tin (C)	Tout (C)	Ts (C)
1	1.16	22.43	25.23	127.78
2	1.16	22.45	25.27	127.83
3	1.48	22.28	24.56	127.85
4	1.48	22.28	24.57	127.83
5	1.97	22.12	23.91	127.79
6	1.97	22.12	23.91	127.78
7	2.51	22.01	23.45	127.82
8	2.51	22.02	23.47	127.83
9	3.00	21.95	23.18	127.84
10	3.00	21.95	23.19	127.82
11	3.43	21.91	23.00	127.80
12	3.43	21.91	23.00	127.79
13	3.85	21.87	22.85	127.83
14	3.85	21.87	22.85	127.82
15	4.40	21.84	22.69	127.78
16	4.40	21.84	22.70	127.81
17	1.16	22.57	25.41	127.76
18	1.16	22.57	25.40	127.76

File Name: L1EG53
Pressure Condition: Vacuum
Vapor Velocity: 10.0 (m/s)

Date #	Vw (m/s)	Tin (C)	Tout (C)	Ts (C)
1	1.70	22.72	25.76	127.99
2	1.70	22.71	25.77	127.99
3	2.13	22.57	25.10	127.93
4	2.13	22.58	25.09	127.91
5	2.51	22.48	24.67	127.98
6	2.51	22.48	24.68	128.05
7	2.89	22.41	24.35	127.98
8	2.89	22.41	24.36	128.05
9	3.32	22.35	24.07	127.99
10	3.32	22.35	24.08	128.05
11	3.59	22.32	23.93	127.99
12	3.59	22.32	23.93	127.96
13	3.86	22.29	23.79	128.00
14	3.86	22.28	23.79	127.97
15	4.40	22.25	23.57	128.01
16	4.40	22.25	23.57	127.91
17	1.70	22.70	25.79	128.03
18	1.70	22.70	25.79	127.97

File Name: L2EG46
Pressure Condition: Vacuum
Vapor Velocity: 10.0 (m/s)

Date #	Vw (m/s)	Tin (C)	Tout (C)	Ts (C)
1	1.70	22.21	26.12	127.97
2	1.70	22.21	26.14	128.12
3	2.13	22.08	25.36	127.99
4	2.13	22.08	25.37	128.06
5	2.51	21.99	24.91	128.07
6	2.51	21.99	24.91	128.00
7	2.89	21.93	24.57	128.05
8	2.89	21.93	24.56	127.98
9	3.32	21.88	24.25	128.05
10	3.32	21.88	24.25	128.07
11	3.59	21.85	24.06	127.99
12	3.59	21.85	24.07	128.03
13	3.86	21.82	23.91	128.03
14	3.86	21.82	23.90	128.08
15	4.40	21.78	23.64	128.03
16	4.40	21.78	23.65	128.03
17	1.70	22.23	26.16	128.03
18	1.70	22.22	26.15	128.00

File Name: L3EG51
Pressure Condition: Vacuum
Vapor Velocity: 10.0 (m/s)

Data #	Vw (m/s)	Tin (C)	Tout (C)	Ts (C)
1	1.70	23.17	27.31	128.03
2	1.70	23.18	27.35	128.03
3	2.13	23.04	26.52	128.02
4	2.13	23.05	26.52	128.05
5	2.51	22.97	26.05	128.01
6	2.51	22.97	26.06	128.08
7	2.88	22.91	25.73	128.00
8	2.88	22.91	25.73	127.99
9	3.31	22.86	25.40	128.05
10	3.31	22.86	25.40	128.03
11	3.58	22.84	25.24	128.04
12	3.58	22.84	25.25	128.00
13	3.85	22.81	25.08	128.04
14	3.85	22.81	25.08	127.91
15	4.39	22.77	24.82	128.01
16	4.39	22.77	24.83	128.01
17	1.70	23.21	27.38	127.95
18	1.70	23.21	27.37	127.97

File Name: L4EG50
Pressure Condition: Vacuum
Vapor Velocity: 10.0 (m/s)

Data #	Vw (m/s)	Tin (C)	Tout (C)	Ts (C)
1	1.70	23.00	26.90	128.02
2	1.70	23.02	26.97	128.00
3	2.13	22.90	26.22	128.05
4	2.13	22.90	26.20	128.03
5	2.51	22.82	25.74	127.97
6	2.51	22.82	25.75	128.02
7	2.88	22.77	25.43	128.01
8	2.88	22.77	25.43	127.94
9	3.32	22.72	25.13	128.00
10	3.32	22.72	25.13	127.98
11	3.58	22.70	24.96	127.93
12	3.58	22.70	24.97	127.99
13	3.85	22.68	24.82	128.02
14	3.85	22.68	24.83	127.98
15	4.39	22.64	24.57	127.97
16	4.39	22.64	24.57	128.06
17	1.70	23.08	27.08	128.01
18	1.70	23.08	27.06	128.02

File Name: L5E648
Pressure Condition: Vacuum
Vapor Velocity: 10.0 (m/s)

Data #	Vw (m/s)	Tin (C)	Tout (C)	Ts (C)
1	1.70	22.82	26.55	128.03
2	1.70	22.82	26.55	127.99
3	2.13	22.69	25.81	127.93
4	2.13	22.68	25.82	127.96
5	2.51	22.60	25.38	127.98
6	2.51	22.60	25.40	128.01
7	2.89	22.54	25.04	128.01
8	2.89	22.54	25.04	128.00
9	3.32	22.48	24.74	127.96
10	3.32	22.49	24.73	127.98
11	3.59	22.46	24.58	128.01
12	3.59	22.46	24.58	127.95
13	3.86	22.43	24.43	127.97
14	3.86	22.43	24.44	128.07
15	4.39	22.39	24.18	128.00
16	4.39	22.39	24.18	127.94
17	1.70	22.84	26.56	127.94
18	1.70	22.84	26.54	127.98

File Name: L5E647
Pressure Condition: Vacuum
Vapor Velocity: 10.0 (m/s)

Data #	Vw (m/s)	Tin (C)	Tout (C)	Ts (C)
1	1.70	22.58	25.90	127.98
2	1.70	22.58	25.92	128.03
3	2.13	22.46	25.24	127.92
4	2.13	22.46	25.24	127.97
5	2.51	22.39	24.83	127.99
6	2.51	22.39	24.81	127.94
7	2.89	22.34	24.52	127.95
8	2.89	22.34	24.54	127.93
9	3.32	22.30	24.26	127.94
10	3.32	22.30	24.25	127.98
11	3.59	22.27	24.09	127.96
12	3.59	22.27	24.10	128.03
13	3.86	22.25	23.97	127.96
14	3.86	22.25	23.97	127.87
15	4.40	22.22	23.75	127.96
16	4.40	22.22	23.75	127.93
17	1.70	22.67	26.00	127.94
18	1.70	22.67	26.01	127.98

File Name: Q1RA20
Pressure Condition: Atmospheric
Vapor Velocity: .25 (m/s)

Data #	Vw (m/s)	Tin (C)	Tout (C)	Ts (C)
1	2.07	21.61	22.63	48.52
2	2.07	21.61	22.63	48.54
3	2.64	21.43	22.31	48.60
4	2.64	21.43	22.30	48.56
5	3.51	21.26	21.97	48.51
6	3.51	21.26	21.96	48.54
7	4.47	21.15	21.73	48.48
8	4.47	21.15	21.73	48.42
9	5.33	21.09	21.58	48.45
10	5.33	21.09	21.58	48.41
11	6.10	21.06	21.49	48.51
12	6.10	21.06	21.49	48.46
13	6.87	21.02	21.40	48.43
14	6.87	21.02	21.41	48.41
15	7.83	20.98	21.31	48.35
16	7.83	20.98	21.31	48.39
17	2.07	21.75	22.76	48.74
18	2.07	21.75	22.76	48.77

File Name: QSTA106
Pressure Condition: Atmospheric
Steam Velocity: 1.0 (m/s)

Data #	Vw (m/s)	Tin (C)	Tout (C)	Ts (C)
1	2.06	22.96	30.66	100.03
2	2.06	22.96	30.68	99.98
3	2.64	22.77	29.48	100.01
4	2.64	22.77	29.48	100.05
5	3.31	22.63	28.55	99.99
6	3.31	22.63	28.55	100.02
7	3.98	22.53	27.85	100.03
8	3.98	22.54	27.86	100.01
9	4.65	22.46	27.31	100.02
10	4.65	22.46	27.32	100.06
11	5.32	22.40	26.88	100.00
12	5.32	22.40	26.88	100.00
13	5.99	22.35	26.50	100.02
14	5.99	22.35	26.52	100.02
15	6.47	22.33	26.30	100.00
16	6.47	22.33	26.30	100.01
17	2.06	23.05	30.88	100.03
18	2.06	23.05	30.87	99.98

APPENDIX B

UNCERTAINTY ANALYSIS

When measuring a physical quantity, there will always be a difference between its actual value and the measured value. The best estimate of this difference is defined as uncertainty of the measured value. The uncertainty depends on equipment calibration and accuracy as well as the operator. Although an uncertainty for a single measurement might be very small, an equation or data reduction that combines two or more measurements may generate results with rather large uncertainties. The uncertainties of the physical quantities in this investigation are combined using an equation suggested by Kline and Mclintok [Ref. 31].

$$W_r = \left[\left(\frac{\partial r}{\partial x_1} W_1 \right)^2 + \left(\frac{\partial r}{\partial x_2} W_2 \right)^2 + \ldots\ldots + \left(\frac{\partial r}{\partial x_n} W_n \right)^2 \right]^{0.5} \qquad (B.1)$$

where

W_r = uncertainty of the desired dependent variable,

x_n = the measured variables, and

W_n = the uncertainties in the measured variables.

A program, designed by Mitrou [Ref. 10] to compute the uncertainties of the modified Wilson plot technique, was used in this investigation. Slight modifications were made to include the difference inside diameters and the testing of ethylene glycol.

The following equation was used to compute the uncertainties on the the enhancements.

$$W_e = \frac{\left[\left(\frac{1}{W_{rsm}}\right)^2 + \left(\frac{1}{W_{rfm}}\right)^2\right]^{-0.5} + \left[\left(\frac{1}{W_{rsmn}}\right)^2 + \left(\frac{1}{W_{sfmn}}\right)^2\right]^{-0.5}}{2} \qquad (B.2)$$

where

W_e = uncertainty in enhancement for finned tube,

W_{rsm} = uncertainty of outside heat-transfer coefficient for a smooth tube at maximum flow rate,

W_{rsmn} = uncertainty of outside heat-transfer coefficient for a smooth tube at minimum flow rate,

W_{rfm} = uncertainty of outside heat-transfer coefficient for a finned tube at maximum flow rate, and

W_{rfmn} = uncertainty of outside heat-transfer coefficient for a finned tube at minimum flow rate.

The following are examples of the uncertainties.

DATA FOR THE UNCERTAINTY ANALYSIS:

File Name:	S4RA17		
Pressure Condition:	Atmospheric (101 kPa)		
Vapor Temperature	=	48.42	(Deg C)
Water Flow Rate (%)	=	20.00	
Water Velocity	=	2.05	(m/s)
Heat Flux	=	6.333E+04	(W/m^2)
Tube-metal thermal conduc.	=	385.0	(W/m.K)
Sieder-Tate constant	=	0.0300	

UNCERTAINTY ANALYSIS:

VARIABLE	PERCENT UNCERTAINTY
Mass Flow Rate, Md	3.00
Reynolds Number, Re	3.12
Heat Flux, q	3.15
Log-Mean-Tem Diff, LMTD	.86
Wall Resistance, Rw	2.63
Overall H.T.C., Uo	3.27
Water-Side H.T.C., Hi	7.13
Vapor-Side H.T.C., Ho	8.25

DATA FOR THE UNCERTAINTY ANALYSIS:

File Name:	S4RA17		
Pressure Condition:	Atmospheric (101 kPa)		
Vapor Temperature	=	48.40	(Deg C)
Water Flow Rate (%)	=	80.00	
Water Velocity	=	7.83	(m/s)
Heat Flux	=	6.887E+04	(W/m^2)
Tube-metal thermal conduc.	=	385.0	(W/m.K)
Sieder-Tate constant	=	0.0300	

UNCERTAINTY ANALYSIS:

VARIABLE	PERCENT UNCERTAINTY
Mass Flow Rate, Md	0.79
Reynolds Number, Re	1.15
Heat Flux, q	3.13
Log-Mean-Tem Diff, LMTD	3.00
Wall Resistance, Rw	2.63
Overall H.T.C., Uo	4.33
Water-Side H.T.C., Hi	6.74
Vapor-Side H.T.C., Ho	5.60

DATA FOR THE UNCERTAINTY ANALYSIS:

File Name:	MBRA03		
Pressure Condition:	Atmospheric (101 kPa)		
Vapor Temperature	=	48.31	(Deg C)
Water Flow Rate (%)	=	20.00	
Water Velocity	=	1.16	(m/s)
Heat Flux	=	6.891E+04	(W/m^2)
Tube-metal thermal conduc.	=	385.0	(W/m.K)
Sieder-Tate constant	=	0.0300	

UNCERTAINTY ANALYSIS:

VARIABLE	PERCENT UNCERTAINTY
Mass Flow Rate, Md	2.99
Reynolds Number, Re	3.09
Heat Flux, q	3.13
Log-Mean-Tem Diff, LMTD	.80
Wall Resistance, Rw	2.67
Overall H.T.C., Uo	3.33
Water-Side H.T.C., Hi	7.12
Vapor-Side H.T.C., Ho	11.99

DATA FOR THE UNCERTAINTY ANALYSIS:

File Name:	MBRA03		
Pressure Condition:	Atmospheric (101 kPa)		
Vapor Temperature	=	48.57	(Deg C)
Water Flow Rate (%)	=	80.00	
Water Velocity	=	4.41	(m/s)
Heat Flux	=	1.000E+05	(W/m^2)
Tube-metal thermal conduc.	=	385.0	(W/m.K)
Sieder-Tate constant	=	0.0300	

UNCERTAINTY ANALYSIS:

VARIABLE	PERCENT UNCERTAINTY
Mass Flow Rate, Md	0.79
Reynolds Number, Re	1.09
Heat Flux, q	2.24
Log-Mean-Tem Diff, LMTD	2.05
Wall Resistance, Rw	2.67
Overall H.T.C., Uo	3.04
Water-Side H.T.C., Hi	6.73
Vapor-Side H.T.C., Ho	5.34

DATA FOR THE UNCERTAINTY ANALYSIS:

File Name:	L4RA07		
Pressure Condition:	Atmospheric (101 kPa)		
Vapor Temperature	= 48.43		(Deg C)
Water Flow Rate (%)	= 20.00		
Water Velocity	= 1.16		(m/s)
Heat Flux	= 8.078E+04		(W/m^2)
Tube-metal thermal conduc.	= 385.0		(W/m.K)
Sieder-Tate constant	= 0.0300		

UNCERTAINTY ANALYSIS:

VARIABLE	PERCENT UNCERTAINTY
Mass Flow Rate, Md	3.00
Reynolds Number, Re	3.10
Heat Flux, q	3.10
Log-Mean-Tem Diff, LMTD	.68
Wall Resistance, Rw	2.67
Overall H.T.C., Uo	3.18
Water-Side H.T.C., Hi	7.12
Vapor-Side H.T.C., Ho	17.46

DATA FOR THE UNCERTAINTY ANALYSIS:

File Name:	L4RA07		
Pressure Condition:	Atmospheric (101 kPa)		
Vapor Temperature	= 48.42		(Deg C)
Water Flow Rate (%)	= 80.00		
Water Velocity	= 4.40		(m/s)
Heat Flux	= 1.212E+05		(W/m^2)
Tube-metal thermal conduc.	= 385.0		(W/m.K)
Sieder-Tate constant	= 0.0300		

UNCERTAINTY ANALYSIS:

VARIABLE	PERCENT UNCERTAINTY
Mass Flow Rate, Md	0.79
Reynolds Number, Re	1.10
Heat Flux, q	1.93
Log-Mean-Tem Diff, LMTD	1.70
Wall Resistance, Rw	2.67
Overall H.T.C., Uo	2.57
Water-Side H.T.C., Hi	6.73
Vapor-Side H.T.C., Ho	5.86

DATA FOR THE UNCERTAINTY ANALYSIS:

File Name:	M1STV103		
Pressure Condition:	Vacuum (11 kPa)		
Vapor Temperature	=	48.44	(Deg C)
Water Flow Rate (%)	=	20.00	
Water Velocity	=	1.16	(m/s)
Heat Flux	=	1.352E+05	(W/m^2)
Tube-metal thermal conduc.	=	385.0	(W/m.K)
Sieder-Tate constant	=	0.0660	

UNCERTAINTY ANALYSIS:

VARIABLE	PERCENT UNCERTAINTY
Mass Flow Rate, Md	3.00
Reynolds Number, Re	3.11
Heat Flux, q	3.06
Log-Mean-Tem Diff, LMTD	.41
Wall Resistance, Rw	2.67
Overall H.T.C., Uo	3.09
Water-Side H.T.C., Hi	3.94
Vapor-Side H.T.C., Ho	9.31

DATA FOR THE UNCERTAINTY ANALYSIS:

File Name:	M1STV103		
Pressure Condition:	Vacuum (11 kPa)		
Vapor Temperature	=	48.44	(Deg C)
Water Flow Rate (%)	=	55.00	
Water Velocity	=	3.64	(m/s)
Heat Flux	=	1.872E+05	(W/m^2)
Tube-metal thermal conduc.	=	385.0	(W/m.K)
Sieder-Tate constant	=	0.0660	

UNCERTAINTY ANALYSIS:

VARIABLE	PERCENT UNCERTAINTY
Mass Flow Rate, Md	0.96
Reynolds Number, Re	1.24
Heat Flux, q	1.39
Log-Mean-Tem Diff, LMTD	.92
Wall Resistance, Rw	2.67
Overall H.T.C., Uo	1.67
Water-Side H.T.C., Hi	3.21
Vapor-Side H.T.C., Ho	3.14

DATA FOR THE UNCERTAINTY ANALYSIS:

File Name: M7STV80
Pressure Condition: Vacuum (1 kPa)

DATA FOR THE UNCERTAINTY ANALYSIS:

File Name: M7STV80
Pressure Condition: Vacuum (1 kPa)

Vapor Temperature	= 48.53	(Deg C)
Water Flow Rate (%)	= 20.00	
Water Velocity	= 1.16	(m/s)
Heat Flux	= 1.899E+05	(W/m^2)
Tube-metal thermal conduc.	= 385.0	(W/m.K)
Sieder-Tate constant	= 0.0880	

UNCERTAINTY ANALYSIS:

VARIABLE	PERCENT UNCERTAINTY
Mass Flow Rate, Md	3.00
Reynolds Number, Re	3.11
Heat Flux, q	3.05
Log-Mean-Tem Diff, LMTD	.30
Wall Resistance, Rw	2.67
Overall H.T.C., Ub	3.05
Water-Side H.T.C., Hi	3.94
Vapor-Side H.T.C., Ho	23.51

DATA FOR THE UNCERTAINTY ANALYSIS:

File Name: M7STV80
Pressure Condition: Vacuum (1 kPa)

Vapor Temperature	= 48.39	(Deg C)
Water Flow Rate (%)	= 80.00	
Water Velocity	= 4.40	(m/s)
Heat Flux	= 3.407E+05	(W/m^2)
Tube-metal thermal conduc.	= 385.0	(W/m.K)
Sieder-Tate constant	= 0.0880	

UNCERTAINTY ANALYSIS:

VARIABLE	PERCENT UNCERTAINTY
Mass Flow Rate, Md	0.79
Reynolds Number, Re	1.11
Heat Flux, q	1.09
Log-Mean-Tem Diff, LMTD	.81
Wall Resistance, Rw	2.67
Overall H.T.C., Ub	1.25
Water-Side H.T.C., Hi	3.18
Vapor-Side H.T.C., Ho	5.13

DATA FOR THE UNCERTAINTY ANALYSIS:

File Name:	S4STA100		
Pressure Condition:	Atmospheric (101 kPa)		
Vapor Temperature	= 100.00		(Deg C)
Water Flow Rate (%)	= 20.00		
Water Velocity	= 2.06		(m/s)
Heat Flux	= 5.192E+05		(W/m^2)
Tube-metal thermal conduc.	= 385.0		(W/m.K)
Sieder-Tate constant	= 0.0510		

UNCERTAINTY ANALYSIS:

VARIABLE	PERCENT UNCERTAINTY
Mass Flow Rate, Md	3.01
Reynolds Number, Re	3.14
Heat Flux, q	3.04
Log-Mean-Tem Diff, LMTD	.11
Wall Resistance, Rw	2.63
Overall H.T.C., Uo	3.04
Water-Side H.T.C., Hi	6.41
Vapor-Side H.T.C., Ho	20.41

DATA FOR THE UNCERTAINTY ANALYSIS:

File Name:	S4STA100		
Pressure Condition:	Atmospheric (101 kPa)		
Vapor Temperature	= 100.00		(Deg C)
Water Flow Rate (%)	= 66.00		
Water Velocity	= 6.47		(m/s)
Heat Flux	= 7.693E+05		(W/m^2)
Tube-metal thermal conduc.	= 385.0		(W/m.K)
Sieder-Tate constant	= 0.0510		

UNCERTAINTY ANALYSIS:

VARIABLE	PERCENT UNCERTAINTY
Mass Flow Rate, Md	0.96
Reynolds Number, Re	1.31
Heat Flux, q	1.08
Log-Mean-Tem Diff, LMTD	.22
Wall Resistance, Rw	2.63
Overall H.T.C., Uo	1.10
Water-Side H.T.C., Hi	5.99
Vapor-Side H.T.C., Ho	6.51

DATA FOR THE UNCERTAINTY ANALYSIS:

File Name:	SMTHSTA65	
Pressure Condition:	Atmospheric (101 kPa)	
Vapor Temperature	= 99.98	(Deg C)
Water Flow Rate (%)	= 20.00	
Water Velocity	= 1.16	(m/s)
Heat Flux	= 4.003E+05	(W/m^2)
Tube-metal thermal conduc.	= 385.0	(W/m.K)
Sieder-Tate constant	= 0.0660	

UNCERTAINTY ANALYSIS:

VARIABLE	PERCENT UNCERTAINTY
Mass Flow Rate, Md	3.00
Reynolds Number, Re	3.11
Heat Flux, q	3.04
Log-Mean-Tem Diff, LMTD	.14
Wall Resistance, Rw	2.67
Overall H.T.C., Uo	3.04
Water-Side H.T.C., Hi	3.94
Vapor-Side H.T.C., Ho	7.91

DATA FOR THE UNCERTAINTY ANALYSIS:

File Name:	SMTHSTA65	
Pressure Condition:	Atmospheric (101 kPa)	
Vapor Temperature	= 100.02	(Deg C)
Water Flow Rate (%)	= 80.00	
Water Velocity	= 4.40	(m/s)
Heat Flux	= 5.301E+05	(W/m^2)
Tube-metal thermal conduc.	= 385.0	(W/m.K)
Sieder-Tate constant	= 0.0660	

UNCERTAINTY ANALYSIS:

VARIABLE	PERCENT UNCERTAINTY
Mass Flow Rate, Md	0.79
Reynolds Number, Re	1.12
Heat Flux, q	.99
Log-Mean-Tem Diff, LMTD	.39
Wall Resistance, Rw	2.67
Overall H.T.C., Uo	1.06
Water-Side H.T.C., Hi	3.18
Vapor-Side H.T.C., Ho	1.93

DATA FOR THE UNCERTAINTY ANALYSIS:

File Name:	L4STA66		
Pressure Condition:	Atmospheric (101 kPa)		
Vapor Temperature	= 99.95	(Deg C)	
Water Flow Rate (%)	= 20.00		
Water Velocity	= 1.16	(m/s)	
Heat Flux	= 6.397E+05	(W/m^2)	
Tube-metal thermal conduc.	= 385.0	(W/m.K)	
Sieder-Tate constant	= 0.0660		

UNCERTAINTY ANALYSIS:

VARIABLE	PERCENT UNCERTAINTY
Mass Flow Rate, Md	3.00
Reynolds Number, Re	3.12
Heat Flux, q	3.04
Log-Mean-Tem Diff, LMTD	.09
Wall Resistance, Rw	2.67
Overall H.T.C., Uo	3.04
Water-Side H.T.C., Hi	3.94
Vapor-Side H.T.C., Ho	25.56

DATA FOR THE UNCERTAINTY ANALYSIS:

File Name:	L4STA66		
Pressure Condition:	Atmospheric (101 kPa)		
Vapor Temperature	= 100.01	(Deg C)	
Water Flow Rate (%)	= 80.00		
Water Velocity	= 4.40	(m/s)	
Heat Flux	= 1.122E+06	(W/m^2)	
Tube-metal thermal conduc.	= 385.0	(W/m.K)	
Sieder-Tate constant	= 0.0660		

UNCERTAINTY ANALYSIS:

VARIABLE	PERCENT UNCERTAINTY
Mass Flow Rate, Md	0.79
Reynolds Number, Re	1.12
Heat Flux, q	.93
Log-Mean-Tem Diff, LMTD	.19
Wall Resistance, Rw	2.67
Overall H.T.C., Uo	.94
Water-Side H.T.C., Hi	3.18
Vapor-Side H.T.C., Ho	5.18

DATA FOR THE UNCERTAINTY ANALYSIS:

File Name:	L4STV67		
Pressure Condition:	Vacuum (11 kPa)		
Vapor Temperature	=	48.49	(Deg C)
Water Flow Rate (%)	=	20.00	
Water Velocity	=	1.16	(m/s)
Heat Flux	=	1.885E+05	(W/m^2)
Tube-metal thermal conduc.	=	385.0	(W/m.K)
Sieder-Tate constant	=	0.0660	

UNCERTAINTY ANALYSIS:

VARIABLE	PERCENT UNCERTAINTY
Mass Flow Rate, Md	3.01
Reynolds Number, Re	3.11
Heat Flux, q	3.05
Log-Mean-Tem Diff, LMTD	.30
Wall Resistance, Rw	2.67
Overall H.T.C., Uo	3.07
Water-Side H.T.C., Hi	3.94
Vapor-Side H.T.C., Ho	23.98

DATA FOR THE UNCERTAINTY ANALYSIS:

File Name:	L4STV67		
Pressure Condition:	Vacuum (11 kPa)		
Vapor Temperature	=	48.49	(Deg C)
Water Flow Rate (%)	=	80.00	
Water Velocity	=	4.39	(m/s)
Heat Flux	=	3.779E+05	(W/m^2)
Tube-metal thermal conduc.	=	385.0	(W/m.K)
Sieder-Tate constant	=	0.0660	

UNCERTAINTY ANALYSIS:

VARIABLE	PERCENT UNCERTAINTY
Mass Flow Rate, Md	0.79
Reynolds Number, Re	1.12
Heat Flux, q	1.06
Log-Mean-Tem Diff, LMTD	.55
Wall Resistance, Rw	2.67
Overall H.T.C., Uo	1.19
Water-Side H.T.C., Hi	3.18
Vapor-Side H.T.C., Ho	6.58

DATA FOR THE UNCERTAINTY ANALYSIS:

File Name:	MSEGV34	
Pressure Condition:	Vacuum (1 kPa)	
Vapor Temperature	= 127.79	(Deg C)
Water Flow Rate (%)	= 50.00	
Water Velocity	= 2.79	(m/s)
Heat Flux	= 5.111E+05	(W/m^2)
Tube-metal thermal conduc.	= 385.0	(W/m.K)
Sieder-Tate constant	= 0.0350	

UNCERTAINTY ANALYSIS:

VARIABLE	PERCENT UNCERTAINTY
Mass Flow Rate, Md	1.25
Reynolds Number, Re	1.47
Heat Flux, q	1.35
Log-Mean-Tem Diff, LMTD	.26
Wall Resistance, Rw	2.67
Overall H.T.C., Uo	1.37
Water-Side H.T.C., Hi	14.34
Vapor-Side H.T.C., Ho	12.31

DATA FOR THE UNCERTAINTY ANALYSIS:

File Name: MSEGV40

DATA FOR THE UNCERTAINTY ANALYSIS:

File Name:	MSEGV34	
Pressure Condition:	Vacuum (1 kPa)	
Vapor Temperature	= 127.81	(Deg C)
Water Flow Rate (%)	= 98.00	
Water Velocity	= 5.38	(m/s)
Heat Flux	= 5.994E+05	(W/m^2)
Tube-metal thermal conduc.	= 385.0	(W/m.K)
Sieder-Tate constant	= 0.0350	

UNCERTAINTY ANALYSIS:

VARIABLE	PERCENT UNCERTAINTY
Mass Flow Rate, Md	0.65
Reynolds Number, Re	1.00
Heat Flux, q	.89
Log-Mean-Tem Diff, LMTD	.42
Wall Resistance, Rw	2.67
Overall H.T.C., Uo	.98
Water-Side H.T.C., Hi	14.31
Vapor-Side H.T.C., Ho	7.41

DATA FOR THE UNCERTAINTY ANALYSIS:

File Name:	M1EGV37	
Pressure Condition:	Vacuum (11 kPa)	
Vapor Temperature	= 127.83	(Deg C)
Water Flow Rate (%)	= 20.00	
Water Velocity	= 1.16	(m/s)
Heat Flux	= 2.166E+05	(W/m^2)
Tube-metal thermal conduc.	= 385.0	(W/m.K)
Sieder-Tate constant	= 0.0350	

UNCERTAINTY ANALYSIS:

VARIABLE	PERCENT UNCERTAINTY
Mass Flow Rate, Md	3.00
Reynolds Number, Re	3.11
Heat Flux, q	3.04
Log-Mean-Tem Diff, LMTD	.25
Wall Resistance, Rw	2.67
Overall H.T.C., Uo	3.05
Water-Side H.T.C., Hi	14.51
Vapor-Side H.T.C., Ho	10.10

DATA FOR THE UNCERTAINTY ANALYSIS:

File Name:	M1EGV37	
Pressure Condition:	Vacuum (11 kPa)	
Vapor Temperature	= 127.81	(Deg C)
Water Flow Rate (%)	= 80.00	
Water Velocity	= 4.40	(m/s)
Heat Flux	= 2.501E+05	(W/m^2)
Tube-metal thermal conduc.	= 385.0	(W/m.K)
Sieder-Tate constant	= 0.0350	

UNCERTAINTY ANALYSIS:

VARIABLE	PERCENT UNCERTAINTY
Mass Flow Rate, Md	0.79
Reynolds Number, Re	1.11
Heat Flux, q	1.22
Log-Mean-Tem Diff, LMTD	.82
Wall Resistance, Rw	2.67
Overall H.T.C., Uo	1.48
Water-Side H.T.C., Hi	14.32
Vapor-Side H.T.C., Ho	3.39

DATA FOR THE UNCERTAINTY ANALYSIS:

File Name:	S4STV74		
Pressure Condition:	Vacuum (11 kPa)		
Vapor Temperature	=	48.45	(Deg C)
Water Flow Rate (%)	=	20.00	
Water Velocity	=	2.06	(m/s)
Heat Flux	=	1.592E+05	(W/m^2)
Tube-metal thermal conduc.	=	385.0	(W/m.K)
Sieder-Tate constant	=	0.0510	

UNCERTAINTY ANALYSIS:

VARIABLE	PERCENT UNCERTAINTY
Mass Flow Rate, Md	3.00
Reynolds Number, Re	3.13
Heat Flux, q	3.05
Log-Mean-Tem Diff, LMTD	.35
Wall Resistance, Rw	2.63
Overall H.T.C., Uo	3.07
Water-Side H.T.C., Hi	6.41
Vapor-Side H.T.C., Ho	18.78

DATA FOR THE UNCERTAINTY ANALYSIS:

File Name:	S4STV74		
Pressure Condition:	Vacuum (11 kPa)		
Vapor Temperature	=	48.46	(Deg C)
Water Flow Rate (%)	=	40.00	
Water Velocity	=	3.98	(m/s)
Heat Flux	=	2.011E+05	(W/m^2)
Tube-metal thermal conduc.	=	385.0	(W/m.K)
Sieder-Tate constant	=	0.0510	

UNCERTAINTY ANALYSIS:

VARIABLE	PERCENT UNCERTAINTY
Mass Flow Rate, Md	1.55
Reynolds Number, Re	1.78
Heat Flux, q	1.70
Log-Mean-Tem Diff, LMTD	.53
Wall Resistance, Rw	2.63
Overall H.T.C., Uo	1.78
Water-Side H.T.C., Hi	6.07
Vapor-Side H.T.C., Ho	8.85

DATA FOR THE UNCERTAINTY ANALYSIS:

File Name:	RSMTH1		
Pressure Condition:	Atmospheric (101 kPa)		
Vapor Temperature	=	48.22	(Deg C)
Water Flow Rate (%)	=	20.00	
Water Velocity	=	1.17	(m/s)
Heat Flux	=	2.591E+04	(W/m^2)
Tube-metal thermal conduc.	=	385.0	(W/m.K)
Sieder-Tate constant	=	0.0300	

UNCERTAINTY ANALYSIS:

VARIABLE	PERCENT UNCERTAINTY
Mass Flow Rate, Md	2.99
Reynolds Number, Re	3.08
Heat Flux, q	3.68
Log-Mean-Tem Diff, LMTD	2.11
Wall Resistance, Rw	2.67
Overall H.T.C., Uo	4.24
Water-Side H.T.C., Hi	7.12
Vapor-Side H.T.C., Ho	5.71

DATA FOR THE UNCERTAINTY ANALYSIS:

File Name:	RSMTH1		
Pressure Condition:	Atmospheric (101 kPa)		
Vapor Temperature	=	48.45	(Deg C)
Water Flow Rate (%)	=	80.00	
Water Velocity	=	4.42	(m/s)
Heat Flux	=	2.995E+04	(W/m^2)
Tube-metal thermal conduc.	=	385.0	(W/m.K)
Sieder-Tate constant	=	0.0300	

UNCERTAINTY ANALYSIS:

VARIABLE	PERCENT UNCERTAINTY
Mass Flow Rate, Md	0.79
Reynolds Number, Re	1.08
Heat Flux, q	6.98
Log-Mean-Tem Diff, LMTD	6.92
Wall Resistance, Rw	2.67
Overall H.T.C., Uo	9.82
Water-Side H.T.C., Hi	6.73
Vapor-Side H.T.C., Ho	10.83

LIST OF REFERENCES

1. Holman, J. P., *Heat Transfer*, McGraw Hill, New York, pp. 407–410, 1981.

2. Wanniarchchi, A. S., Marto, P. J., and Rose, J. W., "Film Condensation of Steam on Horizontal Finned Tubes: Effect of Fin Spacing, Thickness and Height," *Multiphase Flow and Heat Transfer*, vol. 108, pp. 960–966, November 1986.

3. Masuda, H., and Rose, J. W., "Condensation of Ethylene Glycol on Horizontal Integral Fin Tubes," *Proceedings of the ASME-JSME Thermal Engineering Joint Conference*, vol. 1, pp. 525–528, March 1987.

4. Yau, K. K., Cooper, J. R., and Rose, J. W., "Effects of Fin Spacing on the Performance of Horizontal Integral-Fin Condenser Tubes," *Journal of Heat Transfer*, vol. 107, pp. 377–383, May1985.

5. Georgiadis, I. V., *Filmwise Condensation of Steam on Low Integral-Finned Tubes*, Master's Thesis, Naval Postgraduate School, Monterey, California, September 1984.

6. Krohn, R. L., *An Experimental Apparatus to Study Enhanced Condensation Heat-Transfer of Steam on Horizontal Tubes*, Master's Thesis, Naval Postgraduate School, Monterey, California, June 1983.

7. Graber, K. A., *Condensation Heat Transfer of Steam on a Single Horizontal Tube*, Master's Thesis, Naval Postgraduate School, Monterey, California, June 1983.

8. Poole, W. M., *Filmwise Condensation of Steam on Externally-Finned Horizontal Tubes*, Master's Thesis, Naval Postgraduate School, Monterey, California, December 1983.

9. Flook, F. V., *Filmwise Condensation of Steam on Low Integral-Finned Tubes*, Master's Thesis, Naval Postgraduate School, Monterey, California, March 1985.

10. Mitrou, E. S., *Film Condensation of Steam on Externally Enhanced Horizontal Tubes*, Master's Thesis, Naval Postgraduate School, Monterey, California, March 1986.

11. Caken, O., *Filmwise Condensation of Steam on Low-Integral-Finned Tubes*, Master's Thesis, Naval Postgraduate School, Monterey, California, December 1986.

12. Zebrowski, D. S., *Condensation Heat-Transfer Measurements of Refrigerants on Externally Enhanced Tubes*, Master's Thesis, Naval Postgraduate School, Monterey, California, June 1987.

13. Lester, D. J., *Indirect Measurements of Local Condensing Heat-Transfer Around Horizontal Finned Tubes*, Master's Thesis, Naval Postgraduate School, Monterey, California, September 1987.

14. Wanniarchchi, A. S., Marto, P. J., and Rose, J. W., "Film Condensation of Steam on Horizontal Low Integral-Fin Tubes: Effect of Fin Spacing," *Journal of Heat Transfer*, vol. 108, pp. 960–966, November 1986.

15. Katz, D. L., Hope, R. E., and Dasko, S. C., *Liquid Retention on Finned Tubes*, Dept. of Engr. Research, University of Michigan, Ann Arbor, Michigan, Project M 592, 1946.

16. Rudy, T. M., and Webb, R. L., "Condensate Retention of Horizontal Integral-Finned Tubing," *Advances in Enhanced Heat Transfer*, HTD, vol. 18, pp. 35–41, 20th National Heat Transfer Conference, Milwaukee, Wisconsin, August 1981.

17. Rifert, V. G., "Steam Condensation on Profiled Surfaces," *Heat and Mass-Transfer Processes in Porous Media With Phase Transformation*, Academy of Sciences, BSSR, A. B. Lykov (ed.), pp. 373–378, Minsk, 1982.

18. Rudy, T. M. and Webb, R. L., "Theoretical Model for Condensation on Horizontal Integral-Fin Tubes," *AICHE Symposium Series*, vol. 79, no. 225, pp. 11–18, 1983.

19. Honda, H., Nozu, S., and Mitsumori, K., "Augmentation of Condensation on Horizontal Finned Tubes by Attaching Porous Drainage Plates," *Proceedings of the ASME-JSME Thermal Engineering Conference*, pp. 289–296, Honolulu, 1983.

20. Rudy, T. M., and Webb, R. L., "An Analytical Model to Predict Condensation Retention on Horizontal Integral-Finned Tubes," *Journal of Heat Transfer*, vol. 107, pp. 361–368, May 1985.

21. Masuda, H., and Rose, J. W., "Static Configuration of Liquid Film on Horizontal Tubes With Low Radial Fins: Implications for Condensation Heat Transfer," *Proceedings of the Royal Society of London*, vol. A410, pp. 125–139.

22. Honda, H., Nozu, S., and Uchima, B., "A Generalized Prediction Method for Heat Transfer During Film Condensation on a Horizontal Low Finned Tube," *Proceedings of the 1987 ASME-JSME Thermal Engineering Conference*, vol. 4, pp. 385–392, Hawaii, 1987.

23. Beatty, K. T., Jr., and Katz, D. L., "Condensation of Vapors on Outside of Finned Tubes," *Chemical Engineering Progress*, vol. 44, no. 1, pp. 55–77, January 1948.

24. Owen, R. G., Sardesai, R. G., Smith, R. A., and Lee, W. C., "Gravity Controlled Condensation on Horizontal Low-Fin Tube," *Condensers: Theory and Practice*, Inst. Chem. Engrs. Symp. Ser. 75, pp. 415–428, 1983.

25. Wanniarchchi, A. S., Marto, P. J., and Rose, J. W., "Filmwise Condensation of Steam on Externally-Finned Horizontal Tubes," *Fundamentals of Phase Change: Boiling and Condensation*, HTD, vol. 38, pp. 133–141, C. T. Avedisian and T. M. Rudy (eds.), December 1984.

26. Gregorig, R., "Filmwise Condensation on Finely Rippled Surfaces with Condensation of Surface Tension," *Zeitschrift fur angewandte Mathemetik und Physik*, vol. V, pp. 36–49, 1954, trans. D. K. Edwards.

27. Webb, R. L., Rudy, T. M., and Kedzierski, M. A., "Prediction of the Condensation of Steam on Horizontal Integral-Fin Tubes," *ASME Journal of Heat Transfer*, vol. 107, pp. 369–376, November 1985.

28. Adamek, T., "Bestimmung der Kondensationgrossen auf feingewellten Oberflachen zur Auslegung aptimaler Wandprofile," *Warme und Stoffubertrangung*, vol. 15, pp. 255–270, 1981.

29. Honda, H., and Nozu, S., "A Prediction Method for Heat Transfer During Film Condensation on Horizontal Low Integral-Fin Tubes," *ASME Journal of Heat Transfer*, vol. 109, pp. 218–225, 1987.

30. Marto, P. J., "An Evaluation of Film Condensation on Horizontal Integral-Fin Tubes," *Journal of Heat Transfer*, vol. 110, pp. 1287–1305, November 1988.

31. Kline, S. J., and McClintok, F. A., "Describing Uncertainties in Single-Sample Experiments," *Mechanical Engineering*, vol. 74, pp. 3–8, January 1953.

INITIAL DISTRIBUTION LIST

		No. Copies
1.	Defense Technical Information Center Cameron Station Alexandria, VA 22304–6145	2
2.	Library, Code 0142 Naval Postgraduate School Monterey, CA 93943-5002	2
3.	Department Chairman, Code 69He Department of Mechanical Engineering Naval Postgraduate School Monterey, CA 93943-5004	1
4.	Professor Paul J. Marto, Code 69Mx Department of Mechanical Engineering Naval Postgraduate School Monterey, CA 93943-5004	5
5.	Dr. A. S. Wanniarachchi ERC-CRSS University of California at Santa Barbara Santa Barbara, CA 93106	2
6.	Professor John W. Rose Department of Mechanical Engineering Queen Mary College London E1 4NS England	1
7.	Mr. R. Helmick, Code 2722 David W. Taylor Naval Ship Research and Development Center Annapolis, MD 21402	1
8.	Program Director Thermal Systems and Engineering Program National Science Foundation Washington, DC 20550	1

9. Dr. Thomas J. Caulfield, CAPT, USNR (Ret.) 1
Professor, Counselor Education
Canisius College
Buffalo, NY 14208

10. LT Thomas L. Van Petten, USN (Ret.) 1
408 Minutemen Road
Virginia Beach, VA 23462

11. LCDR David J. Van Petten, USNR 1
2267 Easton Court
Waldorf, MD 20601

12. LCDR Paul H. Case, USN 1
USS Samuel Gompers (AD-J)
Fleet Post Office
San Francisco, CA 96641-2515

13. LT Thomas L. Van Petten, USN 2
130 Fairlawn Drive
Eggertsville, NY 14226